

In presenting this thesis in partial fulfillment of the requirements for an advanced degree at Idaho State University, I agree that the Library shall make it freely available for inspection. I further state that permission for extensive copying of my thesis for scholarly purposes may be granted by the Dean of the Graduate School, Dean of my academic division, or by the University Librarian. It is understood that any copying or publication of this thesis for financial gain shall not be allowed without my written permission.

Signature _____

Date _____

Autonomous Ground Vehicle and a Novel EOAT for Infected Plant
Detection and Removal

by

Taher Deemyad

A Dissertation

Submitted in Partial Fulfillment

of the Requirements for the Degree of Doctor of Philosophy

in the Department of Mechanical Engineering

Idaho State University

Summer 2021

Copyright (2021) Taher Deemyad

To the Graduate Faculty:

The members of the committee appointed to examine the thesis of Taher Deemyad find it satisfactory and recommend that it be accepted.

Alba Perez Gracia, Ph.D., Associate Professor
Major Advisor

Anish Sebastian, Ph.D., Assistant Professor, Associate Chair
Major Co-Advisor

Chikashi Sato, Ph.D., Professor
Graduate Faculty Representative

Marco P. Schoen, Ph.D., P.E., Professor
Committee Member

Paul Bodily, Ph.D., Assistant Professor
Committee Member

To my parents: Efat and Mohammadreza

ACKNOWLEDGMENTS

My success in this long journey has been due to the advice and help of many people, who with endless support made it possible for me to become the scientist I am today.

My sincere thanks go to:

My Advisor, Professor Alba Perez Gracia, who with incredible knowledge and patience shaped my understanding of kinematics and robotics. Learning from such a great scientist was an exceptional opportunity for me from my very first day starting a new major in the field of robotics.

My Advisor, Professor Anish Sebastian, whose guidance and continuous support in all aspects of my research and teaching made it possible for me to reach to this point.

Professor Donna Delparte and Professor Arash Rashed, who initiated the idea for this project, and whose knowledge in the field of agriculture proved invaluable during my collaborations with them.

Professor Marco Schoen, Professor Paul Bodily, and Professor Chikashi Sato for kindly accepting to be in my PhD dissertation committee, and for their precious guidance during this work.

Professor Brian Williams, Professor Ken Bosworth, Professor Mary Hofle, Professor Bennett Palmer, Professor Arya Ebrahimpour, and Professor Bruce Savage, whose ready support and immense knowledge helped me greatly during my master's and PhD and have played a significant role in the success of this project.

Professor Soheil Porkhial, Professor Shahrokh Sorkhkhah, and Professor Mohammad Layeghi, my professors during my bachelor's degree, to whom I credit my general knowledge of mechanical engineering. The reason that I am here today is because of their continuous support.

Ryan Moeller, Omid Heidari, Neda Hassanzadeh, Vincent Akula, Mohammadamin Torabi, Ali Tamimi, Mike Griffel and Jared Cantrell, who were my coworkers in this project or helped me in various parts of this work.

All my friends in Idaho, who made ISU my home and a fantastic research environment.

And my deepest thanks to my family: My mother, Efat, who was by my side in all stages of my education; My father, Mohammadreza, who was my main inspiration to engage in science and, specifically, mechanical engineering; My siblings, Tara, Shanti, and Taha, who helped me a lot in various parts of my dissertation; My brothers-in-law Soroush and Saveez and my sister-in-law Marketa for their immense support during my PhD; and my intelligent niece, Irenka, who helped me in editing this dissertation.

TABLE OF CONTENTS

ACKNOWLEDGMENTS	v
LIST OF FIGURES	xi
LIST OF TABLES	xv
LIST OF SYMBOLS	xvii
ABSTRACT.....	xviii
CHAPTER 1. INTRODUCTION	1
1.1 Robots in Agriculture.....	1
1.2 Chassis Design.....	5
1.3 Navigation, Obstacle Avoidance, and Communications	7
1.4 Image Processing	9
1.5 Roguing Mechanism	10
1.6 Singularity Analysis.....	18
1.7 Research Goals	20
CHAPTER 2. CHASSIS DESIGN FOR AN AUTONOMOUS GROUND VEHICLE (AGV)	23
2.1 Potato Field Specifications and Motion Study for AGV	23
2.1.1 Potato Field.....	23
2.1.2 Potato Field Simulation Information	24
2.1.3 Possible Stresses for a Four-Wheel Vehicle	25
2.2 Parts of the AGV and Specification.....	29
2.2.1 Parts of AGV	29

2.2.2	Material Selection & Size of the Chassis.....	30
2.3	Chassis Optimization and Stress Analysis.....	31
2.3.1	Optimization	31
2.3.2	Force	33
2.3.3	Stress Analysis.....	33
2.4	Chassis Final Design.....	40
CHAPTER 3. NAVIGATION & OBSTACLE AVOIDANCE.....		42
3.1	Navigation.....	42
3.1.1	Evaluation of Components.....	45
3.1.2	Integration with Pixhawk.....	45
3.2	Obstacle Avoidance	48
3.3	Results for Navigation & Obstacle Avoidance Tests.....	49
3.3.1	Piksi Multi Accuracy	49
3.3.2	Autonomous Navigation via Waypoints and Obstacle Avoidance	51
CHAPTER 4. IMAGE PROCESSING		52
4.1	Project Overview and Conditions of the Target Environment.....	52
4.2	Equipment and Appropriate Color Space	54
4.2.1	HSL Color Space	54
4.2.2	Equipment.....	55
4.3	Problem Statement and Methods	58
4.4	Results and Discussion	61
4.4.1	The Target Color Domain Detection	61

4.4.2	The Light Range	63
4.4.3	The Minimum Range	64
4.4.4	Finding the Center of the Target Plant.....	65
CHAPTER 5. ROGUING MECHANISM.....		70
5.1	Potato Field Visit and Simulated Model of Potato Field in the Lab	70
5.1.1	Finding the Height of Potatoes with Picture Analysis	70
5.1.2	Potato Field Visit	72
5.1.3	Process for Planting Potatoes Indoor	73
5.2	Analysis of the Possible Options for Roguing Mechanism	78
5.2.1	General Grasping Principles	78
5.2.2	Initial Tests for Grasping Mechanism.....	80
5.2.3	The Best Options	82
5.3	Final Design.....	87
5.3.1	Parts of the Mechanism.....	87
5.3.2	Parts Specification	90
5.3.3	Motion Study	91
5.3.4	Designed Attachment for Tractor	92
5.3.5	Some of the Mechanism Specifications and Information about Extracted Soil.....	93
5.4	Prototype Model and Actual Test	94
CHAPTER 6. SINGULARITY ANALYSIS.....		97
6.1	Kinematic Synthesis of the Five-Fingered Multi-fingered Hand.....	97
6.2	Hand Optimization.....	99

6.3	Underactuated Coupling Mechanisms	101
6.4	The RRSS Mechanism	103
6.5	Singularity Design for RRSS Mechanism	105
6.6	Solution Procedure and a Numerical Example	108
CHAPTER 7. CONCLUSIONS		114
APPENDIX.....		118
A.	STRESS ANALYSIS FOR CHASSIS	118
B.	CHASSIS OPTIMIZATION CODES	144
C.	IMAGE PROCESSING CODES	147
D.	RELATED PUBLICATIONS AND PATENT.....	155
E.	REFERENCES	156

LIST OF FIGURES

Figure 1: Whole process of communication between UAV and AGV from detection sick plant by UAV to roguing by AGV	5
Figure 2: Potato field before and after harvesting [27]	24
Figure 3: Simulated shape and size of the terrain	24
Figure 4: Longitudinal Torsion	26
Figure 5: Vertical Bending.....	26
Figure 6: Lateral Bending	27
Figure 7: Horizontal Lozenging.....	28
Figure 8: Simulated Terrains Encountered in Field	28
Figure 9: AGV components	30
Figure 10: Chassis.....	32
Figure 11: Reaction forces in test 1	34
Figure 12: Reaction forces in test 2	34
Figure 13: Reaction forces in test 3	35
Figure 14: Reaction forces in test 4	36
Figure 15: Reaction forces in test 5	36
Figure 16: Reaction forces in test 6	37
Figure 17: Reaction forces in test 7	37
Figure 18: Displacement in test 2	39
Figure 19: Stress in test 2.....	39
Figure 20: Strain in test 3.....	40

Figure 21: Autonomous ground vehicle (AGV)	41
Figure 22: Commercial implemented GPS [112]	43
Figure 23: RTK system [113]	43
Figure 24: Pixsi Multi Evaluation Kit Main Parts	44
Figure 25: Screenshots of the mission planner's navigation planning feature.....	46
Figure 26: Assembled and painted enclosure, placed on top of robot chassis	47
Figure 27: The “dodge” obstacle avoidance on the Pixhawk using a range-finding LIDAR	49
Figure 28: A geodetic marker in the Pocatello Airport.....	50
Figure 29: Simulated potato field and an average distance between plants in the field.....	53
Figure 30: Planted potatoes indoors with a similar pattern in the field.....	54
Figure 31: Required components for image processing and detect the infected plant.....	56
Figure 32: The location of two cameras in the prototype of roguing mechanism. Camera #1 give us the top view of the plant and Camera #2 give us the front view of the plant	57
Figure 33: The 60cm×60cm area around the target plant in the field and nine 40cm×40cm sub-areas inside of this region.....	59
Figure 34: The 40cm×40cm area with the center point number 1 (example).....	60
Figure 35: Three leaves samples with different color, shape, and size to test the detection codes and check the selected range for HSL parameters	63
Figure 36: Checking the accuracy of the code in various level of brightness A) very bright b) normal c) dark d) very dark.....	64
Figure 37: The blobs with less than 300 pixels will be removed from the image	65
Figure 38: Aerial photo from a potato field	65

Figure 39: The received coordinate from GPS as the center of the target plant (close to Num. 9) and surrounding	66
Figure 40: Nine search regions in Method A	66
Figure 41: A-Center of target plant; B- The center point detected from method A (Yellow star) & method B (Blue star).....	68
Figure 42: Comparison between the error of method A & method B for ten different situations	69
Figure 43: Potato field (left) and simulated shape and size of the potato field (right).....	73
Figure 44: Container filled by gravel for planting potato	74
Figure 45: Cover gravels with a sheet of filter fabric	74
Figure 46: Marking the container for the place of planting potatoes	75
Figure 47: Adding soil up to the middle of the container	75
Figure 48: Planting potatoes with 30cm from each other	76
Figure 49: Adding soil for 30cm on top of the potatoes	76
Figure 50: Using Indoor Reflector Plant Light Bulbs for having enough light for potatoes	77
Figure 51: Fully grown potatoes after 8 weeks	77
Figure 52: a) Vertical motion b) Connection between roots, tubers, and stem of the plant were broken in a vertical motion	81
Figure 53: a) Horizontal motion b) Connections between roots, tubers, and stem of the plant were not broken in the first time but in the next two repeats it was failed	82
Figure 54: a) Twist & vertical motion b) Connections between different parts of the plant were broke....	82
Figure 55: Designed mechanism with multiple blades in circular form	85
Figure 56: Cage form mechanism with two moving blades and a single actuator.....	86
Figure 57: Different views of final design.....	87

Figure 58: Final design Components	88
Figure 59: Actuation of blades by a hydraulic system in the final design	91
Figure 60: Different views of the designed connection part between roguing mechanism and tractors three-point hitch	92
Figure 61: Roguing mechanism with connection part for tractors three-point hitch	93
Figure 62: Amount soil can be extracted from the field	94
Figure 63: Prototype of the mechanism (1/3 of the real size)	95
Figure 64: Process of roguing the sample plant by prototype mechanism.....	96
Figure 65: The tree graph of the 1-(1, 1, 1, 1, 1) hand, left; the kinematic sketch, right	98
Figure 66: First and second positions for each fingertip, left and a schematic sketch of hand in both.....	99
Figure 67: a) Schematic sketches of the hand in position 1 before optimization b) after optimization....	100
Figure 68: The R-R chain for wrist joint and first finger, coupled using the complementary R-R chain .	102
Figure 69: Mechanism with 5 RRSS chains designed for grasping a mobile phone	104
Figure 70: Single RRSS chain	106
Figure 71: Motion of RRSS chain between points 1 and 2 (the points the RR chain was synthesized for) plus singular positions at point 1 and 3.....	111
Figure 72: Angle for θ_{11} at the first singularity position (left), Angle for θ_{12} at the second singularity position (right)	111
Figure 73: Possible singular points for each selected θ_1	112
Figure 74: The relation between θ_1 & θ_2 for the loop closure	113

LIST OF TABLES

Table 1: Name, Quantity, and Weight of Each Part.....	29
Table 2: Specification of Aluminum Alloy 6061.....	30
Table 3: Optimization Results for Three Different Materials for Chassis	32
Table 4: Final Results for Stress, Displacement, and Strain of All 7 Tests	38
Table 5: Piksi Multi Evaluation Kit Main Parts.....	44
Table 6: Comparison of RTK GPS Systems	45
Table 7: Results from Piksi Multi Accuracy Testing.....	50
Table 8: List of components	57
Table 9: Acceptable Range of Parameters in the HSL Format	61
Table 10: Color Detection Test for a Wide Range of Colors.....	62
Table 11: Green Area for each Region in Method A.....	67
Table 12: The X & Y Coordinates for Method A, Method B, and True Center Point.....	68
Table 13: Morphology Chart	84
Table 14: List of Components for Final Design	89
Table 15: The two positions used for the synthesis of finger 1, expressed as dual quaternions	99
Table 16: Twist angles α_{ij} between axis S_i and axis S_j	99
Table 17: Resulting values for the sliding parameters of the joints	100
Table 18: Mechanisms to implement coupling between joint axes	101
Table 19: Two task positions and two points on each R joint axis	109
Table 20: Plucker coordinates for the R joints.....	109

Table 21: Information about the relation between R joints and input values for θ_1 to define two singular positions	109
Table 22: Result for unknown parameters and the center point of S joints for RRSS with two specified singular positions	110
Table 23: Possible singularity points and valid one respect to work-space of robot	113

LIST OF SYMBOLS

σ	Stress
M	Internal bending moment
c	Perpendicular distance from the neutral axis to the farthest point on the section
I	Moment of inertia of the section area about the neutral axis
H	Hue (HSL color format)
S	Saturation (HSL color format)
L	Lightness (HSL color format)
R	Red (RGB color format)
G	Green (RGB color format)
B	Blue (RGB color format)
m	Mass
S (RRSS)	Spherical joint
R (RRSS)	Revolute joint
\hat{P}	Relative displacement
α	Twist Angle
t_s	Sliding parameters of the joints
T	Translation
R	Rotation
θ	Input/output angle
G	Transformation Matrix
J & J*	Jacobian Matrices

Autonomous Ground Vehicle & a Novel EOAT for Infected Plant Detection & Removal

Dissertation Abstract — Idaho State University (2021)

In this work, various parts of an autonomous ground vehicle (AGV) for agricultural purposes are designed. This AGV is part of a larger project that, in a cooperation with an unmanned aerial vehicle (UAV), can detect and remove infected potatoes plants by virus Y (PVY).

In the first part of this work, the design of a prototype chassis for the AGV was analyzed. This prototype is a four-wheel powered vehicle. An optimization routine was used for finding the ideal size and material for the chassis. In the second and third parts, the design, implementation, and performance of autonomous navigation and obstacle avoidance systems for this AGV are discussed. To reach the maximum accuracy for navigation, an RTK GPS has been used. Also, for obstacle avoidance in this AGV, a simple 2D LIDAR sensor was installed and tested. The fourth part is related to detect the exact location of the infected plant by an advanced robot vision system and proper image processing algorithm. This system includes two RGB cameras and utilizes the HSL format of images for image processing. The fifth part of this work is related to design of an efficient end of arm tooling (EOAT). The most appropriate mechanism for complete removing infected plant was designed and a prototype model of it was built and tested after passing the motion analysis in a CAD model. In the last part of this work, a novel singularity analysis for robotic mechanisms has been presented, and the idea is developed by an example of a spatial mechanism (RRSS).

The outcome of this work includes design and implementation of various parts of an agricultural ground vehicle. The motion study and stress analysis for the mechanical sections of this vehicle are analyzed in SolidWorks, and a prototype model of each part is tested in the field. All electronic sections (including various GPS, sensors, cameras, motors, etc.) have been checked

one by one in different situations based on function. Also, codes and algorithm for image processing and navigation were tested in various conditions.

Key Words: Optimization, Stress Analysis, Chassis Design, Autonomous Vehicle, Four Wheel Drive Vehicle, CAD Stress Analysis, Mobile Manipulator, Roguing Mechanism, Agricultural Robot, End of Arm Tooling, Autonomous Virus Removal, Navigation, RTK GPS, Obstacle Avoidance, Agricultural Robot, Autonomous Ground Vehicle, Pixhawk, Robot Vision System, HSL format, Image Processing Algorithm, 2D object detection, Image Segmentation.

CHAPTER 1. INTRODUCTION

1.1 Robots in Agriculture

The population of the world is increasing very fast in recent years. To meet nutritional needs for the expansion of the human population by 2050, a projected 100-110% growth in crop production has been estimated. This change is needed a fundamental change in our traditional agriculture system and is dependent on improvements in the efficiency of the current agroecosystem to minimize the continuation of our damages on the global ecosystem [1]. The productivity of the agroecosystem has improved progressively in large owing to mechanization and automation of production systems [1]; however, as mentioned before, global food demand is expected to double from 2005 levels by 2050. The results of this increased demand will push the agricultural industry and policymakers to once again assess their decision-making and focus. Right now the possible options are continuing the current practices and increasing land in agriculture, or moderate intensification coupled with new technologies. With each transition to combine new agricultural practices and technology, some in the agricultural sector choose to implement while others do not. Social and behavioral circumstances, along with a favorable policy environment, impact adoption rates of new technology and practices [2], [3]. Thus, to implement a co-robot system framework, it is imperative to understand the existing social, behavioral, and policy conditions and the possibility of making agricultural practice changes in the future. The concept of Integrated Pest Management (IPM) [4] was developed to reduce the negative impacts of reliance on intensive chemical use. Continuous monitoring of agricultural farms is a critical component of IPM practice. However, monitoring efficiency in large-scale farming is limited, as acknowledged by many producers. Precision agriculture [5] is a key component of the IPM strategy.

Achievements in computational, information and robotic technologies can play a key role in reducing some of the costly agricultural inputs and in increasing yielding and sustainability. Steps for improved productivity and sustainability in the agroecosystem have been taken with IPM. A greater impact can be accomplished when used in conjunction with precision agriculture. However, its affordable and efficient implementation requires autonomous or collaborative robotics technology. This is the area in which this paper proposes to contribute. The research presented in this paper is a vital part of a larger, more complex problem. The broader scope of the project undertaken aims to answer the fundamental question of whether a multi-agent team comprised of humans, aerial and ground robots, and using multi-sensor fusion and learning techniques, could be the best solution for IPM and under what conditions. Right now, lots of research groups are working on the multi-agent robotic systems for various agricultural applications, for instance [98, 99]. A part of this larger problem is the scalable co-robot which will be the autonomous ground vehicle (AGV) discussed in this paper.

Potato Virus Y (PVY) is one of the common problems between various types of potatoes. The PVY can destroy products of the farmers up to 80%, depending on the potato's type [11, 12, 19]. Recent economic data indicates PVY reduces total potato production in Idaho by about 2.3 million hundredweight (cwt) annually. The direct cost of PVY to the Idaho economy is about \$19.5 million and economic modeling indicates the total impact exceeds \$33 million annually [13]. A wide variety of potatoes are affected by the (potato virus Y) PVY virus and are also referred to as PVY carriers. Most of these varieties show mild or no symptoms when contaminated by the virus [6]. Visual identification of the virus is especially difficult in the early stages [7]. There are many research programs and techniques which are currently used to make crops naturally resistant to PVY, but unfortunately, the virus has quickly changed in the last 10 years and keeps damaging farmers' products [20]. When microbiologists try to use new methods for producing crops with

better PVY resistance, mechanical elimination of infected plants is still remaining a full-proof, but because of the size of the fields and the possibility of the existence of viruses anywhere in the field would be an inefficient method to prevent the spread of PVY once it is already present in a field. Therefore, utilizing multi-robot exploration and task planning algorithms based on unknowingly distributed tasks can be useful in this case [8, 9]. Virus detection methods including serological methods (ELISA) or molecular methods (PCR) are destructive, time-consuming, labor-intensive, and therefore very expensive. A non-destructive and fast method to detect viruses is the use of mid-wave infrared remote sensing [10].

In [14] has shown that remote sensing techniques, coupled with machine learning algorithms, can differentiate virus-infected plants from non-infected neighbors based on electromagnetic energy absorbance and reflectance. On detecting the infected plants, the standard procedure is to send a crew into the field to manually uproot the infected plants. Common disadvantages of this method are: a) Late Detection, as workers identify the infected plants visually, which is essentially further into their growing cycle, b) Time consuming: since this process is done manually; in an average field of a few acres to a few hundred acres it takes weeks or longer to complete the removal process. This allows additional time for the aphids to spread the virus, c) Additional cost on production, d) Significant loss of crops. These factors were the major motivating forces in the design and development of an autonomous ground vehicle (AGV) testbed to identify the infected plants early in the crop life cycle. The AGV would be equipped with various sensors and an automatic roguing mechanism to dispose of the affected potatoes by PVY. The roguing mechanism will be selected between various mechanical designs preferably with a minimum number of actuators and smallest size [15, 16, 17] because the size and weight of the roguing mechanism will affect the final size and weight of AGV too. Also, soft robotic actuators [18] can be considered as one of the possible options in this mechanism.

In the prevalent mechanical removal method, first, some professionals identifying the infected plants and then manually removing them. This method consists of two major sections. The first and most important one is correctly detecting the affected plants by PVY, which is very difficult with eyes. An experienced inspector may be accurate but because of the size of the potato fields, checking the whole field by the human is still very slow and because of the limitation of time between the moment we can find out the PVY in plants (they must be mature) and when they are starting to spread out the disease to other, detection PVY by people is useless [21]. Therefore, remote sensing techniques are usually preferred [22]. Remote sensing uses cameras that can sense ranges of the electromagnetic spectrum that human eyes cannot. In hyperspectral remote sensing, the electromagnetic spectrum is dividing into hundreds of narrow “bands” of light, making hyperspectral imaging able to discover infected plants even before symptoms happen [23, 24]. Hyperspectral cameras can be attached to autonomous vehicles or quadcopters to make remote sensing a powerful technique. Remote sensing combined can be combined with both of these systems, a modern-day Unmanned Air Vehicles (UAV) and an Autonomous Ground Vehicles (AGV) to scan, detect, and eliminate the potatoes infected by PVY from the field with minimum human interaction. The communication between these systems and schematic of the whole process from detection to elimination of the infected potatoes is showed in Fig. [1].

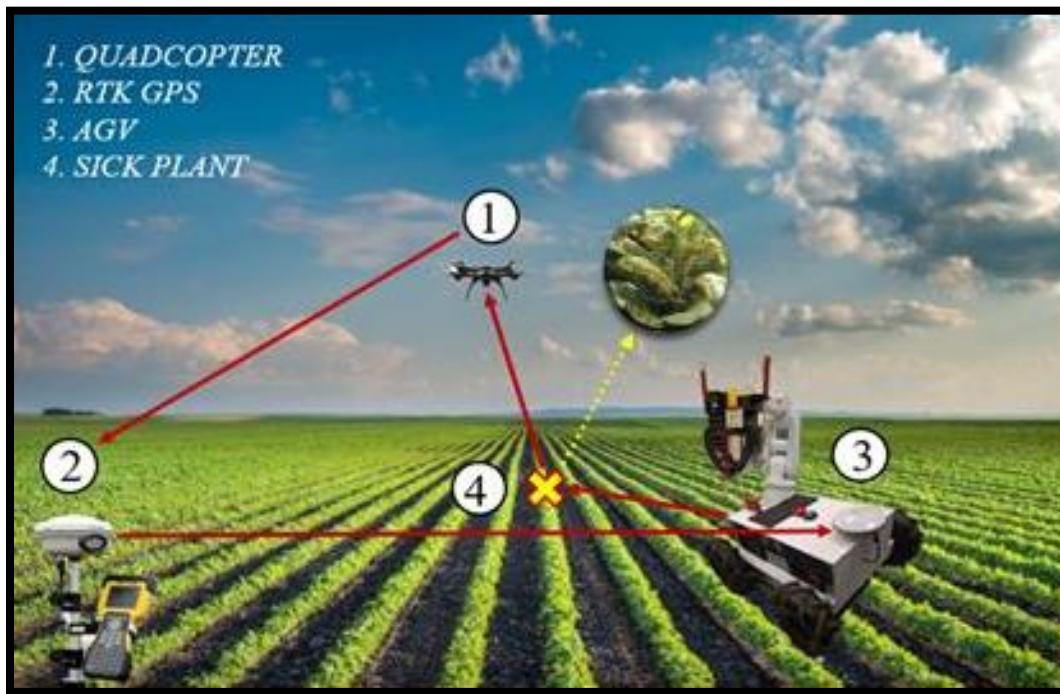


Figure 1: Whole process of communication between UAV and AGV from detection sick plant by UAV to roguing by AGV

In this system, UAV and AGV working with each other. First, a UAV that is equipped with a hyperspectral camera and high accuracy GPS goes over the potato fields and taking images to find the location of the sick plants. Then the GPS coordinates will be sent to AGV, which will lead autonomously to the target location for roguing and removing the infected crops. However, the plant still has to be removed. For removing the infected crops, the AGV would be equipped with a robotic arm and an automatic roguing mechanism. The roguing mechanism will be selected between various possible mechanical designs preferably with minimum actuation and weight [15-17].

The focus of this work is over the designing of AGV and all required attachments for detection and removal of sick plant which will be discussed about each of them in detail.

1.2 Chassis Design

In this project, for designing an AGV, we need a proper chassis for this vehicle as one of the main parts of any vehicle. However, there are some differences between designing a chassis for

a regular vehicle and an agricultural vehicle. These differences mostly related to the maximum weight an agricultural vehicle supposed to carry, shape of the field which this vehicle need to go through, and task that have to be done by it. In this part, some of the advances in chassis design for AGVs and modern agricultural ground vehicles will be explained.

In [101], the process of design of an unmanned ground vehicle for agricultural purposes with an ability of landing a drone on it was explained. In this project, a novel design was used to keep the vehicle chassis horizontal, even on rough terrains or steep slopes.

In [102], for adaptation the vehicle with different based on the farm shapes and crop heights, the chassis is mechanically adjustable. This adjustment is done manually by loosening bolts and adjusting the chassis to the new size. In another research in [103], an advanced agricultural vehicle with focus on maintain a level position of vehicle on uneven terrain was designed and analyzed. In this design, a rapid active method was suggested for levelling the vehicle platform as soon as the slope begins to prevent or reducing vehicle body inclination. This system includes a platform mechanism, a four-wheel vehicle chassis and a control system.

Additional to the novel chassis designs with ability of level adjustment, in the point of view of safety, analyzing various type of stresses that are applying on chassis is very important for designers. In [104], by using finite element method, the stress analysis of a truck chassis structure design with various thicknesses was analyzed. The minimizing the thickness of chassis, will help designers to reduce the price of the final product. Also, for reducing the stress at critical point of the chassis frame in [104], the thickness of side member and cross member and position of cross member from rear end of chassis compare to original design has been changed.

One of the main challenges for designing chassis of agricultural vehicle is the presence of bumps and ruts in the farms which causes more stress over the chassis. In [105], bending and torsion

stress within two cases for a standard dump truck has been studied and analyzed. Stresses analyzed based on the finite element method for the vehicle chassis when only one side of the chassis is passing the bumps, and then when both wheels are getting over the bumps.

With all of these advances in designing novel chassis for agricultural vehicles and research on stress analysis of chassis, still a comprehensive study on various possible stresses over the agricultural vehicle chassis seems necessary. Based on this necessity, in this work, a complete stress analysis is provided for the chassis of an autonomous ground vehicle for agricultural purposes.

1.3 Navigation, Obstacle Avoidance, and Communications

Lots of research groups are working on novel robotic systems for agricultural purposes, whether it be for fertilization, pesticide application, or inspection [28]. Robots can be better than traditional large machinery as they can be more selective where they spray, conserving resources. Additionally, in some cases, it is more cost-efficient to send a robot than a human operator [29].

Recently, GPS as new technology has been a favorite solution for autonomous robot navigation [30]. One of the difficulties in using an autonomous agricultural robot in the fields is related to obstruction of the GPS signals by buildings and trees. Also, cloudy weather can have the same effect on GPS signals.

The GPS network is just one of many in the Global Navigation Satellite System (GNSS). GNSS receivers work by measuring the time needed for a signal to reach the receiver from a satellite. Transmitted signals traversing through the atmosphere may be slowed down or interfered with, and causing an error, especially in cloudy weather.

One proper solution for improving the accuracy of navigation systems is using Real-Time Kinematic (RTK) system with an error of less than 0.1 m (3.93 inches). These systems became very popular in recent years for navigation of agricultural vehicles [106-109]. An RTK system contains

two main units; a base station unit and a rover unit. The base station unit is stationary and the rover unit is mounted on the AGV. The base station transmits position information in real-time to the rover, which helps the rover make corrections to its location, thereby achieving higher accuracy.

While the distance between two potato plants, in the field, is around 0.3 m (12 inches), the average error of commercial GPS is 2-4 m. This will make a problem for accurate navigation of AGV and reaching the target location. Although the bulk of the growing season for potatoes is during the summer months when the weather is generally calm and usually potato fields are far from the buildings and trees, still the accuracy of AGV navigation would be significantly increased by using RTK GPS. Therefore, to improve the accuracy of the navigation system of AGV in this project, a RTK GPS has been utilized.

Additional to a high precision GPS system, an autonomous vehicle need an obstacle avoidance system to not hitting possible objects in the path. Using the LIDAR sensors in autonomous vehicles is a common way for detection objects and avoid hitting them. Autonomous vehicles for agricultural purposes facing various unknown objects that moving with different speeds in the fields which make it more difficult to avoid hitting them.

In [110], advantages of MEMS based 3D LIDAR sensors had been compared to the vision/stereo vision in the domain of agricultural robotics and typical 3D sensors used on mobile robots. Also, an application for such sensors which can be used for the detection and segmentation of plants and ground had been presented. In [111], single multi-beam LIDAR scans had been used for object detection and terrain classification.

In this work, a simple 2D LIDAR sensor is utilized for having some general tests and finding a proper algorithm but for the final version in future, the AGV will be equipped by a 3D LIDAR sensor.

1.4 Image Processing

Diseases always affect on quality and quantity of farmers' products. As it was explained, the main point for protection of the field from spread out the diseases is identifying and destroying the infected plants. For having a more accurate decision about infected plants, we need to acquire information about various signs of each disease [31-34]. When detection of the sick plants seems too hard with just searching the field by sight (especially for large field) computer vision technology helping us by finding the segments of disease spots from leaf images find the infected plants. [31, 32, 35].

On the other hand, with recent improvements in the science of robotics and autonomous systems, image processing playing a more critical role for correct decision making, path planning, obstacle avoidance, and generally act as the vision system for robots. The image processing would be hard in an area like an agricultural field. When dust is one of the problems, dealing with lots of changeable conditions from a point to another point makes it even harder [36].

Most of the image processing technics are focus on the size and color of objects. In most of them, change the color picture of the object to gray or black and white formats and analyzed it. While loses of contrasts, sharpness, shadow, and structure of the color image are some of the characteristics of converting the colored images to gray images, the scientists working on improving on this method [37]. However, in the agricultural fields, based on the weather condition, we are facing a wide range of the amount of sunlight which causes a different level of shadow and changes the lightness of the picture. Also, there is a possibility of lots of unexpected objects on the farm. Plus, the size of the target objects which can be different types of fruits or vegetables is not equal!

Except for working with black and white or gray pictures, another option can work with original color pictures (Red-Green-Blue, RGB) which has its own problem. The problem is we have

to work with three variables which makes it too complicated. Two other alternatives options rather than RGB are converting the picture to HSL (hue, saturation, lightness) and HSV (hue, saturation, value) [38].

In this project because we are working on agricultural fields and as it was discussed the range of the light would be vary based on place and time. Therefore, if we convert the images to HSL format we can consider the whole range of lightness and eliminate one of three components. Also, because we are looking for the location of potato plants, we can just focus on green color and find an exact range of hue and saturation for green color which will be matched by leaves of potatoes.

1.5 Roguing Mechanism

The agriculture products as the major humans' living resources such as food, medicine, energy, fiber always been in the center attention of human. After, the industrial revolution, the agriculture industry took lots of benefit from developing and using mechanical systems in agriculture and related technologies [96]. In the last years of the last century, with advances in the field of robotics [97], farmers started to replace the old form of mechanical system by fully or partial automatic systems in various farming tasks; such as pesticide/herbicide spraying, irrigation and harvesting products. However, the shape, size, growing environment, general health of crops are completely different area which has yet to see significant automation. The complexities associated with different types of crops make it a big challenge for engineers to find an appropriate solution for each individual product.

The field of robotic in agriculture as was discussed is very vast. Because in this research we are focus on roguing the sick potatoes from the field, let's narrow down our search on the research programs just related to the harvesting, grasping, and roguing mechanisms. These research topics

are mostly focused on two major parts: Control and kinematic design. Here, a summary of some of these research outcomes in both areas will be presented.

In [39] an air actuated gripper with a parallel jaw is designed and built for the seedling. In this design, in most cases, there is not any damage happened to the plants. Also, the jaws could only be fully open or fully closed. A reduction in the jaw motion between the open and closed was tested for this design and the amount of required applied force to the soil plug was found to be able to grip the soil plug without damaging the seedling.

A proper end-effector plays an important role in a good performance of a seedling transplanting robot. In [40], two types of grippers, "Swinging Needles" and "Sliding Needles" were designed and compared in three different areas of the robotic transplanting process: seedling picking, holding, and planting. The results show Sliding Needles gripper was much better than the Swinging Needles for seedling transplanting. Then, a seedling sensing was added to the Sliding Needles gripper to make it adaptable to a wide range of seedling sizes and shapes and the final design was "Sliding Needles with Sensor". In process of picking, the gripper becomes close to a seedling from one side. Then, it enters the root system at a slanted angle and swinging the needles to grasp the plug and lift it from the tray.

Some of the advantages of this design:

1. The simple gripper with low-cost actuators.
2. Holding a wide range of seedlings in various sizes of plug trays and growing flats by the gripper.
3. The gripper working on the root of the seedling rather than the stem.

4. The fingers in the gripper can penetrate, grasp, hold, and release with minimum damage to the roots.
5. Using sensors for identifying the presence of a seedling on the gripper [40].

About the amount of applied force for a proper grasp, the Force/Torque (F/T) sensor does not show any reaction in a perfect grasp (Fruit stay in its equilibrium position), thus the grasping forces will be only "internal" forces. In reality, after the grasp, the fruit will be moved from the equilibrium position. Additionally, forces should be distributed and controlled through the grasping process to prevent damages to the fruits [41].

In [42], by using a robotic arm connected to a pneumatic parallel jaw gripper with some special fingers a vegetative propagation was processed for geranium cuttings in a robotic work cell. Fingers are made of aluminum, spring steel, and rubber. For handling the geranium cuttings, a 4-Arc spring steel parallel gripper and aluminum fingers were used. The gripper without damages the main stem handled the cuttings tightly and remove them from the field-of-view of the camera. Two main steps to reach this goal are finding the point for cutting the main stem and finding the position and orientation of the grasp point along the main stem.

A fruit-harvesting robot was designed for harvesting melons in a greenhouse autonomously [43]. In this robot, a gripper grasps the melon and removes it from the vine when its controller adjusts the wrist and grasp motions. A flexible joint connects this gripper to the robot arm to absorb side loads from horizontal motions during the process of picking the fruits.

A multipurpose agricultural robot with four different end-effectors for harvesting, berry thinning, spraying, and bagging was designed to work in the vineyard. This robot contains a manipulator, a visual sensor, a traveling device, and end-effectors which can do several things based on various end-effectors [44].

The harvesting end-effector is grasped and cut rachis and thus able to harvest bunches without any damage. The berry thinning end-effector includes three parts and designed to collect berries in a unified bunch shape. The spraying end-effector with keeping the speed of motion and distance between the nozzle and target constantly sprayed the target evenly. Finally, the bagging end-effector was able to put one by one and nonstop bags on growing bunches [44].

The specific fruit harvester robot was built and tested in a laboratory with an artificial tree to check localization accuracy for the laser rangefinder and dependency of that on external conditions, velocity of the arm, positioning accuracy, and repeatability; and performance of the gripper-cutter. This research contained a deep study for geometric, kinematic, and dynamic to find the most appropriate manipulator structure, and the final outcome of the tests was showing excellent results for accuracy of range-finder and harvesting arm action with some weakness in the performance of gripper-cutter [45].

For grasping general horticulture products and specifically focus on tomato harvesting, an appropriate gripper with two fingers was designed and connected to a robotic arm. This project using pneumatic actuation to control the amount of force required for a suitable grasp and using sketches and drawings to find feasible solutions for on-field problems. There are various possible mechanical designs that depend on the object and required force can be used for two finger gripper such as two rigid fingers with two contacts grasp or articulated fingers with four (or more) contacts grasp with or without an extra contact in the palm. Also, there are two possible mechanical designs with scissors to cut the stalk: scissors connect to the last knuckle of a finger, or scissors connect to the palm [46].

A cluster harvesting end-effector was designed in [47] which is connected to a manipulator, is designed to grasp a stem, cut, and hold it. The upper and lower fingers of this gripper move by electrical actuators. A limit switch was attached to the end-effectors for sensing the main stem,

while two limit switches that acting as pressure sensors were on the lower fingers to recognize a stem.

For improvement in the efficiency of the robot for harvesting tomato, an end-effector was developed in [48] for a tomato cluster that can harvest a whole fruit cluster. The end-effector of fruit cluster harvesting requires multi-directional access to grasp and cut the stem from any direction. Selective compliance assembly robot arm (SCARA) was used for manufacture and test of end-effector which can harvest the entire tomato cluster with 4-6 fruits in a greenhouse.

The theories of contact grasp stability and spatial for an entire system were expanded and analyzed in [49]. Then, from the vision processing approach, the related data for plate and curved finger synthesis to grasp unknown tomato fruits based on tomato images was presented. Plus, stability tests were implemented for grasping tomatoes with two parallel fingers based on using both types of fingers (plate and curved fingers). Finally, based on vision feedback can reach a programmed control for grasp stability of two-fingered tomato by prediction of stable grasp regions.

An end-effector with three various parts, a mechanism for grasping fruit, a size-judging mechanism, and another mechanism for cutting the peduncle was developed when it has required force for grasping the fruit and cutting the tough stem [50].

In [51] an agricultural robot was developed a parallel type handling manipulator for harvesting heavy vegetables such as watermelons, pumpkins, cabbage, lettuce, etc. The manipulator contains three joints: first two joints run by hydraulic actuators when the third joint connects the gripper to a rail and is driven by a DC servo motor. The hand is designed for grasping watermelons has a small DC motor and four one DOF fingers.

For grasping watermelons design a hand with four 1 DOF fingers and a small DC motor. For grasping watermelon, the manipulator will move the gripper right above the targeted watermelon

and the hand goes down and grasp just watermelon when avoiding leaves and vines. This hand has a passive joint in the wrist with a passive force closure under gravity and friction [52].

In [53], the guidelines for designing power assist robots to lift heavy stuff in industries were analyzed. An assist robot system was developed with just 1-DOF when dynamics and control of it were in the perception of the human weight. The robot system was designed to carry objects with various sizes and three different lifting orders in normal working conditions – unimanual, bimanual, and cooperative lift. To improve the system performances, an innovative control was applied to decrease extreme load forces in both usual and worst-cases (unusual working conditions).

A robotic design for grasping the orange, with controlling the pressure over orange grasp it and the arm move away. By using located force sensor on the wrist of the robot, the control system can find the location of the stalk and cut it with a circular micro-saw [54].

In the new robotic system, three actuators were used rather than two actuators, for controlling the jaw and clippers, and one for a sliding tray placed at the bottom of the pincers and slides out before the stalk is cut. The expansion of the lower jaw and the existence of this tray, lets the orange remain trapped inside. When the orange reaches the unloading area, the tray will come back in and the orange drops automatically, and the grasping device returns the jaw to the resting position to be ready for picking another one [54].

A mechanism was designed in [55] for harvesting the radicchio. Because the radicchio needs accurate stem cutting, a double four-bar linkage manipulator and a special two-finger gripper were suggested for harvesting and cut a plant approximately 10 mm underground. While the gripper works with flexible pneumatic muscles and both manipulator and end-effector are pneumatically actuated.

In [56], a robotic arm was designed for grasping the asparagus and cut its stem. This robot arm has two fingers and a cutting knife which are attached to the tip on this arm. In the robotic arm, a cylindrical cam mechanism with two cylindrical bodies, an inner cylinder (with three straight grooves) and an outer cylinder (three spiral grooves), and one arm shaft was used to increase the speed of expanding function of the robotic arm in a compact body. A DC motor will rotate the outer cylinder when the inner cylinder is fixed to the main body. Therefore, three bearing shafts going forward or backward with the rotation of the outer cylinder when the arm shaft is fixed. And there are 5 steps for this robotic arm: 1) Rotate the arm 2) translate the arm to target 3) grasp the target asparagus 4) cut the stem 5) carry the asparagus to the box.

The gardening robots are movable manipulators with the camera placed in the end-effector which gives them the ability to locate plants in the garden, water plants, and locate and grasp fruit. To perform an appropriate grasp, a closed-loop control algorithm [57], will be used to line up the gripper and fruit when the force sensor will help to detect failed grasping attempts may not very useful in the case of the gripper grasps any other part of the plant!

In [58] a vision-guided grasping system was developed and tested for *Phalaenopsis* tissue culture plantlets (PTCPs). Because the leaf of *Phalaenopsis* is very fragile and is easily damaged by the gripper the plantlet is usually grasped at the root or the stem. The appropriate grasping point on the roots was found using an image-processing algorithm. Also, for finding the 3D coordinates of the grasping location, a binocular stereovision algorithm was applied.

The Robot Gesture Library (RoGuE) is a motion-planning method to create gestures and four robots are connected to RoGuE: 1) Barrett hands with three-finger and 7-degrees of freedom, 2) ADA (Assistive Dexterous Arm) is a 6-degree of freedom hand with an actuated gripper and two fingers. 3) Curi is an omnidirectional humanoid mobile robot hand with two 7-degree of freedom

arms 4) PR2 is a bi-manual mobile robot with two 7degree of freedom arms and each gripper has only two fingers [59].

In [60], there is a 7 DOF robotic system in which a serial link manipulator with 6 DOF is mounted on a prismatic base, and the whole of that is connected to an end-effector for grasping apple. The selected end-effector for picking apple contains three identical tendon-driven fingers plus two links for each of them and three actuators.

Soft robots have become more and more popular in robotic systems nowadays. One of the areas for using these robots is for agriculture purposes. Soft end-effectors and grippers are playing important role in grasping and handling soft fruit and vegetables, for instance for lettuce harvesting or suction mechanisms for picking apples. The amount of applied force for each task is important too. Basically, more focus to control base on the force rather than position. In other words, for grasping and manipulation applications in Agri-Food, both high accuracy and unexpected strength are required. For making something more like a human, some elastic structures with variable stiffness actuators can be used [61].

In this project, the main task for AGV is removing all parts of the sick plant completely out of the field. Although there are lots of advances in designing robotic mechanisms for agricultural purposes still there is not many mechanisms that specifically designed for grasping and pull out or digging out all parts of the sick plants out of the soil. Therefore, in this work, all possible options for extraction of sick potato plants are analyzed and finally a novel mechanism will be designed for complete extraction of the sick potato plants while it can be used for other plants with similar shape and size too.

1.6 Singularity Analysis

In general singularity in robots is define as a condition caused by the collinear alignment of two or more robot axes resulting in unpredictable robot motion and velocities [100]. Singularity configuration of a robot is one of the serious challenges for designers and is one of the problem in designing various mechanisms and ones for agriculture are not an exception. Therefore, in the last part of this research, we trying to define a general solution for singularities in mechanisms and that would be supported by singularity analysis in a multi finger hand as an example.

A wristed, multi-fingered hand includes a single serial chain spanning several serial chains, with a kinematic tree topology. Kinematic analysis of tree topologies for applications in modular robots and robotic hands can be found in [62-64].

The design of multi-fingered hands has been studied from the point of view of selecting the right number of fingers and the mobility and connectivity of each finger for grasping and manipulation in [65-68]. In [69], algorithms were created to combine properties of mobility and force closure for the type synthesis of general hands.

The creation of the robotic hand once the hand topology has been selected follows two more steps. First, the joints need to be placed so that the hand can reach the desired task, which is a dimensional synthesis problem. Kinematic dimensional synthesis of tree topologies presents particular challenges that have been explored in [70-72]. Dealing with a coordinated action of all the fingertips leads to a simultaneous task for all end-effectors, in which case relative motion among them has to be considered too.

Obtaining the type and number of joints and the location of the joint axes has to be followed by a process in which the designer needs to decide where to physically implement the joints along the axes. This process does not change the kinematic task but has a great influence on hand

dynamics, force transmission, self-intersection, and overall hand size and inertia. Some of these parameters can be designed with an optimization process such as the one in [73] and automatically implemented [74].

A final step of detailed design is needed to design transmissions, actuator placement, and coupling systems if the hand is going to be underactuated. At this level, the design is usually done for the single finger, such as the designs of individual, underactuated fingers in [75, 76] or finger configurations [77]. For the design in detail, most of the current efforts deal with what we can denote as planar fingers, that is, fingers for which all the joint axes are parallel, and also in some cases with perpendicular axes. To have functional hands with arbitrarily oriented axes, different types of transmissions and coupling methods need to be explored.

The characterization of singularities for closed loop or parallel mechanisms has been widely studied. Single-loop linkages were the first ones to be studied and are the focus of this work. Among many works, we highlight [78], where the mobility problem for four-bar linkages was studied by finding the global extrema of a quadratic function on a cylinder and solving it as the geometric problem of the intersections between a circle and a hyperbola. Later, [79] described three possible types of singularities based on Jacobian matrices for the loop equations. More recently, [80] shows that the singularities of the configuration space and degeneracy of the kinematics of a chain are not always related to each other. Focusing on the RSSR linkage, [81] analyzed the first type of singularity. Works involving design include [82], where the general reason for losing rank and find ill-condition in synthesis was analyzed and solved with an optimization procedure. In [83], Grashof conditions were discussed for closed-loop RSSR mechanisms, and the use of a geometrical approximation to find conditions that make crank-rocker mechanisms. Most of the works found focus on avoiding singularities or creating singularity-free trajectories such as [84], with an algorithm based on a Probabilistic Road Map that can generate trajectories avoiding singularities.

In this work, a single chain of RRSS mechanism explained as the supporting example for the methodology. Unlike the approaches in [15], which the intention was to use SS chains to couple RR fingers for the design of wristed, multi-fingered robotic hands, in this work, the focus is on designing the mechanism for specific singular configurations at desired positions. This approach can be useful to make sure the designed mechanism will stop at specific locations, or have motion between two specific points, corresponding to the two singular points. At the end, the derived equations are explained, and examples are included to test the method.

1.7 Research Goals

This dissertation aims to address the design and implementation of an AGV and EOAT for in-situ virus detection and removal. This project includes the following objectives:

1. Design and implementation of an optimized prototype chassis for AGV

Potato fields are fraught with rough terrain and deep irrigation ruts. Navigation of such terrain is very challenging and demanding on the robot chassis. For reaching the ideal size and material for this chassis, an optimization method is required. Also, based on the shape of potato fields, different stress analyses have to be conducted to help narrow down the chassis design and material for the prototype.

2. Design and implementation of an autonomous navigation system using an RTK GPS

In this project a high-precision GPS is required for navigating the AGV to the infected potatoes with PVY and remove them from the field completely. This autonomous robot is in-line with emerging technologies in the field of precision agriculture. The navigation system in this project is based on a Pixhawk microcontroller for ease of use and affordability. Also, to reach the maximum accuracy an RTK GPS module from Swift Navigation with a maximum 10 cm error has

been used. After installation of all components to the AGV, both electrical and mechanical, they are protected with a cover from water, hit, and sunlight.

3. Design and implementation of an obstacle avoidance system using a LIDAR sensor

To avoid hitting any object or person in the field, this AGV has to be equipped by an obstacle avoidance system. For finding the most appropriate obstacle avoidance system and algorithm, some information about general condition of a potato field, possible obstacles, and speed of each of them required. Finally, after selecting the proper system, it has to be tested to make sure about its performance in a real condition.

4. Design and implementation of an image processing software

The next part is related to the implementation of a vision system and image processing for this autonomous vehicle. When the AGV reaches to target location, the infected plant has to dig out and spoiled by an automatic roguing mechanism that is attached to vehicle. As it was mentioned the RTK GPS has around 10cm error and we know the average distance between potatoes plants would be around 30cm but in reality, this distance varies in the field case by case. Therefore, for finding the exact location which has to be clean out, this roguing mechanism has to be equipped with a special robot vision and image processing system to detect the center of the sick plant. This system includes two 8 Mega Pixel Pi cameras to find the center of the target plant in vertical and horizontal directions. Also, because this system is working in the potato field with various ranges of sunlight during the day and on different weather conditions, for having better image processing in various brightness, the HSL format of images has been utilized for better color detection.

5. Design and implementation of EOAT for roguing the sick plant from the fields

The ultimate goal in this project is the elimination of sick plants from the field but this aim is not reachable unless having a proper design for roguing mechanism. For having an efficient end of arm tooling (EOAT), a wide range of research is required about potato field condition, soil

property, strength in connectivity between various parts of the plant such as roots, stem, and tubers. Also, all possible mechanisms have to be checked and some alternative options selected for the final design.

6. Singularity analysis of mechanisms and manipulators

Singularity of mechanisms is one the major factors of design and very challenging topic for designer specifically when we are working with autonomous systems. In this project, the roguing mechanism would be attached to AGV by an appropriate mechanism (robotic arm). Therefore, as a part of this project, a novel singularity analysis for robotic mechanisms (general case) has been presented and the idea is developed by an example of a spatial mechanism (RRSS). One of the advantages of this method is ability of using it for either to avoid singularity for a specific range of robot motion or defined specified singular positions for robot based on designer requirements.

CHAPTER 2. CHASSIS DESIGN FOR AN AUTONOMOUS GROUND VEHICLE (AGV)

The chassis is the base frame for any vehicle that other major parts of vehicle like the wheels and motor(s) will be attached to it. So, one of the first step in designing a vehicle would be design a proper chassis based on total weight of vehicle and the duty which vehicle is designed for it (a chassis for a sport car would be different from a truck). Base of designing an autonomous vehicle is not big different from regular vehicle. Therefore, in the first part of this project (designing AGV), we will start with presenting the process and results for designing the chassis for this vehicle.

2.1 Potato Field Specifications and Motion Study for AGV

2.1.1 Potato Field

The first step before designing the chassis and performing stress analysis is collecting all possible information about the environment in which this vehicle will be operated. This would give a better idea of the types of stresses the vehicle will be subjected to, and the type of analysis that needs to be done. In this research, lots of information about a potato field condition was collected from consulting with experts, local potato growers, visiting a potato field, and making accurate measurements. The most important information which is required for design a proper chassis is related to shape of the field, irrigation routine and soil condition.

The potato field are full of rough terrain and deep irrigation ruts which during potato growing season are most of the time muddy and wet. Most popular methods of irrigation for potatoes are sprinklers, center pivot, wheel line, and solid set systems. Potatoes prefer a well-

drained, light, deep, loose soil and finding rocks in a potato field are very rare. Fig. 2 shows a potato field before and after harvesting.



Figure 2: Potato field before and after harvesting ^[27]

2.1.2 Potato Field Simulation Information

Based on the information about the shape of a potato field and size ruts and bumps which was measured in the field visit, we created a simulated environment, which is shown in Fig. 3. This information was used to design the AGV chassis. As shown in Fig. 3, the height of each bump was 30 cm and the distance between the two bumps was 60 cm.

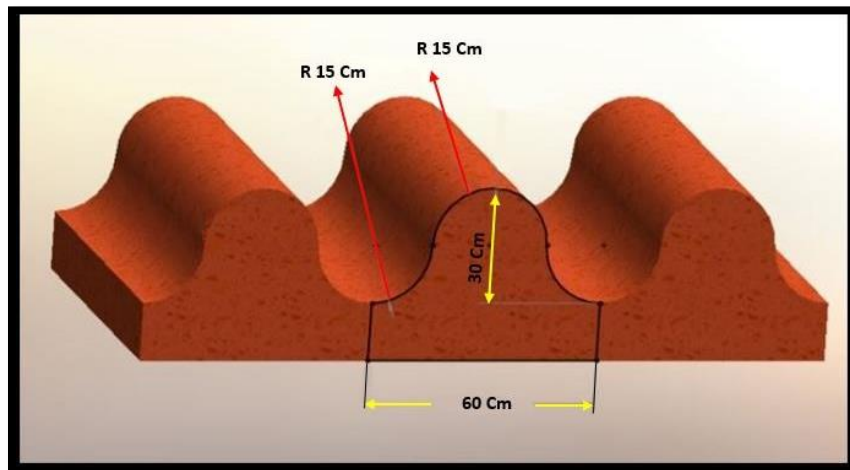


Figure 3: Simulated shape and size of the terrain

2.1.3 Possible Stresses for a Four-Wheel Vehicle

In this stage of research, we need simple initial platform for AGV to carry and test the sensors and navigation system. The final AGV probably partially or completely will have different design based on the size and attached equipment. To make this design simple as much as possible, we didn't use any gear box, suspension system, and steering system. For having more power, avoiding vehicle to stuck on the muddy land, and removing the steering system, an all-wheel drive vehicle with four electrical motors was designed for this prototype. In this system with change the speed of the wheels vehicle will be able to spin around itself. This vehicle is using two 12V & 8 Ah batteries and is able to work between 2-3 hours with each time charging the batteries. Other information about required power calculation and finding most appropriate motors for this AGV has been done in [25] by Moeller et al. From the calculations in [25], the maximum possible incline which this AGV can move on would be 43.5° and because potato farms must be navigated by irrigation equipment and tractors, this high of a slope is rare.

The focus of this section is designing chassis for this vehicle as one of the main parts of this AGV. Although final chassis design may have some differences from this one but most of the stress analysis process because of similarity in the field condition and design constraint would be same.

In general, there are four main types of deformation for an automotive chassis [85].

1. Longitudinal Torsion:

If the force is applied in two opposite directions (up-down) on two opposite corners of the vehicle, a torsion load will affect the chassis. This load would cause a twist on the frame of the chassis (Fig. 4).

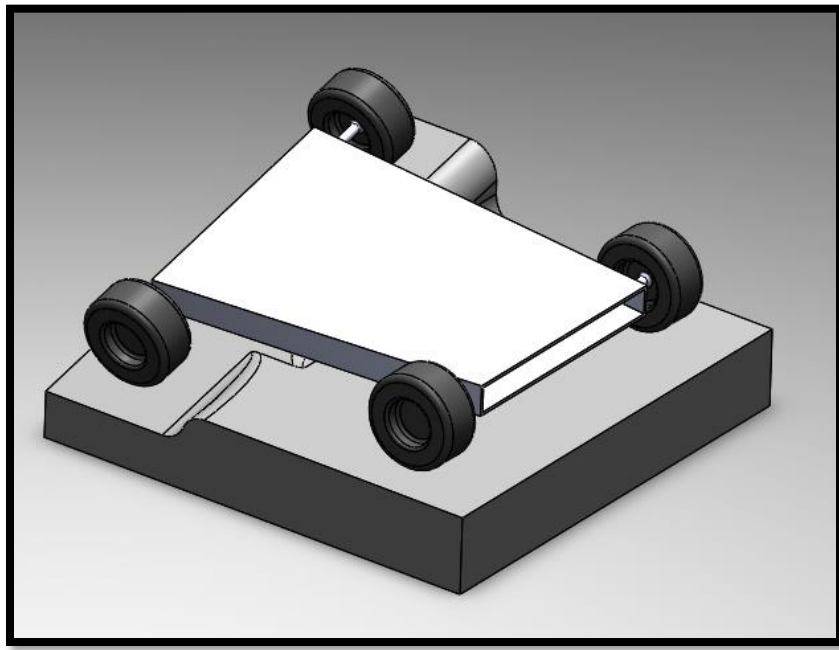


Figure 4: Longitudinal Torsion

2. *Vertical Bending:*

This force is made by the weight of all the various components of the vehicle like chassis, battery, motors, etc. plus all external loads like any moving parts on the vehicle for example a robotic arm. The reaction force would be acting on the axles in the upward direction (Fig. 5).

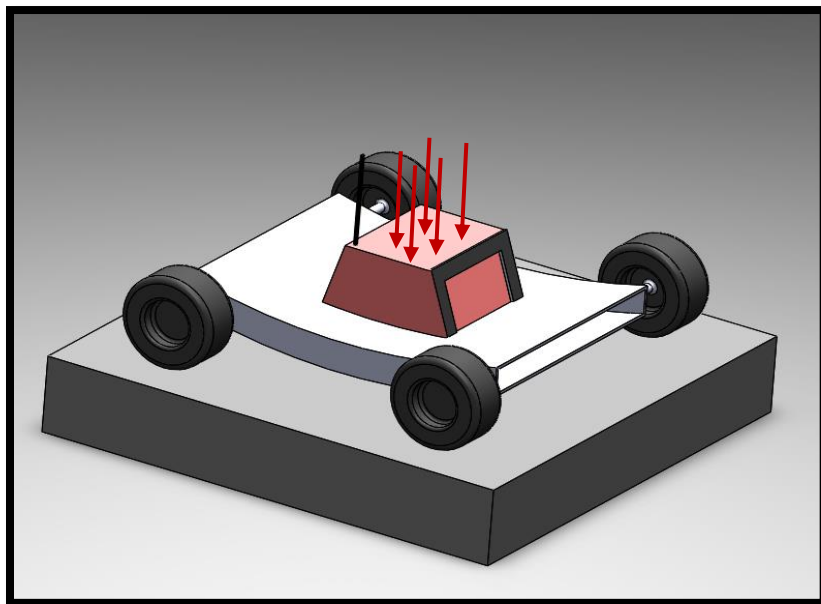


Figure 5: Vertical Bending

3. Lateral Bending:

In this case, a lateral load causes a bending on the chassis because of sideways load along the length of the body of the vehicle. For instance, the force from the wind, road camber, or centrifugal forces (Fig. 6).

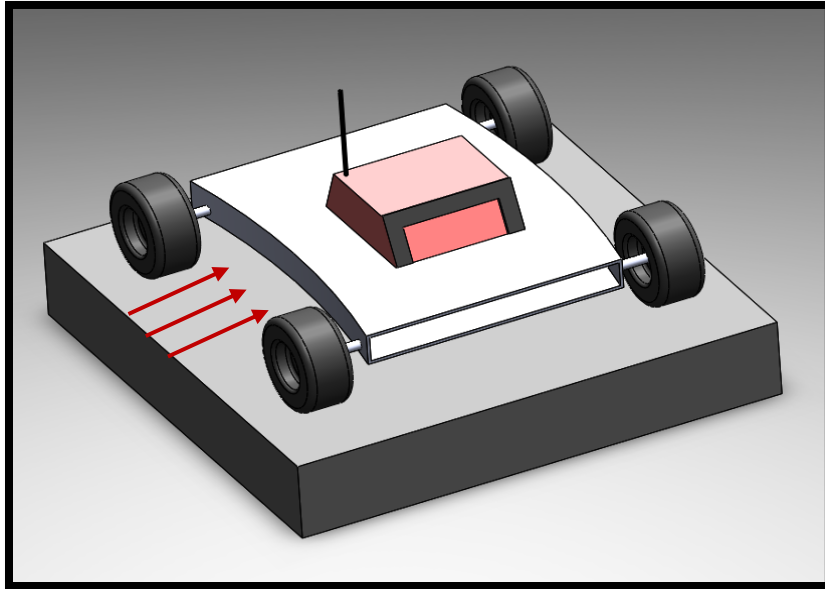


Figure 6: Lateral Bending

4. Horizontal Lozengeing:

This type of deformation happens when loads on two opposite sides of the vehicle are applied in opposite directions (forward-backward forces). These forces are made by the difference in the height of the roadway or the reaction force from the road over the vehicle going forward (Fig. 7).

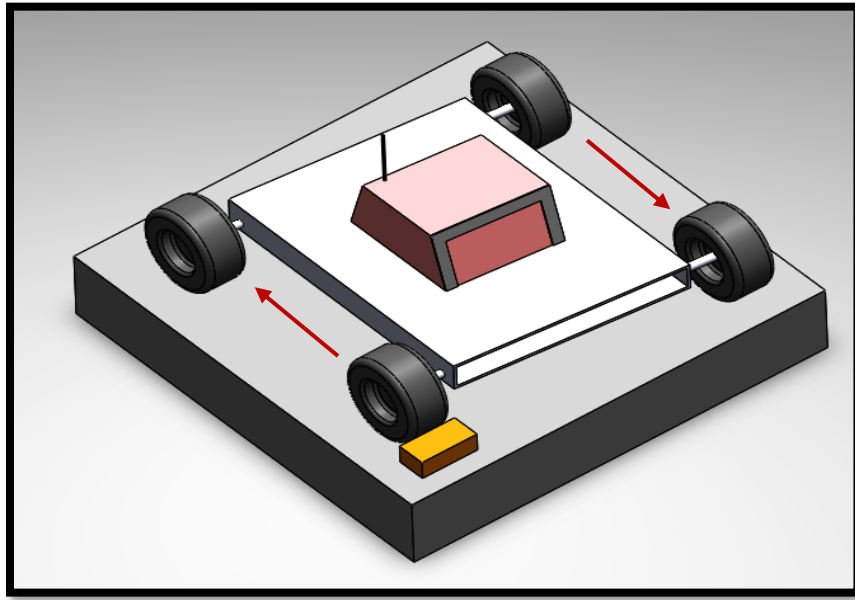


Figure 7: Horizontal Lozenging

However, according to the shape of the potato field and different possible paths which this vehicle is supposed to drive Fig. 8, the maximum force affecting the chassis is the vertical load made by its weight. So, among all the deformations mentioned above, the focus of this research is on the vertical bending and torsion stresses caused by the weight of the vehicle.

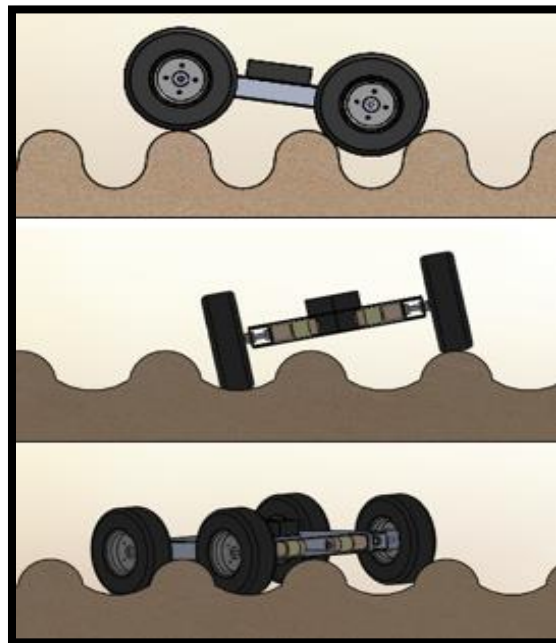


Figure 8: Simulated Terrains Encountered in Field

2.2 Parts of the AGV and Specification

2.2.1 Parts of AGV

As shown in Table. 1 and Fig. 9, this vehicle contains 10 components. Each wheel is independently actuated with individual electric motors to maximize power and for better control of the vehicle. The chassis of this vehicle is made of three main pieces, bottom plate, top plate, and two motor mount tubes. Motor mount tubes are welded to the bottom plate, and the top of the tubes are bolted to the top plate. Based on the tasks and ruggedness of the field, four 25Cm (10-inch) pneumatic wheels with aggressive treads were selected for this vehicle. The quantity and weight of each of the components are provided in Table. 1.

Table 1: Name, Quantity, and Weight of Each Part

#	Part	QTY	Wt kg-(lb)
1	Wheel	4	14.97-(33)
2	Shaft	4	0.454-(1)
3	Top Plate	1	1.36-(3)
4	Bottom Plate	1	1.36-(3)
5	Battery	2	2.27-(5)
6	Motor	4	0.91-(2)
7	Motor Mount Tube	2	1.36-(3)
8	Motor Mount Plate	4	0.454-(1)
9	Clamp Collars	8	0.23-(0.5)
10	Steel Ball Bearing Flanged	4	0.23-(0.5)

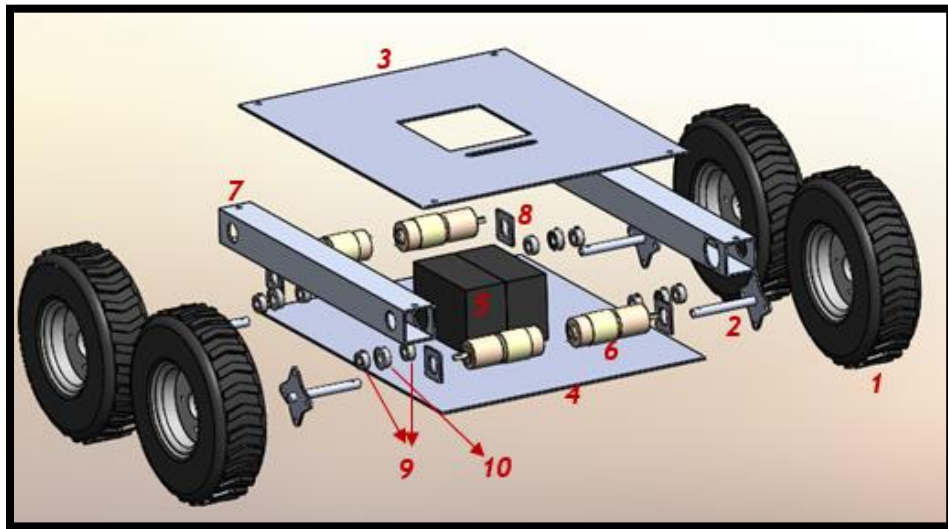


Figure 9: AGV components

2.2.2 Material Selection & Size of the Chassis

Except for the chassis which was designed, analyzed, and built for this project, the other components were selected and ordered from different vendors to satisfy the overall design requirements. To find the appropriate material for the chassis, between Aluminum Alloy 6061, Steel ASTM A36, and Steel AISI 4130, Aluminum alloy 6061 was selected because of higher stiffness and lower weight. Relevant material properties are presented in Table. 2. The size of the bottom and top plates are $53.3\text{cm} \times 43.2\text{cm} \times 0.3175\text{cm}$ ($21\text{in} \times 17\text{in} \times 0.125\text{in}$) and the Motor Mount tube has a thickness of 0.3175cm (0.125in).

Table 2: Specification of Aluminum Alloy 6061

Properties	Value
Yield Strength	55.15 MPa
Tensile Strength	124 MPa
Elastic Modulus	69000 MPa
Poisson's Ratio	0.33
Mass Density	2700 kg/m ³
Shear Modulus	26000 MPa

2.3 Chassis Optimization and Stress Analysis

We selected a rectangular modular shape for the AGV chassis to accommodate all the components and to allow for future modifications. On mounting all the components, the maximum possible load was applied to the chassis. In this section, material selection for the chassis and the best overall size and weight are discussed. These were calculated based on an optimization algorithm. Thereafter, force analysis of the chassis will be discussed. Finally, seven stress analysis tests are provided to ascertain that this vehicle will not fail in its intended operating environment.

2.3.1 Optimization

The Genetic Algorithm was utilized to optimize the overall shape, minimize the weight without compromising the structural integrity of the AGV. The overall weight of the vehicle, and the terrain to be navigated, and the onboard instrumentation are the critical factors that dictate the required power from actuators and the capacity of batteries that could be used. We do not have control over the weight of the onboard instrumentation or the battery pack. Therefore, we targeted the weight of the chassis. This was the objective function considered for optimization. Additionally, there were several equality and non-equality constraints on this optimization. For instance, the minimum thickness for available metal plates at the local hardware store is 0.003m, or the maximum stress over the chassis (multiplied by a factor of safety) must be less than the yield strength of the specified material, which was considered in constraints. The maximum stress over the chassis will be calculated from Equation 1.

$$\sigma_{bend-max} = \frac{M \times c}{I} \quad (1)$$

M = the internal bending moment

c = the perpendicular distance from the neutral axis to the farthest point on the section

I = the moment of inertia of the section area about the neutral axis

This optimization was repeated for three different materials and the minimum total weight of chassis for each of them was found. Symbols for different parts of the chassis were shown in Fig. 10. The size of each of the components after optimization is provided in Table. 3. Based on constraints which were used in this optimization (for instance minimum thickness equal 3mm), the optimum size is similar and equal to minimum possible size for all three materials (as was expected). Aluminum Alloy 6061 has minimum weight as compared to others. So, it was selected for the chassis. Because of the availability and size of the other parts of the vehicle, some of the dimensions for the chassis in the final design were a little different from this table (but very close to the calculated value).

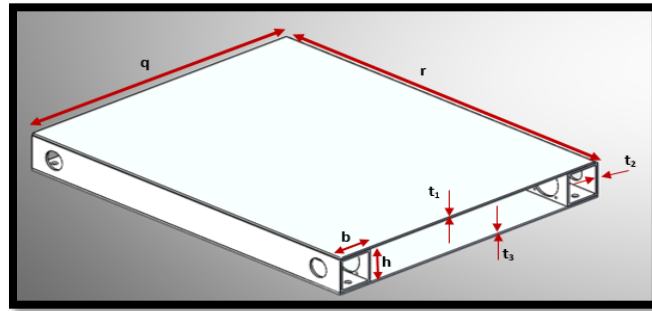


Figure 10: Chassis

Table 3: Optimization Results for Three Different Materials for Chassis

Material	Aluminum Alloy 6061	Steel ASTM A36	Steel AISI 4130
t1 (m)	0.003	0.003	0.003
t2 (m)	0.003	0.003	0.003
t3 (m)	0.003	0.003	0.003
b (m)	0.05	0.05	0.05
h (m)	0.05	0.05	0.05
q (m)	0.4	0.4	0.4
r (m)	0.5	0.5	0.5
W (kg)	4.7628	13.8474	13.8474

2.3.2 Force

As it mentioned before, potato fields are made of loose soil and finding rocks in a potato field are uncommon so hitting a hard object in a potato field would be very rare, also if that is happened, with having damping of the wheels and based on the speed of vehicle, which is low, the forces created by small impacts while traveling can negligible. Based on that the main force over this AGV comes from its own weight. The total weight of the vehicle including all components is 23.5868 kg (52 lbs). This weight makes a total force of 231.386 N which causes a vertical load of 57.847 N over each wheel of this vehicle. However, for all stress analysis tests in this research, a factor of safety (F.S.) of 4 was chosen. Therefore, after importing the F.S. on the calculation, the final force over each wheel will be 231.386 N.

2.3.3 Stress Analysis

Seven different stress analyses have been described in this section. For all stress analysis, a solid mesh with a size of 0.0051m (0.2in) and a maximum aspect ratio of 13.933 was used.

Test 1: Bending Stress #1

This bending stress analysis is for a scenario when three wheels of the vehicle are at a lower level than the fourth one (Fig. 11). In this case, three connection links for the wheels will be assumed fixed (triangles in Fig. 11) and a vertical load will be concentrated on the fourth wheel (upward arrow).

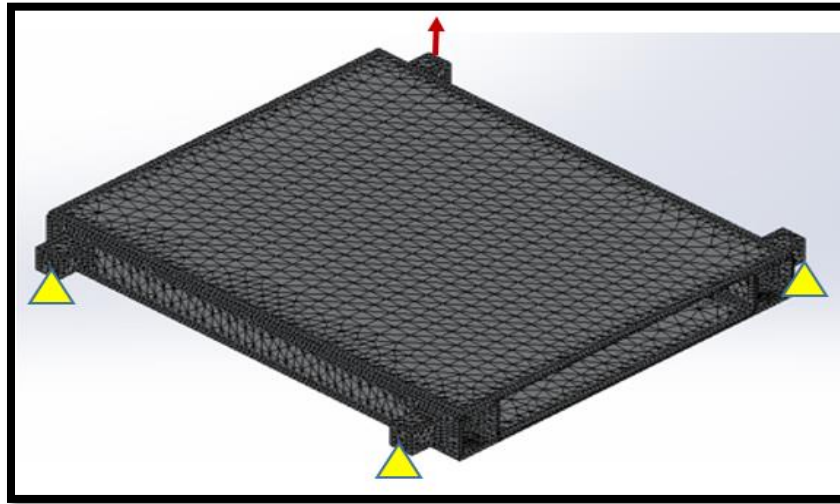


Figure 11: Reaction forces in test 1

Test 2: Bending Stress #2

In this case, the two wheels on the left are at a lower level than the wheels on the right. Therefore, the weight of the vehicle causes bending stress on the chassis. In Fig. 12, two connection links for left wheels are assumed fixed (triangles in Fig. 12) and load distributed between connections links of right wheels are in the same direction (both reaction forces are in the upward direction denoted by the arrows pointing up).

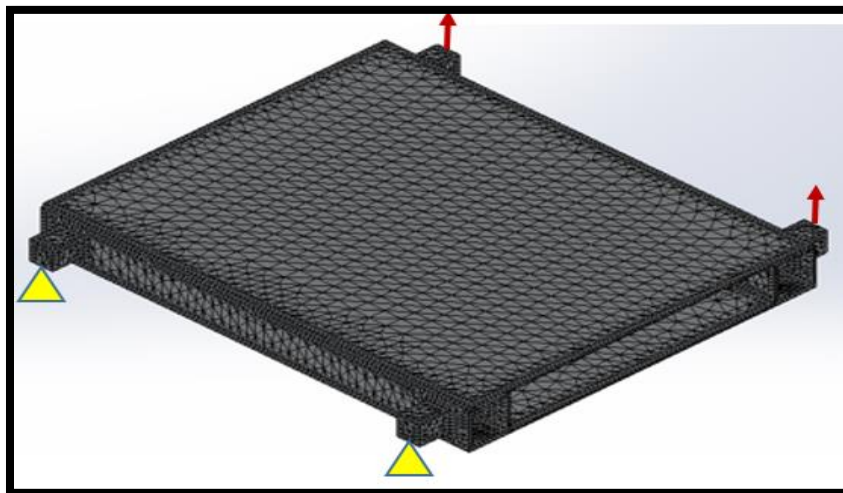


Figure 12: Reaction forces in test 2

Test 3: Bending Stress #3

In this case, two wheels in front of the vehicle are at a lower level than the wheels on the rear of the AGV. So, it would be similar to the second test and the weight of the vehicle causes bending stress on the chassis but this time two connection links for the front wheels are fixed and loaded in the same direction (both reactions forces upward direction) distributed between connection links of rear wheels (Fig. 13)

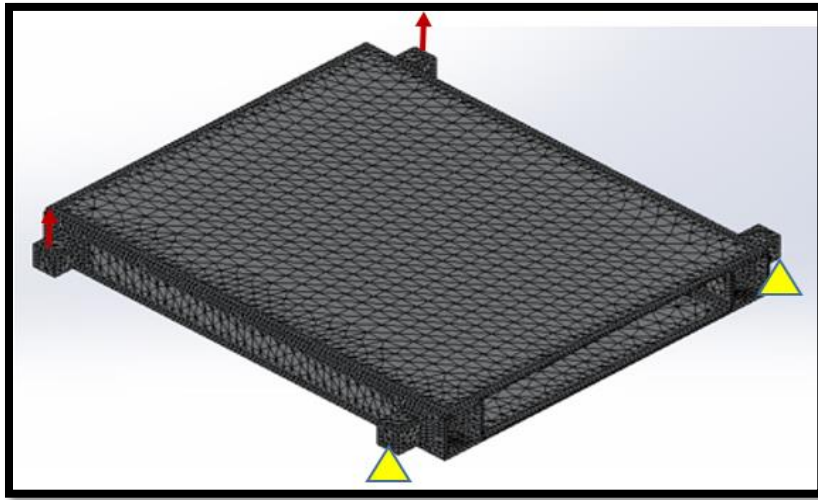


Figure 13: Reaction forces in test 3

Test 4: Bending Stress #4

This analysis loads the chassis when two diagonally opposite wheels are at a higher elevation than the other two wheels. Fig. 14 shows this situation when two connection links of two diagonally opposite wheels are fixed and two others are affected by the upward load which makes a bending on the chassis.

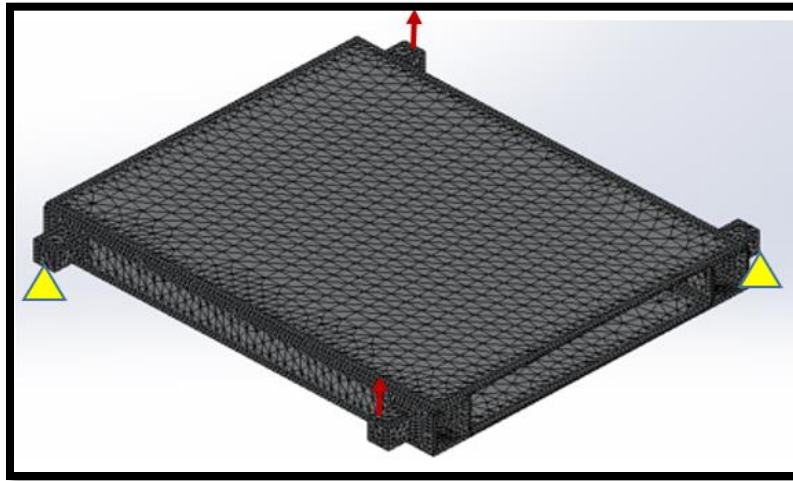


Figure 14: Reaction forces in test 4

Test 5: Torsion Stress #1

This test is similar to the second test with the only change in the way the load is affecting the connection links for the right wheels. As it is shown in Fig. 15, one of the loads is going up when the other one is going down which causes torsional stress rather than bending over the chassis.

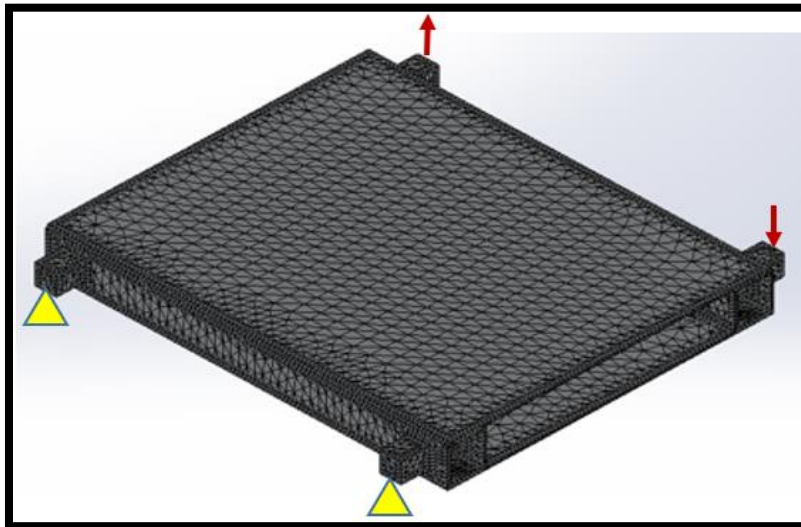


Figure 15: Reaction forces in test 5

Test 6: Torsion Stress #2

This test is similar to the third test, but the load is acting opposite to each other. One of the loads on the back is going up when the other one is pointing down which causes a twist on the chassis and makes torsional stress rather than bending over the chassis (Fig. 16).

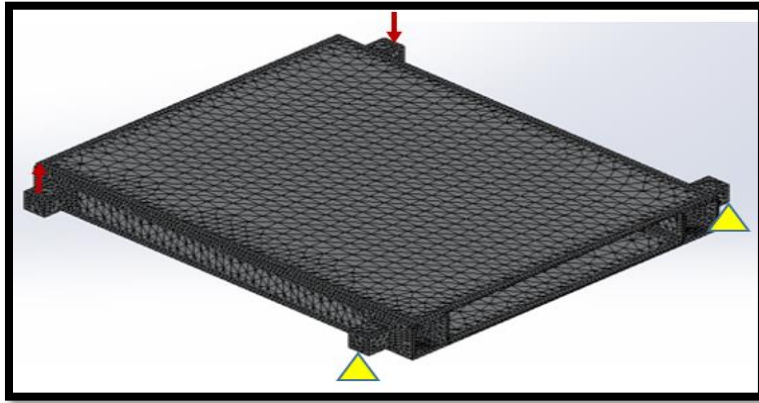


Figure 16: Reaction forces in test 6

Test 7: Torsion Stress #3

The last test is torsional too. Fixed links and the position of the load are the same as the fourth test with only a difference in the direction of load. From Fig. 17, one of the loads is going up when the other one is going down which causes torsional stress.

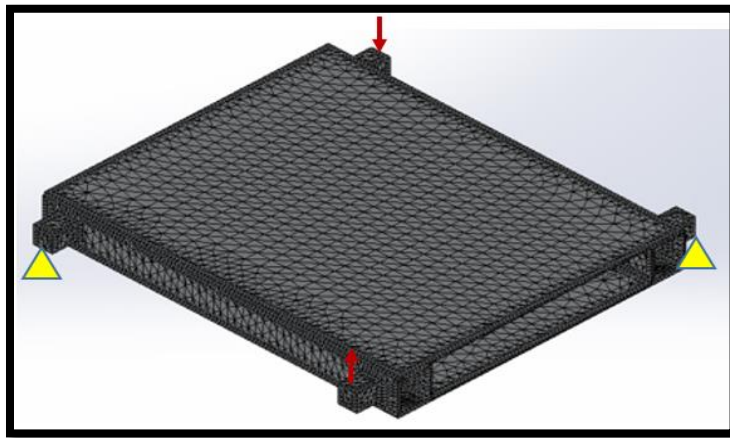


Figure 17: Reaction forces in test 7

The final results for all seven stress analyses are presented in Table. 4. The maximum stress and displacement occurred in test 2 when two wheels in the left and two wheels in the right are not at the same level, and this caused bending stress over the chassis. However, maximum strain occurred in the third test when the front and back wheels were not at the same level. This also made bending stress on the chassis. Difference between max displacement and max strain is related to the shape of this chassis. In this chassis, there is one tube along in each side of the chassis. In test #2, the force applies to the right side of chassis, so, tubes are not affected by this force and there will be around 2 times more displacement compare to test #3 (Table 4). On the other hand, in test #3 the force applies to the front of chassis. Because part of this force applies on tubes, in this case, chassis can show more strength against the force. Also, from Table 3, the length (0.5m) and width (0.4m) of this chassis are different which cases more strain when force apply to the front of it (test #3). Thus, in test #3, there will be more strain and deformation in material with a less displacement compare to test #2.

Table 4: Final Results for Stress, Displacement, and Strain of All 7 Tests

Test	Stress (N/m²)	Strain	Displacement (m)
1	2.826e+7	2.469e-4	2.170e-4
2	5.065e+7	4.136e-4	6.013 e-3
3	4.514e+7	4.783e-4	3.707e-4
4	2.181e+7	1.972e-4	1.619e-4
5	2.185e+7	1.596e-4	3.369e-4
6	2.185e+7	2.263e-4	1.579e-4
7	3.703e+7	3.933e-4	3.653e-4

Displacement and stress for test 2, respectively are showed in Fig. 18 & Fig. 19. Also, strain for test 3 is presented in Fig. 20.

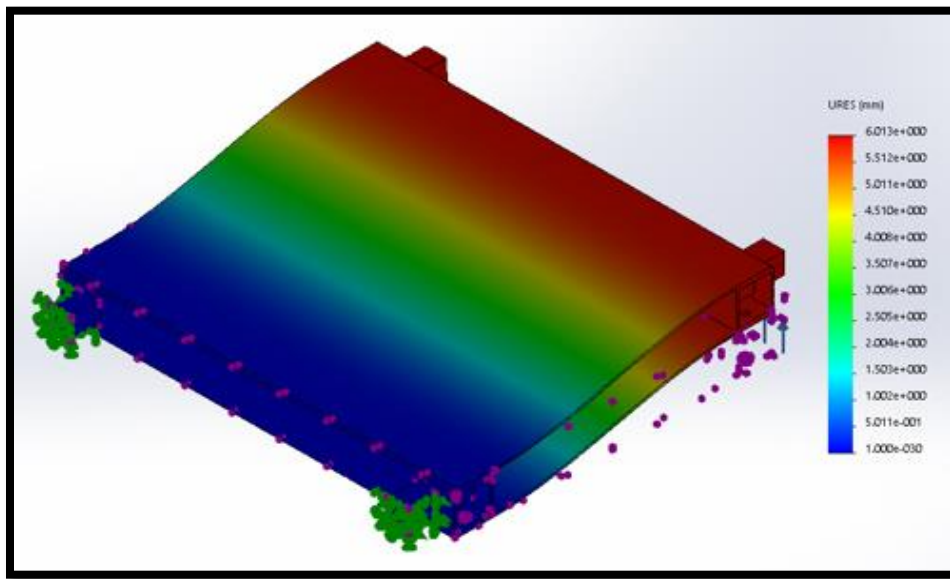


Figure 18: Displacement in test 2

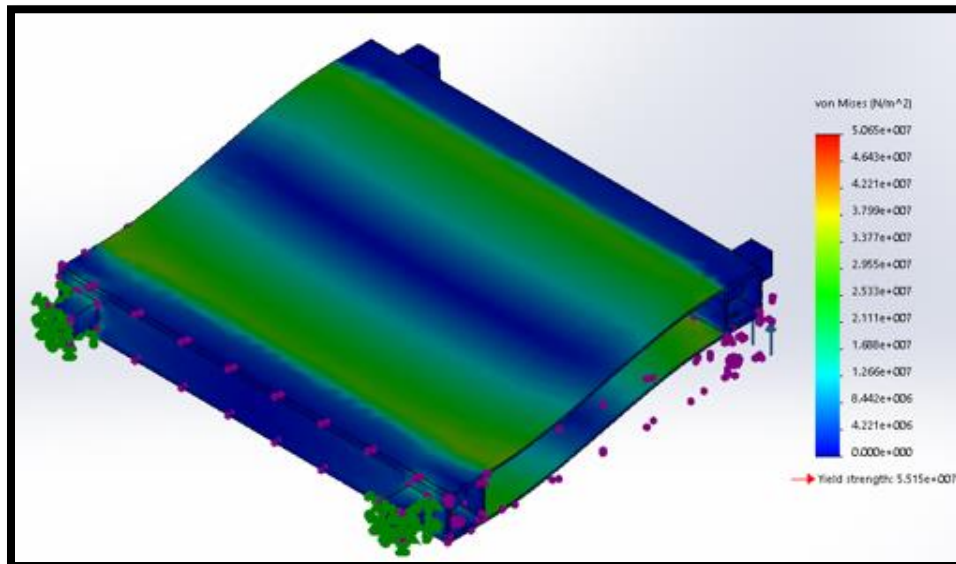


Figure 19: Stress in test 2

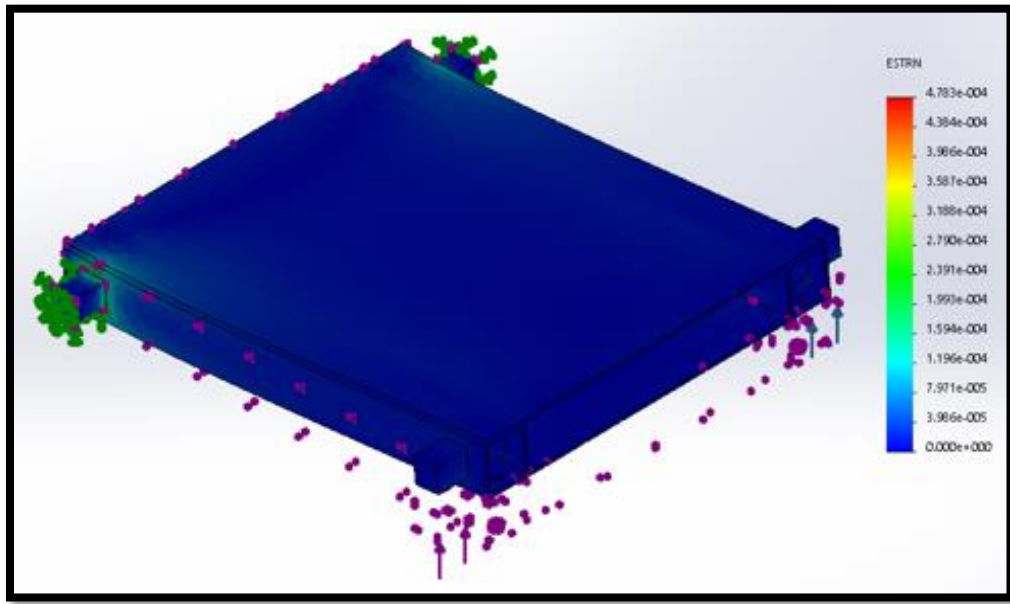


Figure 20: Strain in test 3

2.4 Chassis Final Design

The stresses on the chassis in comparison to the maximum stress ($5.065 \times 10^7 \text{ N/m}^2$) and yield strength of aluminum alloy 6061 ($5.515 \times 10^7 \text{ N/m}^2$), show that the designed chassis wouldn't fail for any simulated condition in the field. This chassis has been built and has been tested in the field and has performed as per expectations. There is sufficient space on top of the chassis for all electronic equipment like a GPS, micro-controller and in the future a robotic arm platform. Fig. 21 shows the actual built-to-specification prototype.

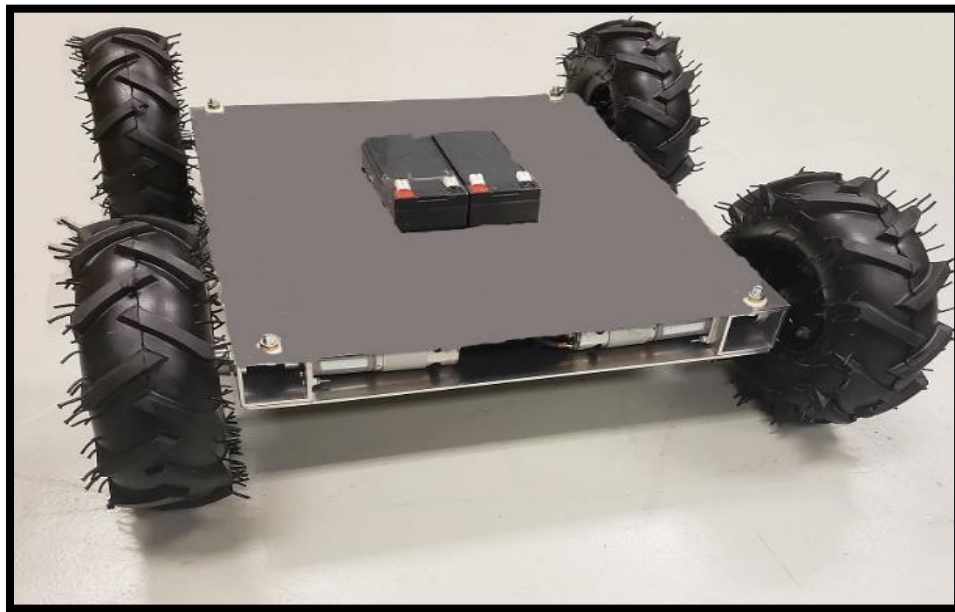


Figure 21: Autonomous ground vehicle (AGV)

*** Further Information: Deemyad, et al. “Chassis Design and Analysis of an Autonomous Ground Vehicle (AGV) using Genetic Algorithm”. In 2020 Intermountain Engineering, Technology and Computing (IETC) (pp. 1-6), IEEE.**

CHAPTER 3. NAVIGATION & OBSTACLE AVOIDANCE

This part of the work which is related to navigation and obstacle avoidance system has been a team effort. So, in this section, I am going to present a general idea of these systems and then I will cover the parts that were my responsibility. for more details about electrical parts, more information can be found in Moeller's thesis [114].

3.1 Navigation

The GPS network is just one of many in the Global Navigation Satellite System (GNSS). GNSS receivers work by measuring the time needed for a signal to reach the receiver from a satellite. Transferred signals traversing through the atmosphere may be slowed down or interfered with, causing an error. The average error of commercially implemented GPS is 2-4 m (Fig. 22). The distance between two potato plants, in the field, is around 0.3 m (12 inches). This limited resolution would fall well short of the resolution required in the field. Therefore, to improve the accuracy of the navigation system for this AGV, a Real-Time Kinematic (RTK) system with an error of less than 0.1 m (3.93 inches) was utilized. An RTK system contains two main units: a base station unit and a rover unit. The base station unit is stationary, and the rover unit is mounted on the AGV. The base station transmits position information in real-time to the rover, which helps the rover make corrections to its location, thereby achieving higher accuracy (Fig. 23).

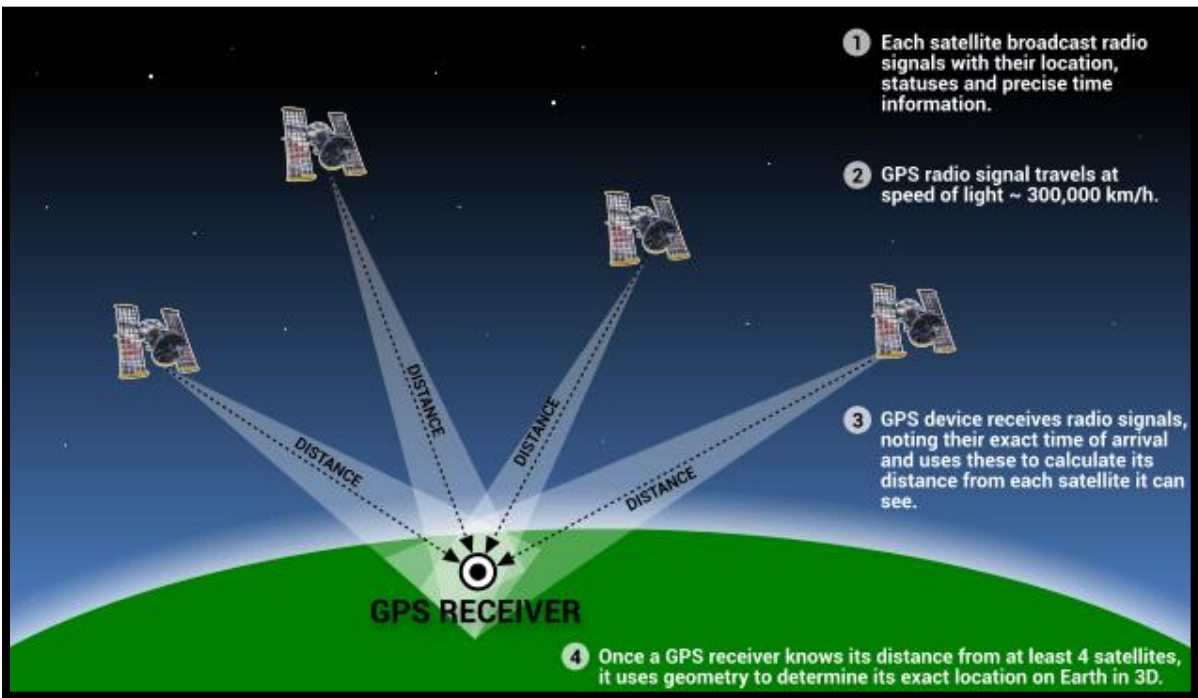


Figure 22: Commercial implemented GPS ^[112]

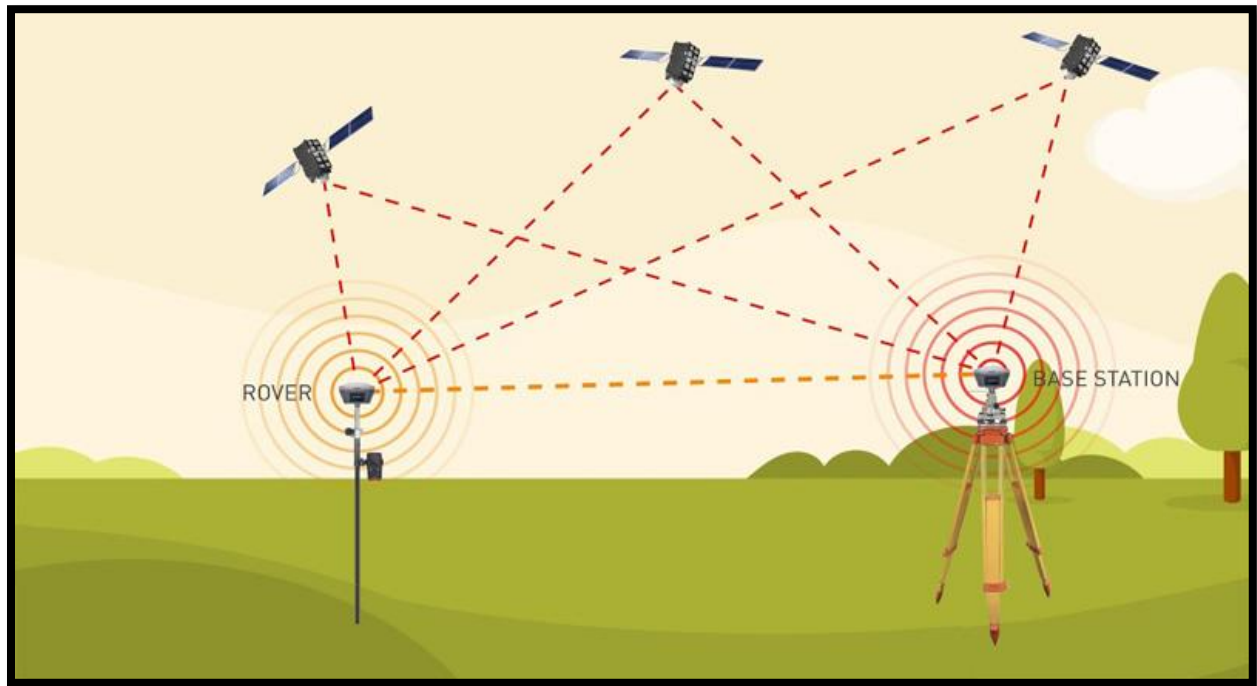


Figure 23: RTK system ^[113]

In this robot, an RTK GPS was combined with magnetometers to provide the robot with its position and heading. A Pixhawk was used for the microprocessor, which calculates the error

between the current position/heading and the desired position/heading and then adjusts wheel speed to correct itself. The Piksi Multi Evaluation Kit from Swift Navigation was chosen for the RTK GPS. The Piksi Multi has a powerful Xilinx Zynq 7020 with dual-core ARM Cortex processors and a 666 MHz clock speed. This allows it to perform RTK calculations quickly, obtaining an RTK fix in seconds. It is also relatively inexpensive as compared to other RTK GPS solutions. The base station and rover units each contain four major parts as shown in Table 5 & Fig. 24.

Table 5: Piksi Multi Evaluation Kit Main Parts

Item #	Name	Quantity
1	Evaluation board	2
2	Lithium-ion battery	2
3	Free Wave radio modem	2
4	Survey grade GNSS antenna	2

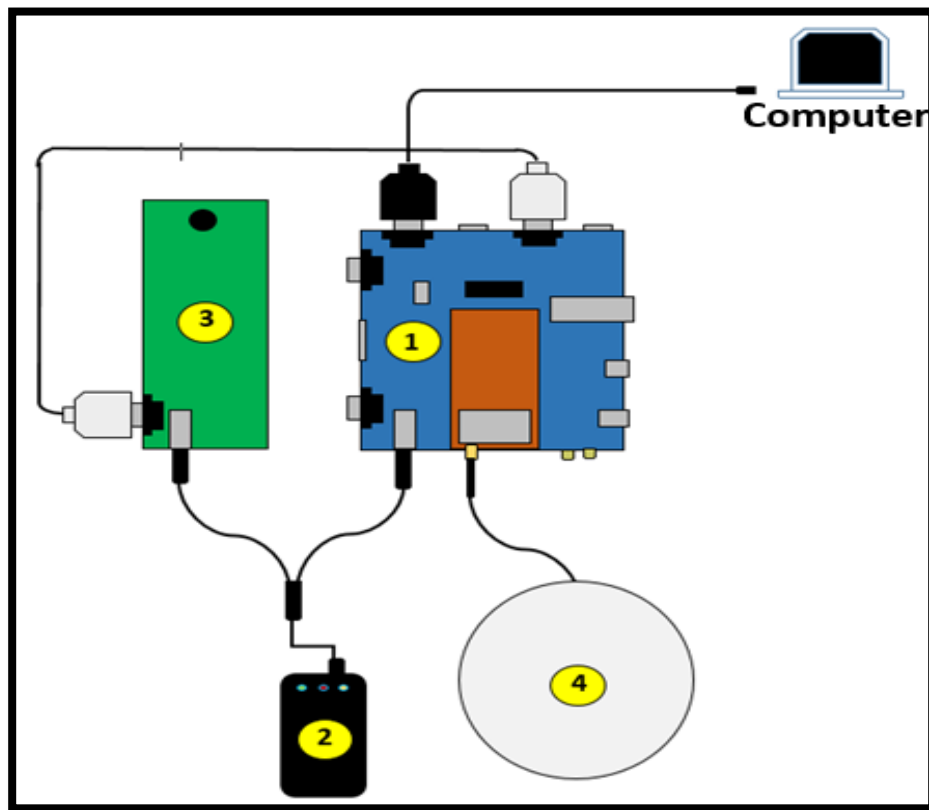


Figure 24: Piksi Multi Evaluation Kit Main Parts – Both the base station and rover contain these four parts

Table 6 has a comparison of similar systems and their most recent prices.

Table 6: Comparison of RTK GPS Systems

Name	Cost
Piksi Multi Evaluation Kit	\$ 2,295.00
Trimble R8s	\$ 10,200.00
Spectra Precision SP80	\$ 12,495.00
Geomax Zenith35 Pro	\$ 9,995.00

3.1.1 Evaluation of Components

Before using the actual AGV, the components were tested using the radios that Swift Navigation provided. To set up the Pixsi Multi in RTK mode, the base station and rover radios have to program to communicate with each other. Then, all components in Table 5 are wired to each other as shown in Fig. 24. The survey-grade GNSS antenna and Free Wave radio modem are connected to the evaluation board. The radio modem and evaluation board are powered by a lithium-ion battery. Finally, the evaluation board is connected with a USB cable to a computer. Swift Navigation provides free software called Swift Console to configure and interface with the Pixsi Multi. 900 MHz or 2.4 GHz radios can be used during the evaluation of the GNSS receivers.

3.1.2 Integration with Pixhawk

In this project, the Swift Navigation radios were only used for evaluation and we utilized Pixhawk telemetry radios on AGV. Therefore, RTK corrections could be sent over the same radio link that the mission planner shared with the Pixhawk, and the mission planner had to retrieve the corrections from the Swift Console.

As shown in Fig. 25, the AGV starts its tasks from the Home location (H). The waypoints are chosen by the user in Mission Planner and sent to the Pixhawk via telemetry radios. When auto mode is turned on, the Pixhawk begins navigating from its current position to the next waypoint in a straight line. Between every two waypoints, we can define some other tasks for AGV for instance taking a picture by camera or using a gripper. Finally, the AGV will be navigated to the Home location by Mission Planner.

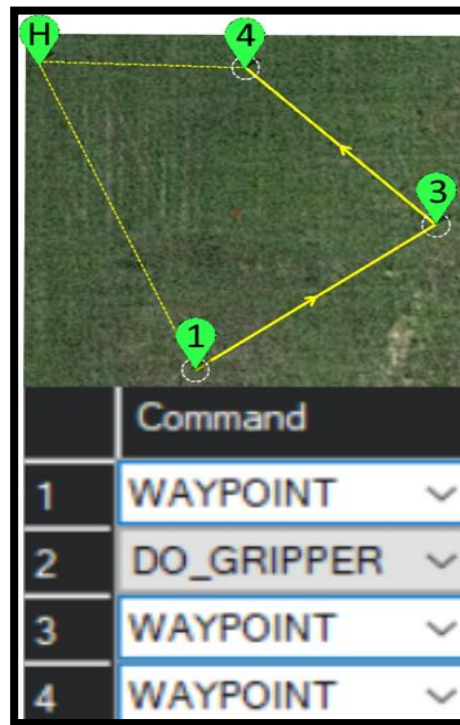


Figure 25: Screenshots of the mission planner's navigation planning feature

Because this AGV is supposed to work in an open area (potato field), to protect all electrical components from sun, rain, and mud, we need to cover whole sensitive parts with a waterproof frame. This frame was painted to become resistant to direct sun rays. The prototype of AGV which includes all attachments and electrical components is shown in Fig. 26.



Figure 26: Assembled and painted enclosure, placed on top of robot chassis

3.2 Obstacle Avoidance

One of the important things in design an autonomous system is avoiding hitting unexpected objects (obstacles) in the path from the start point to the destination. These obstacles can be stationary or moving at different speeds. Based on the work environment and speed of the autonomous system, we will need a different type of sensors to avoid any accident. In a potato field, we are facing with few types of obstacles and most of them are stationary or moving very slowly such as rocks, the center pivot irrigation equipment, tractors, humans, and animals (which very rare but possible). For these types of obstacles, a simple range-finding LIDAR will suffice but for more security, the AGV would be drive slow in the field and making a loud sound for giving awareness to humans and animals.

The firmware onboard the Pixhawk can work with a LiDAR sensor to avoid hitting any obstacle in the way. Fig. 27 shows the parameters that configure the obstacle avoidance protocol known as “dodge” avoidance. In this method when the LIDAR detects an object that is too close which is defined by `RNGFND_TRIGGER_CM`, it stops, turns for a specific degree, and drives straight for a certain time, and then drive back to a direct path to the next waypoint.

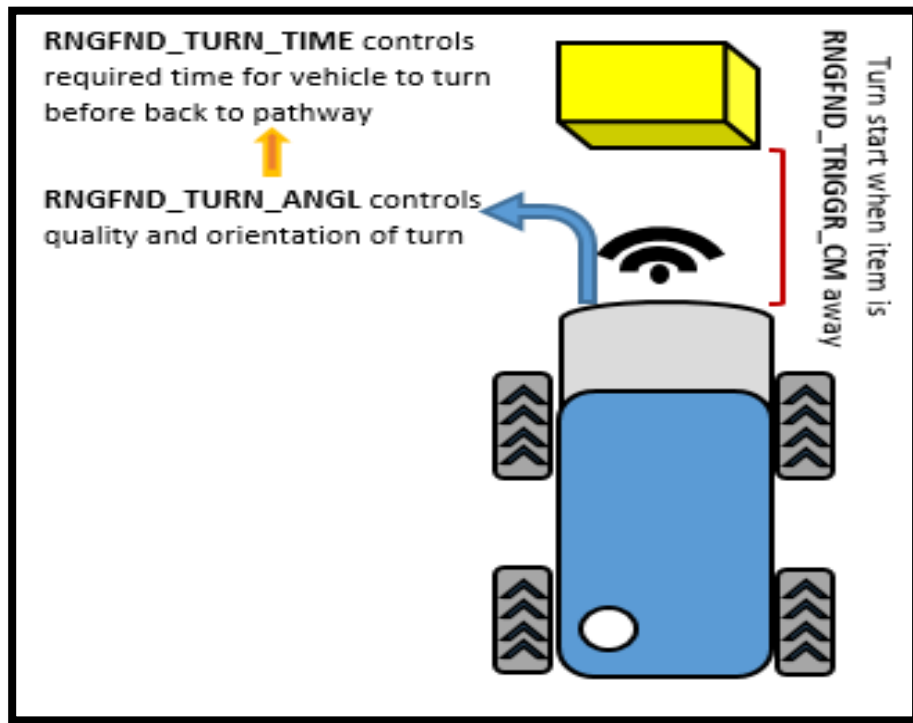


Figure 27: A graphic explaining the parameters involved in setting up “dodge” obstacle avoidance on the Pixhawk using a range-finding LIDAR

3.3 Results for Navigation & Obstacle Avoidance Tests

3.3.1 Piksi Multi Accuracy

Based on the test results the claimed accuracy for RTK GPS (less than or equal to 10 centimeters) was correct. Using National Geodetic Marker sites, we were able to verify that the Piksi Multi is accurate to 5.6 centimeters.

Finding a location with a pre-specified GPS coordinate that is accurate enough to verify the coordinates found by the Piksi was very challenging. A couple of methods were considered. The easiest but most expensive is to survey a spot on the ground. This requires special equipment and training but can be done practically anywhere outside. The more difficult method is to find a geodetic marker, a previously surveyed position marked with a permanent landmark. The online

National Geodetic Survey Data Explorer gives access to all such publicly recorded markers. However, many are located on privately held land and are difficult to access.

The marker used was at the Pocatello Regional Airport (Fig. 28). Using the evaluation boards from Swift Navigation, the base station Piksi was placed on one geodetic marker and the rover Piksi on another several hundred meters away. 50 GPS fixes were collected and converted into the UTM 12N projected coordinate system (for ease of calculation). Pythagorean's theorem was used to find the difference between the rover's estimated GPS location and the coordinates listed on the geodetic marker's datasheet. The average error was 5.6 centimeters. Because of difficulties related to the testing location, only this test was done. Airport security was required, and the airport could only accommodate us for a short time. The results for this test are shown in Table 7.



Figure 28: A geodetic marker in the Pocatello Airport

Table 7: Results from Piksi Multi Accuracy Testing

Test #	Accuracy (cm)	Base Station Test Location		Geodetic Permanent Identifier (PID)
1	5.6	42° 54' 47.03909" N	112° 35' 23.36463" W	AB8163

3.3.2 Autonomous Navigation via Waypoints and Obstacle Avoidance

The performance of the autonomous navigation was satisfactory. In the tests, the AGV had problems finding its heading and would spin around until finding it again. However, this would not be a big deal, and probably will be solved by using higher quality magnetometers or more careful calibration. We didn't check the accuracy of navigation again during autonomous navigation since accuracy had already been confirmed.

The WASP LIDAR was also tested. In this test, the SiK telemetry radios were bypassed with a USB cable. In this setup, the distance between the LIDAR and an obstacle placed in front of the AGV was within a few centimeters of the reported value in Mission Planner. However, obstacle avoidance was not tested with the telemetry connection.

*** Further Information: R. Moeller, T. Deemyad and A. Sebastian, "Autonomous Navigation of an Agricultural Robot Using RTK GPS and Pixhawk." In 2020 Intermountain Engineering, Technology and Computing (IETC) (pp. 1-6), IEEE.**

CHAPTER 4. IMAGE PROCESSING

In this chapter, the robot vision system and method used for image processing in this project are described. Based on the previous sections in this project, the GPS coordinate for the sick plants were sent to the AGV and it is autonomously navigated to the area around the target location for roguing the sick plant from the farm. However, the problem in this stage is about finding the center point of the sick plant. That is very important for us to extract the sick plant completely from the ground, without contacting nearby plants and transferring the infection to them. But even the most accurate GPS (like RTK GPS which we are used in this project with just 10cm error) still has some error. Therefore, for solving this problem, after AGV reaches the intended location for finding the exact location of the target plant, we will use two cameras and an image processing algorithm to find the center of the sick plant.

4.1 Project Overview and Conditions of the Target Environment

Before working on a specific image processing algorithm, we needed to collect more details of the environment (potato field) and specifications related to the target object (potato plant). To get preliminary environment information we visited a local potato field and based on our observations, collected three major sets of data. First of all, this system is supposed to work in an open area where weather conditions are unpredictable. One of the most important and commonly occurring ones is changes in the amount of sunlight during a day. These could be due to any number of reasons; for example – clouds in the sky shadows in the field, etc. This would have a direct impact on the type of image processing algorithm that could be used. The second point that needed consideration, related to the color variations of the target object due to the lighting changes and other possible dynamic elements in the surroundings. In this project, this system must detect a sick

potato plant with high accuracy for removal. A potato plant, based on age, soil conditions, and weather can have a large range of shades of the color green. On the other hand, some of the other common colors in the potato fields which have to be filtered are soil color, other reflected light/shadows from irrigation equipment, rocks, water on the field, etc. One other factor to bear in mind is the shape of the potato field, distance between plants, and size of the plants at the time of roguing. Based on our observations and measurements from the field visits, a simulated model of a potato field was made in SolidWorks which was used in future calculations and image processing algorithm development. This simulated model is shown in Fig. 29. As shown, a potato field is fraught with rough terrain and deep irrigation ruts. The distance between the top points of the two bumps is around 60cm. The plants are grown on the top/crests of the bumps and the average distance between two plants is around 30cm. The cross sign in Fig. 29, shows the target sick plant between eight healthy adjacent plants in the potato field.

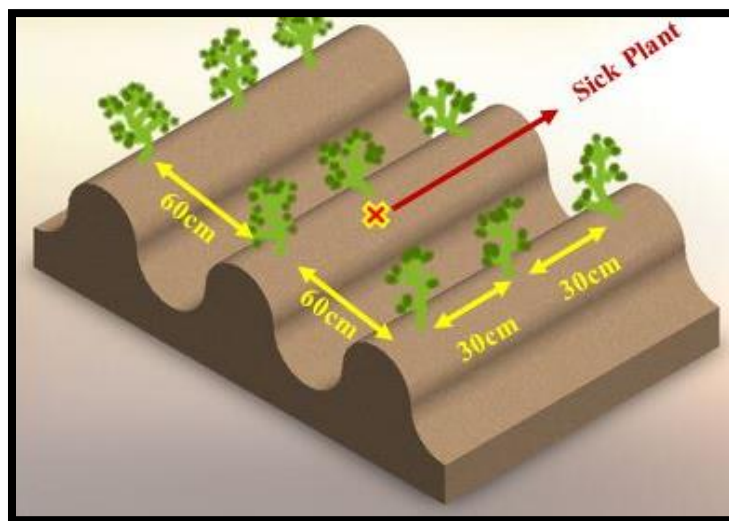


Figure 29: Simulated potato field and an average distance between plants in the field

Usually, PVY can be detected in potato plants, in the very first stages when they are young. This is the best time to detect and get the infected plants out of the field before they transfer the diseases to other plants from the connection between their leaves. However, this time usually very short each year. For having more tests and checking our codes, we planted some potatoes indoor to

accelerate and increase the number of tests. We used the same pattern and shape of the field for planting a single row of potatoes. (Fig. 30).



Figure 30: Planted potatoes indoors with a similar pattern in the field

4.2 Equipment and Appropriate Color Space

4.2.1 HSL Color Space

In this project, segmentation by color is preferred to other methods of segmentation such as edge detection or depth map. Edge detection would not be a good option because concern of this project is finding the center of the target plant, not separation the objects in the images. Also, working with depth map would be hard because it is required 3D imaging and if we want to use 2D images and depth map, user must define different layers for the image while this system supposed to work autonomously in the potato field. For segmentation by color, we are facing a large range of colors (all green domain). Therefore, using a gray or black & white scale would not be a good option for all of this range. On the other hand, working with color spaces is usually very complex. Plus, this system has to utilize in outdoor with a wide range of brightness. Between all color space models, the HSL can be the best option. In this model, H, S, L are Hue, Saturation, and Lightness respectively. A wide range of Lightness (almost whole range) can be selected and play with two remaining components to find the most appropriate map for the target color range.

The images are taken by cameras are in RGB (Red-Green-Blue) format which has to be converted to HSL format. For this conversion, we will use the following sets of equations from [93]:

$$\begin{aligned}
 R' &= R/255 \\
 G' &= G/255 \\
 B' &= B/255 \\
 C_{max} &= \max(R', G', B') \\
 C_{min} &= \min(R', G', B') \\
 \Delta &= C_{max} - C_{min}
 \end{aligned} \tag{2}$$

Hue:

$$H = \begin{cases} 0^\circ & \Delta = 0 \\ 60^\circ \times \left(\frac{G' - B'}{\Delta} \bmod 6 \right) & C_{max} = R' \\ 60^\circ \times \left(\frac{B' - R'}{\Delta} + 2 \right) & C_{max} = G' \\ 60^\circ \times \left(\frac{R' - G'}{\Delta} + 4 \right) & C_{max} = B' \end{cases} \tag{3}$$

Lightness:

$$L = (C_{max} + C_{min})/2 \tag{4}$$

Saturation:

$$S = \begin{cases} 0 & \Delta = 0 \\ \frac{\Delta}{1 - |2L - 1|} & \Delta \neq 0 \end{cases} \tag{5}$$

Where H, S, and L can get any values between 0-1. We will set up an appropriate range for each of them based on the color range we need to be detected which will be explained in the result section.

4.2.2 Equipment

For testing the codes for image processing before final installation and using in the AGV, we preferred to have some tests in the lab to make sure about the accuracy of our codes and algorithm. Therefore, we attached our cameras to a 1/3 scale prototype model of roguing

mechanism while the roguing mechanism, itself was attached to an IRB 120 robotic arm with the ability to control manually or automatically. In the final model we will use two cameras but, in this stage, using just one camera would be enough. The duty of the second camera is to check the results from the first camera from a different view to make sure the first camera detects the center of the target plant correctly.

In this work, we wrote the codes in Matlab while for the final design we can keep them in Matlab format or convert them to Python or any other programming languages. Some of the components were used in this experiment are shown in Table 8 and Fig. 30.

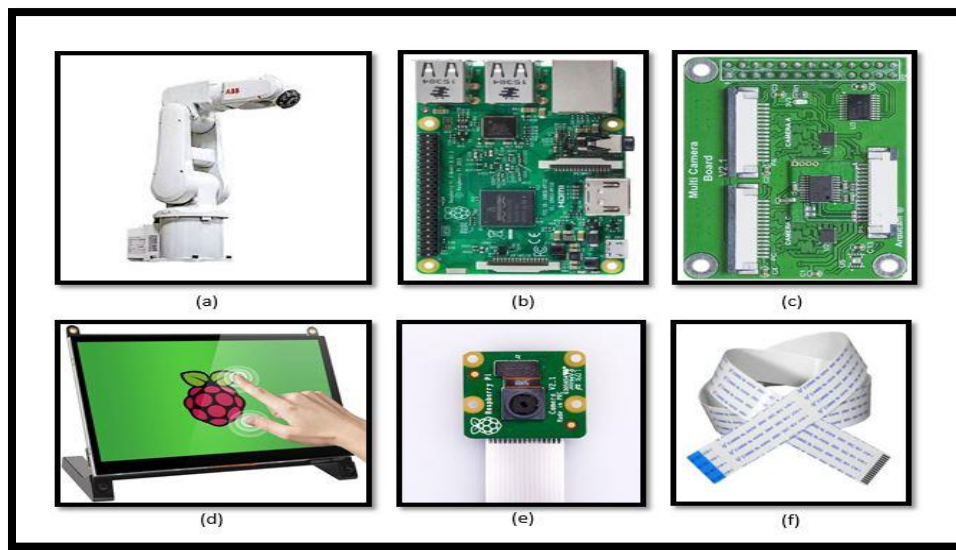


Figure 31: Required components for image processing and detect the infected plant

Table 8: List of components

#	Parts	Description	Qty
a	Robotic Arm	IRB 120	1
b	MicroController	Raspberry Pi 4 B	1
c	Multi-Camera Adapter	Arducam Multi-Camera Adapter Module V2.1	1
d	Monitor	Raspberry Pi Touchscreen Monitor, 7" Touch Screen	1
e	Cameras	Raspberry Pi Camera Module v2 with Sony IMX219 8-megapixel sensor	2
f	Ribbon Flex Extension Cable	1 meter	2

Fig. 32 shows how the cameras are connected to roguing mechanism. The first camera gives us a top view of the plant while the second camera gives us the front view of the plant. As it was discussed before, in this work we just work with Camera #1 and images from the top view.

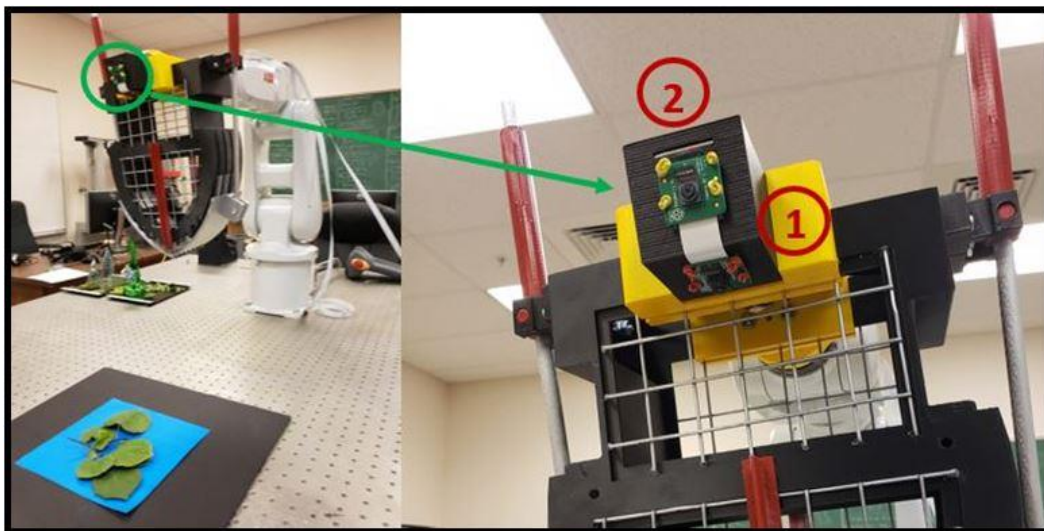


Figure 32: The location of two cameras in the prototype of roguing mechanism. Camera #1 give us the top view of the plant and Camera #2 give us the front view of the plant

4.3 Problem Statement and Methods

Let before starting to discuss the proper algorithm for the target plant detection, talking about all problems which this vision system can face in a potato field and find a solution for each of them in our codes. The first problem is related to the range of the color for the target object. The color of the leaves for plants varies case by case and this makes it hard to detect. The second problem is related to the amount of light during a day and various weather conditions. Both of these problems can be solved by defining a proper range for H, S, and L values. The third problem is related to other small weeds with green color which are growing close to the main target plant and we want to ignore them. For solving this problem, we can define a threshold for the minimum size we want to detect as an object and ignore anything less than this size (assume as the noise) in our image detection. The fourth problem and most complicated one is related to detect the target plant between other adjacent plants and find the center of this plant which will be used for roguing mechanism.

For solving the last problem, let's take a look at the location of the sick plant and adjacent plants from the top. Fig. 33 shows an area of 60cm×60cm of the field around the sick plant. In this figure, the yellow cross in the middle of the picture is the target plant (number 5). As mentioned before, the AGV will navigate to this location using an RTK GPS with a possible 10cm error. This error boundary is shown by a red circle in figure. However, because we are working with pixels, using a square shape would be easier. Therefore, we will define a square boundary which is shown by the blue crosses (eight other numbers) in the figure. These are other possible locations that the AGV may reach by mistake and assume them as the center of a target plant. Two adjacent plants in which are on the left and right side of the sick plant with a distance of 30cm from it.

Let's divide this 60cm×60cm square into nine 40cm×40cm squares as shown in Fig. 33 with yellow, red, and black colors. In this way, any of the cross points 1 to 9 would be the center of

one of these squares. Therefore, regardless of that the GPS guides the rover to the correct location for the target plant (number 5) or by the mistake guides it to a wrong location (any number 1-9 except 5), the camera has to search the area of $40\text{cm} \times 40\text{cm}$ around that point, find the target plant and detect the center of it.

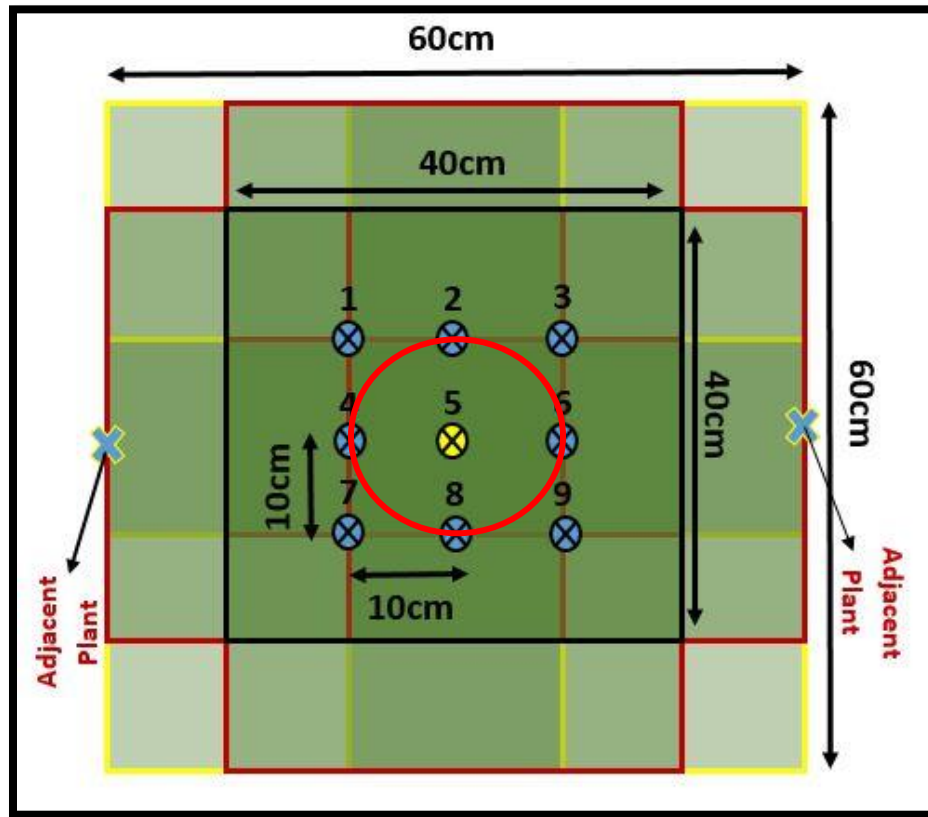


Figure 33: The $60\text{cm} \times 60\text{cm}$ area around the target plant in the field and nine $40\text{cm} \times 40\text{cm}$ sub-areas inside of this region

For making it clear, let's look at one of the possible situations as an example. Imagine point number 1 from GPS is sent to the AGV as the center of the target plant. We assumed the distance between camera and land is fixed and after the AGV reaches this location, the camera takes a picture from the top with the center of point 1 and a frame of $40\text{cm} \times 40\text{cm}$. This area is shown in Fig.34. Now from this image, we have to find the location of the target plant and the center of that which is number 5.

In this case, we can use two different algorithms for finding the center of the target plant. In this section, we will explain both algorithms and in the next section, we can compare the result for each of them and select the best one.

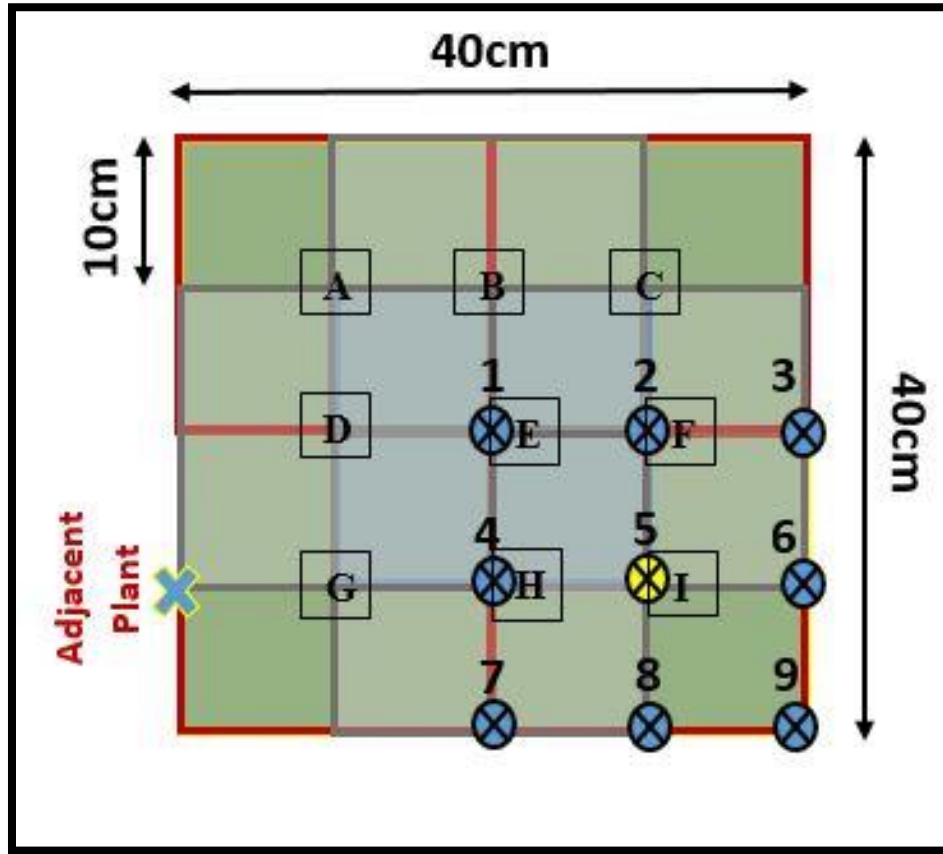


Figure 34: The 40cm×40cm area with the center point number 1 (example)

A) In the first algorithm, the whole 40cm×40cm camera frame is divided into nine 20cm×20cm subframes, as it's shown in Fig. 34 with the center of A to I. Then, the green area (the area that belongs to plants) for each of these nine squares will be calculated and the square with the maximum green area will be found. Finally, the center of that square will be selected as the center of the target plant. For instance, in the above example that would be I.

B) In the second algorithm, the whole 40cm×40cm camera frame will be searched for green areas. Each of the connected green areas (one piece) will be selected as one blob. The area for each

blob will be calculated and the largest blob will be selected as the target plant. Finally, the center of that blob would be chosen as the center of the target plant (the result should be close (or exactly) similar to the first algorithm which that means point I).

4.4 Results and Discussion

As it was explained before, in this project we have a focus on four main topics for accurate plant detection. These are color, light, size of objects, and location for the center of the target plant. The methods and results for each of them will be explained and discussed in this section.

4.4.1 The Target Color Domain Detection

To detect the plant from the background and other objects in a potato field, we need to find an appropriate range of H, S, and L for the detection of potato plants with various colors. After lots of tests for various possible green colors for the leaves of potato plants, a proper range for H, S, and L values in HSL format was found which is shown in Table 9.

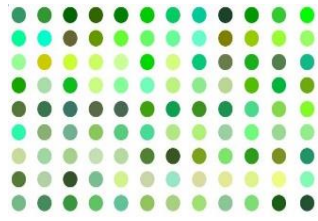
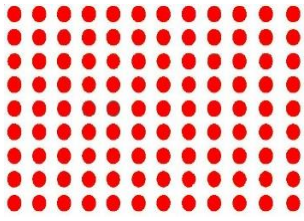
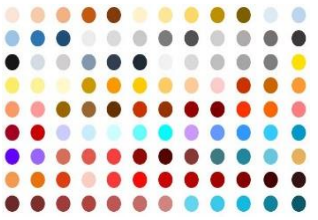
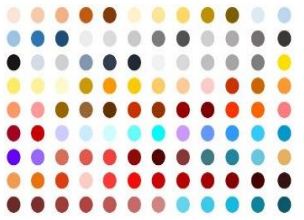
Table 9: Acceptable Range of Parameters in the HSL Format

HSL Format	H	S	L
Minimum	0.157	0.1373	0.1176
Maximum	0.49	1	0.85

For testing these ranges and check if we can detect most of the green color domain while ignoring all other colors (especially colors related to possible objects in a potato field such as sky,

rocks, soil, etc.), a wide range of green color was selected and presented in Test A, Table 10. Any of these points which can be detected by the codes will be replaced with red color. As you can see all of the points in the selected green color domain had been detected. On the other hand, in Test B, a variety of other colors (except green) was selected, and the test had been repeated. As it's shown, none of them was detected by this code.

Table 10: Color Detection Test for a Wide Range of Colors

Test	Color Range	Results After Image processing
A	<u>Green Color Range</u> 	<u>Detected points are red</u> 
B	<u>Other Possible Colors</u> 	<u>Detected points are red</u> 

For making sure about the results of the codes in a real case, we repeated the tests on the leaves of several different plants with various shapes, colors, and sizes. Three samples of them are shown in Fig. 35. None of these leaves belongs to the potato plant but they were chosen because on the potato field based on the time of the roguing and other field conditions the size, shape, and color of potato leaves can be different, and we have to be ready for any situation.

As you can see, for all three cases the camera can detect the leaves of the samples perfectly with minimum error!

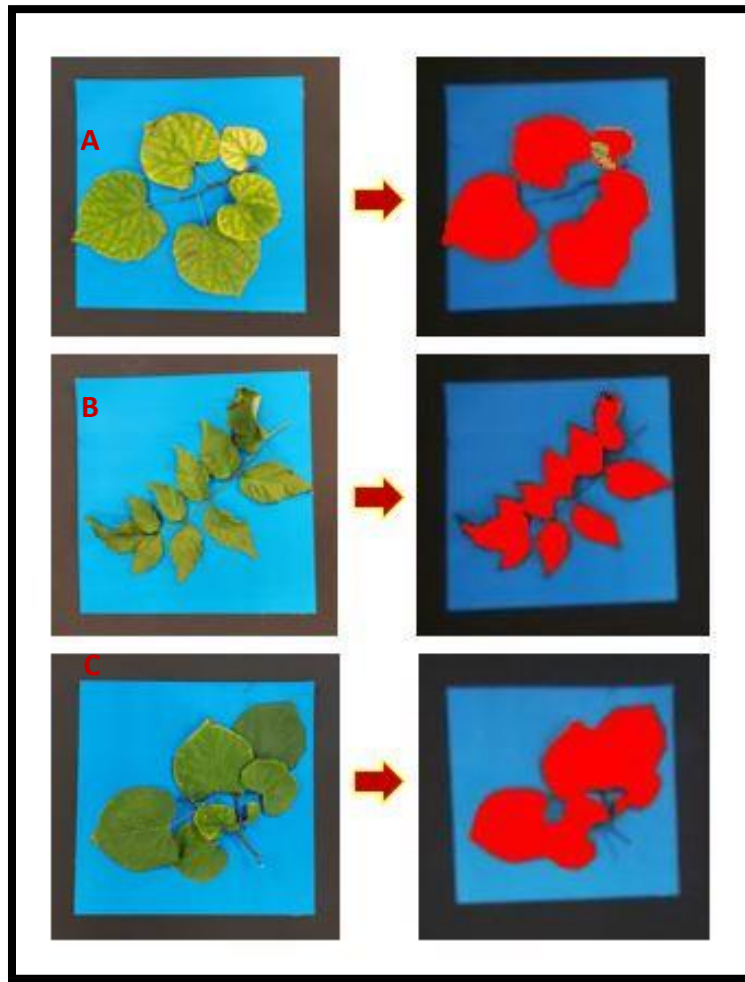


Figure 35: Three leaves samples with different color, shape, and size to test the detection codes and check the selected range for HSL parameters

4.4.2 The Light Range

The second thing that needs to be checked is related to the amount of light in the potato fields. The light can be various because of the time of the day operating the AGV or the weather condition (cloudy or sunny). Fig. 36 is presented four levels of brightness, from very bright to very dark conditions. The results in three conditions; very bright, normal, and dark, show the system can detect the plant with high accuracy in these three conditions but in a very dark scenario, it can detect around 50% of the target plant. So, this system is not recommended for the very dark condition.

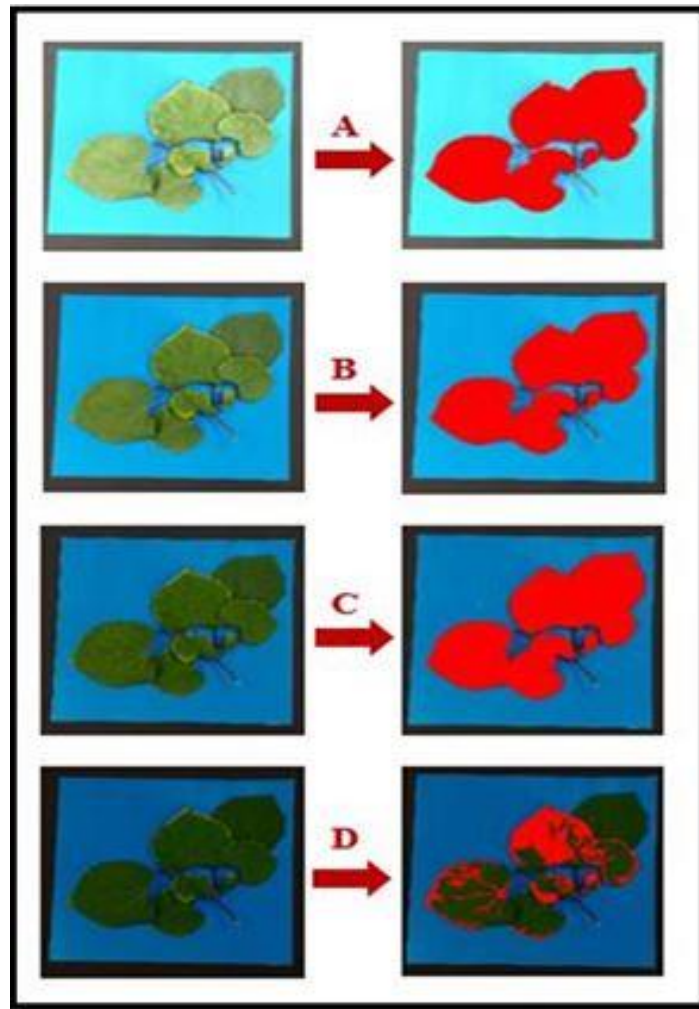


Figure 36: Checking the accuracy of the code in various level of brightness A) very bright b) normal c) dark d) very dark

4.4.3 The Minimum Range

In the potato field, may some small weeds be grown close to the main plants. This may cause an error in finding the exact center for the target plant. Therefore, we defined a minimum range for detecting an object, and any value less than that would be ignored by the system. In our code, any object with less than 300 pixels will be removed from the image. In the example that is presented in Fig. 37, we used the leaves of the Noble tree. As it is shown some part of it that was close to each other was detect as a one-piece but the rest of it is not detected.

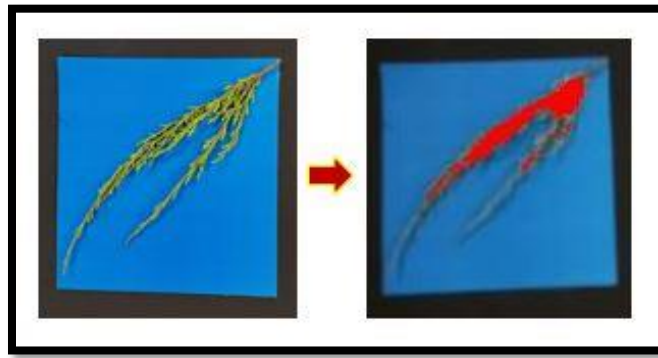


Figure 37: The blobs with less than 300 pixels will be removed from the image

4.4.4 Finding the Center of the Target Plant

Two algorithms were presented in the previous section for finding the center of the target plant. We tested and evaluated both methods with lots of samples. Let's explain one of these samples here as an example and discuss the results. Fig. 38 shows an aerial photo from a potato field. The plant in the middle of this photo is the target plant. The blue points show the boundary for possible coordinates that can be received from GPS and the red point (Num. 5) is the exact center of the target plant. To test both algorithms in the worst scenario, let's imagine GPS send a wrong coordinate to AGV and somewhere close to the discussed boundary with maximum distance from the correct center point, for example very close (but not exactly) to point Num. 9.

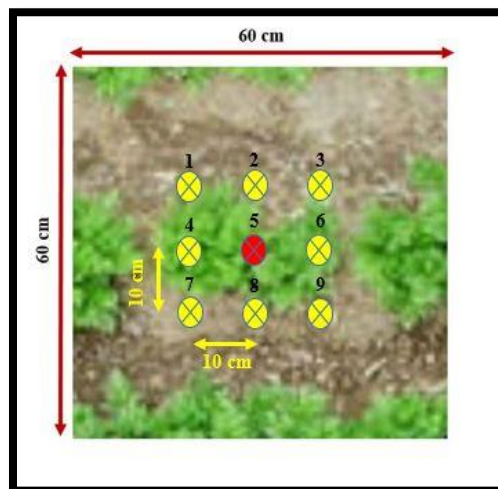


Figure 38: Aerial photo from a potato field

This situation is presented in Fig. 39. As you can see, this is shown an area of 40cm×40cm with the center close to point Num. 9.

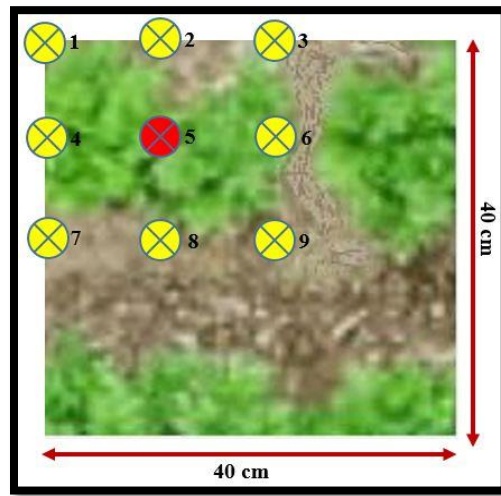


Figure 39: The received coordinate from GPS as the center of the target plant (close to Num. 9) and surrounding

i. Method A

In method A, as it was explained before, the camera frame will be divided into nine equal 20cm×20cm regions. This division is shown in Fig. 40 with center point A to I for each of these regions.

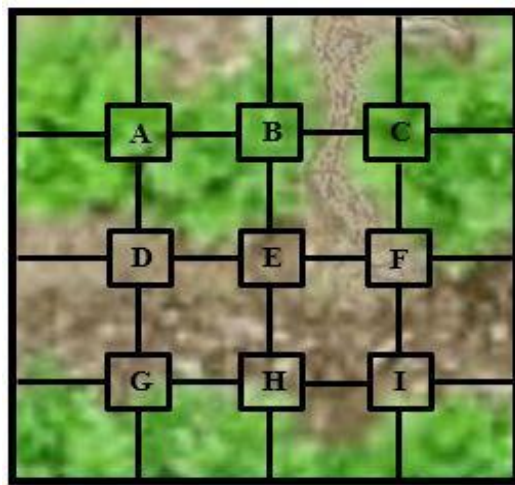











Figure 40: Nine search regions in Method A

In this method, the green area for each of these regions would be calculated and the region with a maximum green area would be selected as the target region. Then, the center of that region will be selected as the center of the target plant. Table 11 shows the green parts in each region and the total value for the green area in each of them. As it's shown the region A, with 6764 pixels has the maximum green area.

Table 11: Green Area for each Region in Method A

Region A	Region B	Region C
		
6764 Pixels	5867 Pixels	6672 Pixels
Region D	Region E	Region F
		
4760 Pixels	4349 Pixels	4749 Pixels
Region G	Region H	Region I
		
4040 Pixels	3461 Pixels	3605 Pixels

ii. Results for method B

In method B, the whole camera frame will be searched to find the largest blob and chose the center of it as the center of the target plant.

The final result for both methods is shown in Fig. 41-B and can be compared to the true center point in Fig. 41-A. As you can see both results are close to each other while method B is more accurate. In reality whenever one of those 9 points in Fig. 38, selected as the center of the picture, method A will find the center of the target plant with 100% accuracies. However, if the selected point is in the range of 10cm but not exactly one of those points (somewhere between two of these points with less than 10cm error), method A can have some error between 0 to 5cm. On the other hand, method B is constant about the results and most of the time find the center of the target plant with high accuracy.

The accuracy for each of these two methods is compared in Fig. 41 and Table 12. The error for method A in this example is because point 9 is not selected to be exactly in the center of the picture.

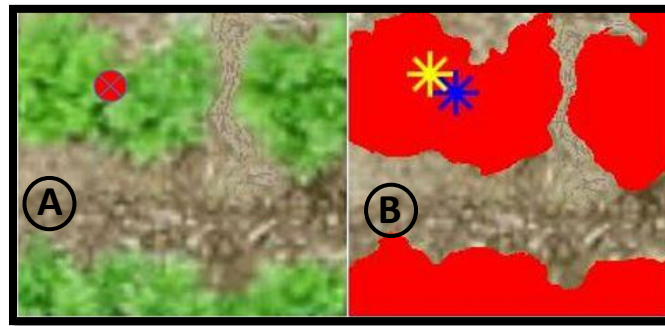


Figure 41: A-Center of target plant; B- The center point detected from method A (Yellow star) & method B (Blue star)

Table 12: The X & Y Coordinates for Method A, Method B, and True Center Point

Center Point	X_Center (Pixel)	Y_Center (Pixel)
Method A	47.5	47.5
Method B	63	59
True Point	63	61

As you can see, the value of X and Y in method B is very close to this value for the real center point of the target plant (only 0.4mm error in the Y direction). But method A has a bigger error (around 3cm error in both directions). However, for having a better comparison between the two methods and select the best one, we repeated the test of both methods many times on various samples. The results for ten of them are shown in Fig. 42. In the graph green and blue lines shows the error for method A and method B from the actual center of the plant respectively. The values of these errors are presented in the table below the graph. While method A has a large fluctuation from 1 cm to 5 cm error, method B has a constant pattern with 1 cm to 2cm error which is acceptable. For these ten tests which are shown in Fig. 42, the mean and median of error values for method A are 2.9 cm and 2.8 cm respectively while these values for method B are 1.8 cm and 1.9 cm. So, we can say Method B in general is more accurate and reliable.

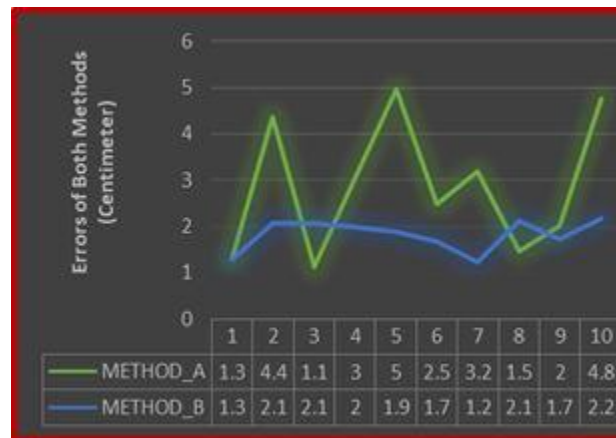


Figure 42: Comparison between the error of method A & method B for ten different situations

*** Results for this image processing software have been submitted to “International Conference on Computer Vision (ICCV), 2021”.**

CHAPTER 5. ROGUING MECHANISM

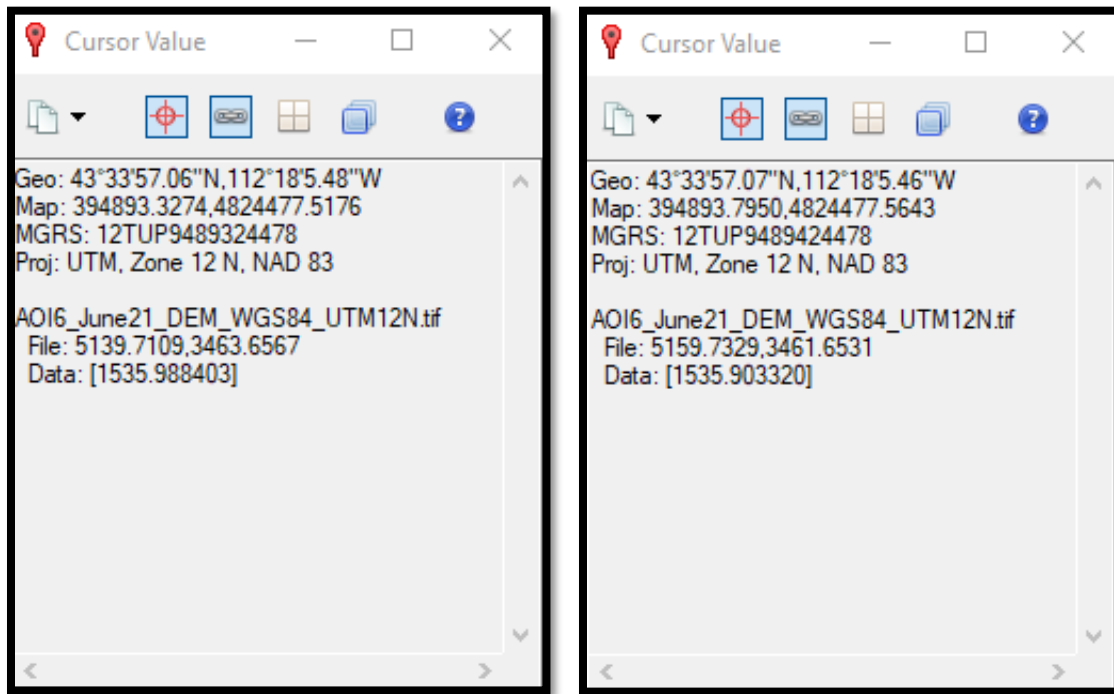
The final goal of this project is extraction of sick plant from the field, and this would not be possible without having a proper extraction mechanism with ability of complete removal the sick plant. In this section, the design process and requirements for this extraction mechanism will be analyzed and finally the most appropriate one based on these requirements has been designed and a prototype of it will be presented.

5.1 Potato Field Visit and Simulated Model of Potato Field in the Lab

Before starting to design the mechanism, we need to know more information and details about the potato field where this mechanism is supposed to work. For reaching this information, we had an image analysis and potato field visit. Based on these data and our observation, we made a simulated model of it in SolidWorks which will be used in future calculations for our design.

5.1.1 Finding the Height of Potatoes with Picture Analysis

Potatoes are planted in April and take 3-4 weeks to see leaves. After 6-8 weeks, the leaves are completely green (early June). The following results are from pictures taken from a drone last year over a potato field. This data analyzed with ENVI software in the department of geoscience. In this software, the elevation of each point in the field can be calculated (the color of each pixel has a different elevation (dark-light)). These results for June 21 shows in the following slides.

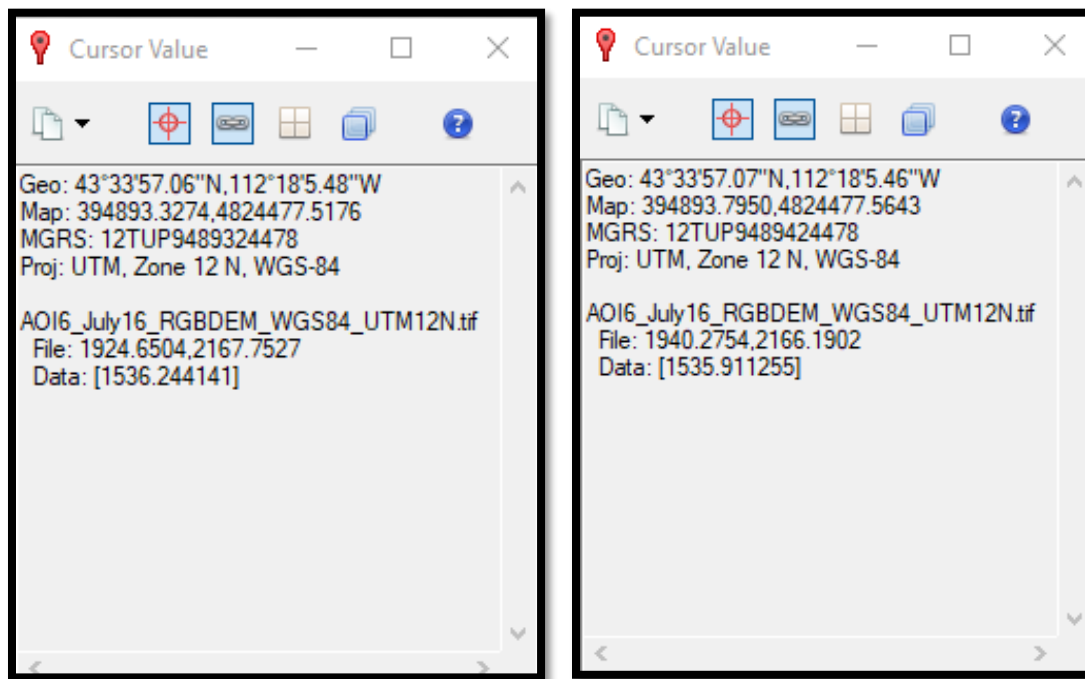


Potato plant elevation on June 21

From the information in these slides, we can calculate the height of the plants (June 21).

Elevation (Height of plant): $1535.988403 - 1535.903320 = 0.085083\text{m} = 8.5083\text{cm}$ (6)

However, this is just a sample (an average) but in general, the height of the plant in a different part of the field is different and is variable between 3cm to 10cm. (depend on soil condition & and fertilization). This test was repeated for July 16 with the same method and information are mentioned in following slides.



Potato plant elevation on July 16

From these slides, we will have:

$$\text{Elevation (Height of plant): } 1536.244141 - 1535.911255 = 0.332886\text{m} = 33.2886\text{cm} \quad (7)$$

This calculation is just for a random point in the field with an average size of the plants and the same as the previous one is just a sample. In general, the height of the plant would vary on the field between 20cm to 35cm when they are fully grown.

5.1.2 Potato Field Visit

The season of growing potatoes in the field is too short and we just had a few weeks for our tests and analysis during the year. We had a chance to visit a potato field just once at the end of the season. From that visit, we find out the connection between fully growth plant and potatoes tubers below the soil is very weak, and with just a little force over stem they are broken, and tubers remain below the soil! However, for making sure about the results we needed to test more samples and check them when they are still young.

Fig. 45 shows a potato field, and the area should clean up (hatch area) from the sick plant in a simulated model of the potato field.

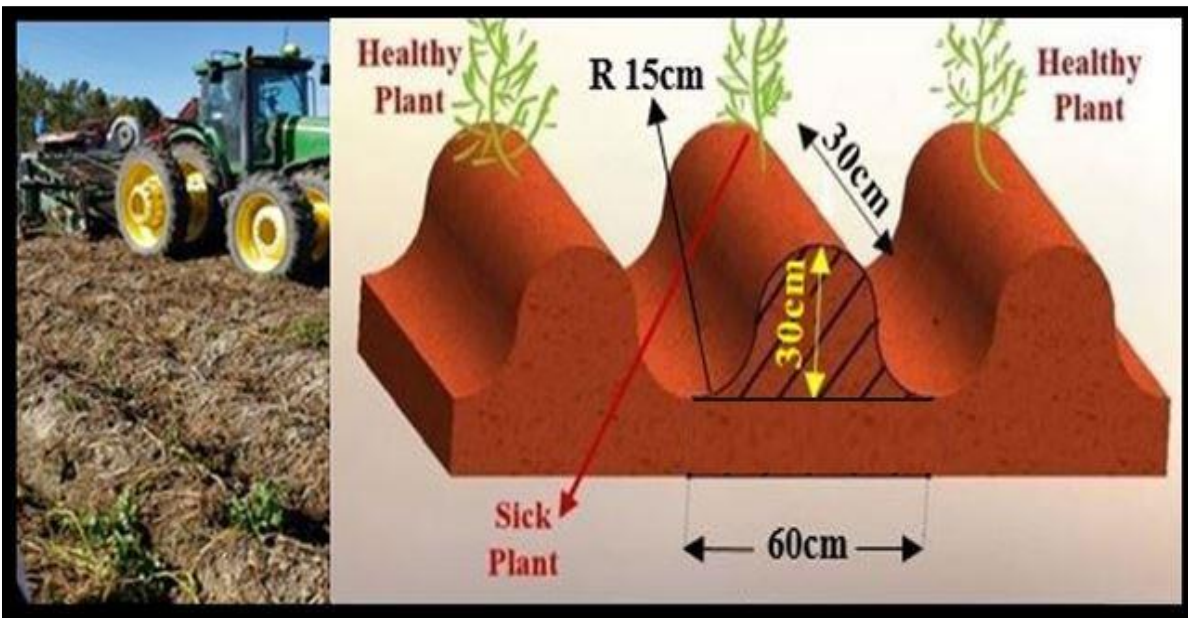


Figure 43: Potato field (left) and simulated shape and size of the potato field (right)

5.1.3 Process for Planting Potatoes Indoor

As it was mentioned before, to have more tests over the potato plants we need to have more samples. Therefore, we plant some potatoes indoors with a similar condition to the field. The following steps are the steps for planting the potatoes indoors:

- 1) Making some small holes on the bottom of the container (around 30 holes with an estimated radius of 2mm-3mm)
- 2) Cover the bottom of the container with two layers of gravel to help draining water slower (Fig. 46)



Figure 44: Container filled by gravel for planting potato

- 3) Cover gravels with a sheet of filter fabric to make sure water will not wash the soil out of the container during watering potatoes (Fig. 47). However, this filter doesn't let any water pass through, so make several holes on it to give some space for draining the extra water out of the container.



Figure 45: Cover gravels with a sheet of filter fabric

- 4) Fig. 48 showed the measuring 15 cm from the gravel surface which is marked on the sidewalls of the container. It was marked because potatoes have to be planted on top of this amount of soil.

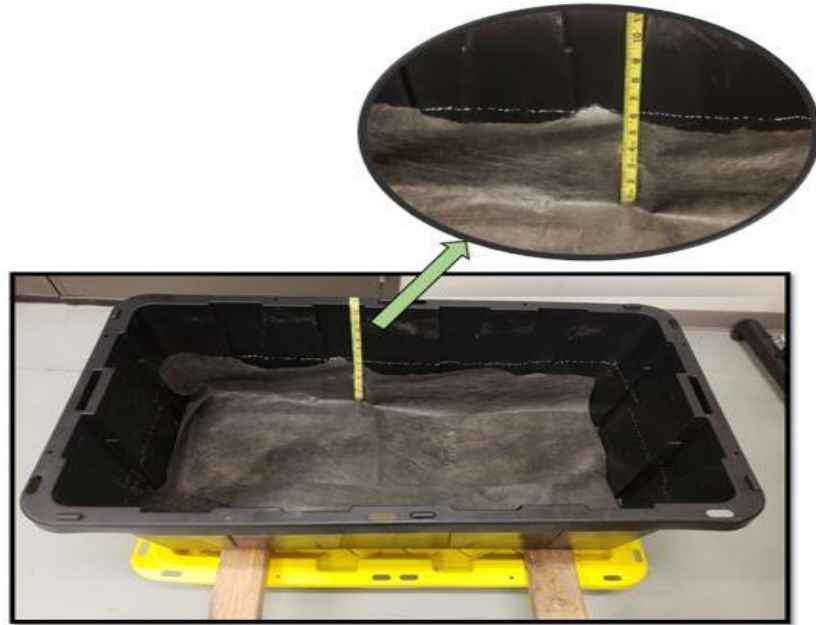


Figure 46: Marking the container for the place of planting potatoes

- 5) Fill out the container with moisture control potting mix up to 6 inches from gravels surface. Potato needs loose soil because they need room for their roots to grow faster and better so shovel the soil very well before adding it to the container (Fig. 49).



Figure 47: Adding soil up to the middle of the container

- 6) Look at potato seeds to find an eye on them and put them on the soil when the eye is face-up (Fig. 50). Each potato seed at least should have 15cm free space in any direction (to have enough space for growing roots).



Figure 48: Planting potatoes with 30cm from each other

- 7) Add more soil on top of the potato seeds for 6 inches (Fig. 51).



Figure 49: Adding soil for 30cm on top of the potatoes

- 8) Potatoes need at least 6-8 hours of sun. However, because we are growing the potatoes indoors, we used two (120W, 120V) Indoor Reflector Plant Light Bulb for this case and use

the smart plugs to control the amount of light and prevent over-lightening which causes damage to the plants (Fig. 52).



Figure 50: Using Indoor Reflector Plant Light Bulbs for having enough light for potatoes

- 9) The last step is watering the plants. They need water as much as see some water drain out of the bottom holes of the container. Repeat this process each 10-14 days (when the soil become completely dry)
- 10) After 6-8 weeks, we will have a fully grown potato plant and ready for various tests (Fig. 53).



Figure 51: Fully grown potatoes after 8 weeks

5.2 Analysis of the Possible Options for Roguing Mechanism

5.2.1 General Grasping Principles

Totally, there are five possible grasping principles that can be considered for designing a gripper:

- a) **Pinching:** In this gripper, force is applied by two or more fingers to hold and move an object when this force is a local normal force. The friction between fingers and the object helps the gripper to hold it during movement. In this type of gripper, a large amount of force is applied to the object. (Hard grip)

Discussion:

This type of gripper probably cannot be a good one in the case of the roguing potato because of the following reasons:

- The stem and leaves of potato plants are slippery and robot fingers cannot grasp them perfectly
- Even if the gripper can grasp properly the stem of the potato plant, that may cause some broken infected potato leaves which make the virus spread out to other potatoes
- This type of virus affects all parts of a plant, so it has to take the whole infected plant out of the field. On the other hand, the connection between stem, roots, and potato seeds is very weak and there is a high possibility some part of the infected potato (root or some of the seeds) stay in the field and cause the disease to spread out.

- b) **Enclosing:** The object will fully or partially be surrounded by fingers with large surfaces. The total necessary force will be found from the summation of all normal force vectors of the surfaces in touch with the object. In general, undergoes high accelerations, each of these forces can be larger than the force exerted by the object, but if the object doesn't

have an acceleration, none of them are larger than force from gravity (soft grip). Also, the object can be released by opening the fingers large enough.

Discussion:

There are two different ways we can design enclosing gripper for roguing potato:

1) Some grippers which just grasps completely the top part of potato plant (stem, leaves, etc.).

When this design has some advantages in the first two problems mentioned before for pinching gripper, it still has the last issue and when it takes the whole stem and leaves out of the field, the roots and tubers can still stay in the field.

2) The other design can be a kind of closed shovel/bow rake that takes the whole infected potato plant include everything below the soil plus some of the soil surrounded just for safety. This one can be a possible option in our case.

c) **Pinning, penetration:** In this gripper, several sharp-pointed pins are pressed into the object and don't let the object move anymore.

Discussion:

There are two types of them:

1) Short pins penetrate the surface of flat objects. It can be used for grasping the stem/leaves which will have the same issues as the first two grippers.

2) Long pins for going deeper inside of disorderly objects. Some long pins (like a fork) can go inside of the soil in the middle of potato tubers and take them out. The problems facing this design are:

- Each main seed divided into many tubers which finding and put a pin inside of each of them is hard

- Number of tubers for each plant is vary, therefore a specific design cannot work for various plants

- d) Underpressure, suction, vacuum:** This gripper is not just dependent on a vacuum, but it uses a certain amount of underpressure in the gripping area. For release, the object just needs to remove the underpressure.

Discussion:

Additional to the issues mentioned for the pinching gripper, because of the size of the stem which is very small, and the thickness of leaves which are very thin and fragile, a vacuum will not work for this case.

- e) Surface effects, surface phase transitions:** In this case, the surface of the gripper will be cool down very fast to a temperature much lower than the freezing point of water. If this surface is in contact with a wet object, it makes an ice layer which causes a sufficient holding force. For release just need to warm up the contact area.

Discussion:

This case also has similar issues as the vacuum gripper. Thus, this one is also not working for roguing potatoes.

5.2.2 Initial Tests for Grasping Mechanism

Early on testing for designing the prototype, involved analyzing the force that could be applied to the connections between the stem and the tubers and shortlist any grippers which may satisfy this requirement.

There are different motions that can be applied by a gripper mechanism (for example: a human hand) for pulling plants out of the soil. We analyzed motions of different mechanism to see if the entire plant and tubers could be pulled out of the soil without breaking the plant. For this we

conducted experiments to identify the maximum gripping force which might snap the stem thereby leaving the tubers in the soil. One of the challenges faced here, was that the forces varied significantly between plants. If we were to proceed with a design based on the gripping force itself, we would have to find actuators with a wide range to manipulate the force on the stem.

- a) Grasping the plant from the stem and moving it several times up and down (kind of vertical shaking). With this motion, we tried to loosen the soil around the tubers and the base of the plant before pulling the plant completely out (Fig. 54-a). As shown in Fig. 54-b, the connection between stem, potato tubers, and roots broke due to this motion. The potato tubers and roots remained in the soil, which would not help with the complete removal of the plant as desired.

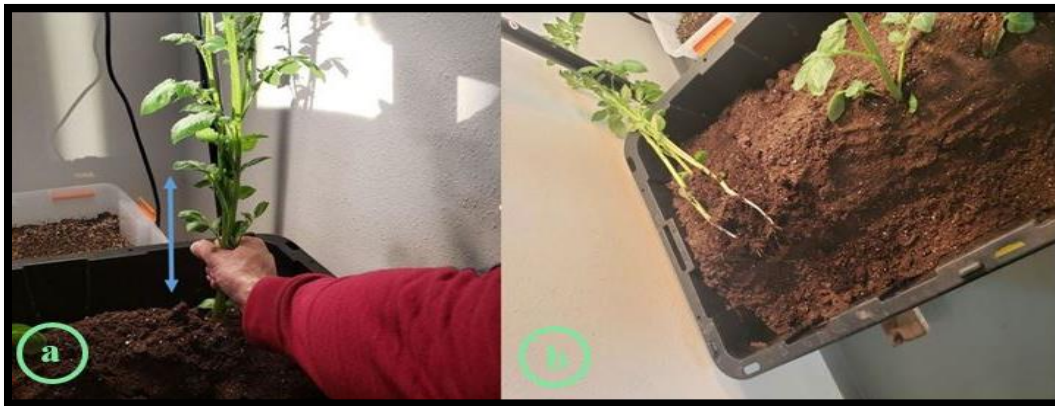


Figure 52: a) Vertical motion b) Connection between roots, tubers, and stem of the plant were broken in a vertical motion

- b) Grasping the plant by the stem and moving it several times front and back (kind of horizontal shaking). This motion was used to facilitate the loosening of the connection between the soil and tubers (Fig. 55-a) before pulling the plant out of the soil. This test was repeated 3 times. As it is shown in Fig. 55-b, for the first time, the whole plant includes stem, potato tubers, and roots came out of the soil and the test was successful but in the next two attempts the test was failed and the connection between stem and tubers broke.



Figure 53: a) Horizontal motion b) Connections between roots, tubers, and stem of the plant were not broken in the first time but in the next two repeats it was failed

- c) Grasping the plant from the stem and twisting it around the stem axis, and at the same time pulling the plant out of the soil (Fig. 56-a). As shown in Fig. 56-b, we observed the same results as the other two methods, the connection between stem, potato tubers, and roots was broken. Therefore, the potato tubers and roots remained in the soil again failing to facilitate the desired outcome.



Figure 54: a) Twist & vertical motion b) Connections between roots, tubers, and stem of the plant were broke

5.2.3 The Best Options

To satisfying the project requirements, a list of these requirements which must be considered for designing a roguing mechanism are list here.

- 1) Infected plant must be removed completely from the field (this includes whole parts of the sick plant: tubers, roots, stem, leaves, etc.)
- 2) Make sure, the selected design will not cut the plant which causes remaining some parts of the plant in the field
- 3) The mechanism has an easy actuation (minimum number of dofs)
- 4) Applying minimum force over each parts and links during extraction process

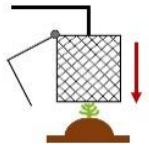
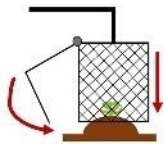
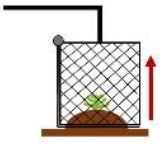


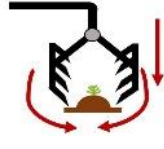

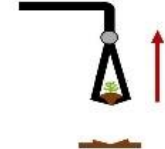
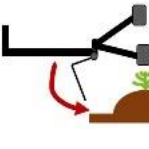
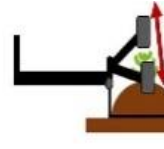
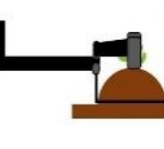
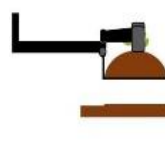
According to the results in the last two sections and listed design requirements, between all possible options, we shortlisted three mechanisms as the best choices for roguing the potatoes. The morphology chart for these three mechanisms is presented in Table 13.

The first design is made of a cage and blade for cutting soil. The cage goes down while surrounding the target plant. Then the cutting blades cut the soil (which includes potato tubers and roots of the plant) from one side and the whole mechanism goes up and dumps all of the material in a disposal container. (Table 13 – design A)

The second design is made of two rake-shaped arms. When these arms reach the top of the plant, it goes down and closes from both sides to cut the soil and grab the infected potato tubers, roots, and body of the plant. Then, it will pull up and dump all of the collected material in a disposal container. (Table 13 – design B)

The third design is a combination of a pinching gripper and a cutting blade. In this design, first, the whole mechanism goes down into the soil and the gripper closes to engulf the top part of the plant, while the blade cuts the soil grabbing the potato tubers and plant roots. Finally, the mechanism lifts and discards all the collected material into a disposal container. (Table 13 – design C)

Table 13: Morphology Chart

TYPE	1	2	3	4
A				
B				
C				

However, each of the above designs has some problems. In design “C”, because of the variety in the shape of the bushes, it would be hard to grasp only the top portion of the plant which includes all branches, leaves, and stem by the gripper completely. Also, cutting that much soil with just a single blade will require applying significant force on the blade. In design “A”, we would have a better performance for collecting the entire plant, but still have the same issue, significant forces on one blade. While in design “B” the soil would be cut easier due to splitting of forces on two arms. But because of the shape of the rakes and the sides of the arms being open, there is a significantly higher risk of losing a part of the infected plant in the field.

Therefore, the best design would be a combination of the mechanisms A and B which includes the advantages of both of them while eliminating their weaknesses. Several mechanisms based on this information were developed which two of them are shown in Fig. 57 & Fig. 58.

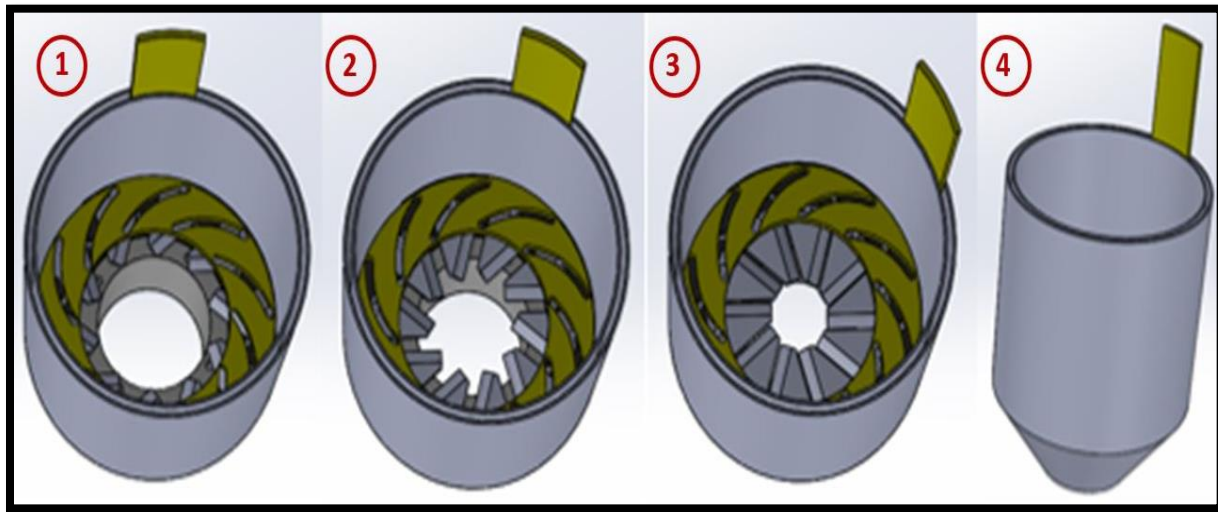


Figure 55: Designed mechanism with multiple blades in circular form

Fig. 57 is shown a mechanism that includes multiple small blades that can hide inside of the body of the mechanism. First, the body of the mechanism is pushed down to cut the soil around the plant and goes enough deep (below the roots of the plant) then with pushing the yellow handle up or down these blades can open or close in the form of a circular pattern (like the diaphragm of a camera). Therefore, the soil below the roots of the plant would be cut and kept the whole plant inside of this mechanism. The main problem with this design was the thickness of the body which was required for blades to hide. Also, there is possibility of cutting part of plant (tubers) which causes transferring infection to other healthy plants.

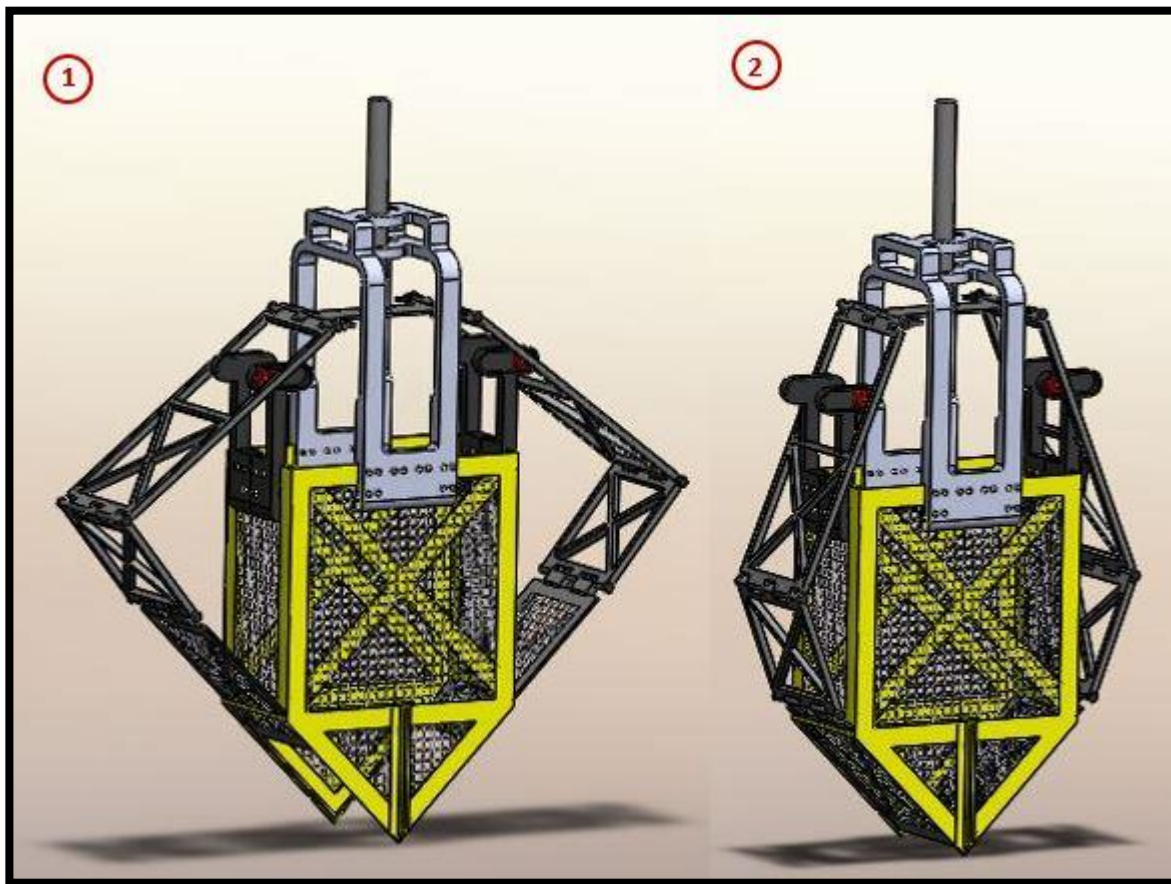


Figure 56: Cage form mechanism with two moving blades and a single actuator

Fig. 58 is shown another mechanism. This mechanism includes a big cage as the main body which is supported by cross beam and T-shape angle bars. Rather than solid walls for the body of this mechanism, we used Gridwall Panel to decrease the weight of the mechanism and to let the unnecessary soil goes out of the cage. First, the mechanism stand on top of the plant goes down and the mechanism with the sharp part of its body will cut the soil while the plant is inside of the cage. Then two moving blades cut the soil from the sides and the whole plant include stem, leaves, roots, tubers, etc. remain in the cage. Two moving blades are connected to the single actuator with two frames. One of these frames has two wheels as an attachment which will move inside of two fixed rails. This would cause the motion of the actuator which is up & down, to be changed to the sliding motion for cutting blades with angle. The CAD model of this mechanism was tested and passed the motion test. We built a prototype of this mechanism, but we found out there is a large pressure over

the wheels especially when the blades want to cut the soil! So, this design was not accepted too but we used lots of the main ideas from this mechanism in the final design.

5.3 Final Design

5.3.1 Parts of the Mechanism

As discussed in the previous section, the final design was generated based on combining the strengths of the three designs previously described. As it is shown in Fig. 59, the mechanism will contain a cage to making sure any part of the infected plant (including tubers, stem, leaves, roots, etc.) will remain in the field after roguing by this mechanism. Also, we will utilize two cutting blades to apply less force over each blade to reduce overall wear and chances of failure. In addition, two attached hydraulic actuators will be used to provide the necessary force to pierce the soil to a specified depth.



Figure 57: Different views of final design

Fig. 60 shows all the components for this mechanism. The description and quantity for each of these components is provided in Table 14.

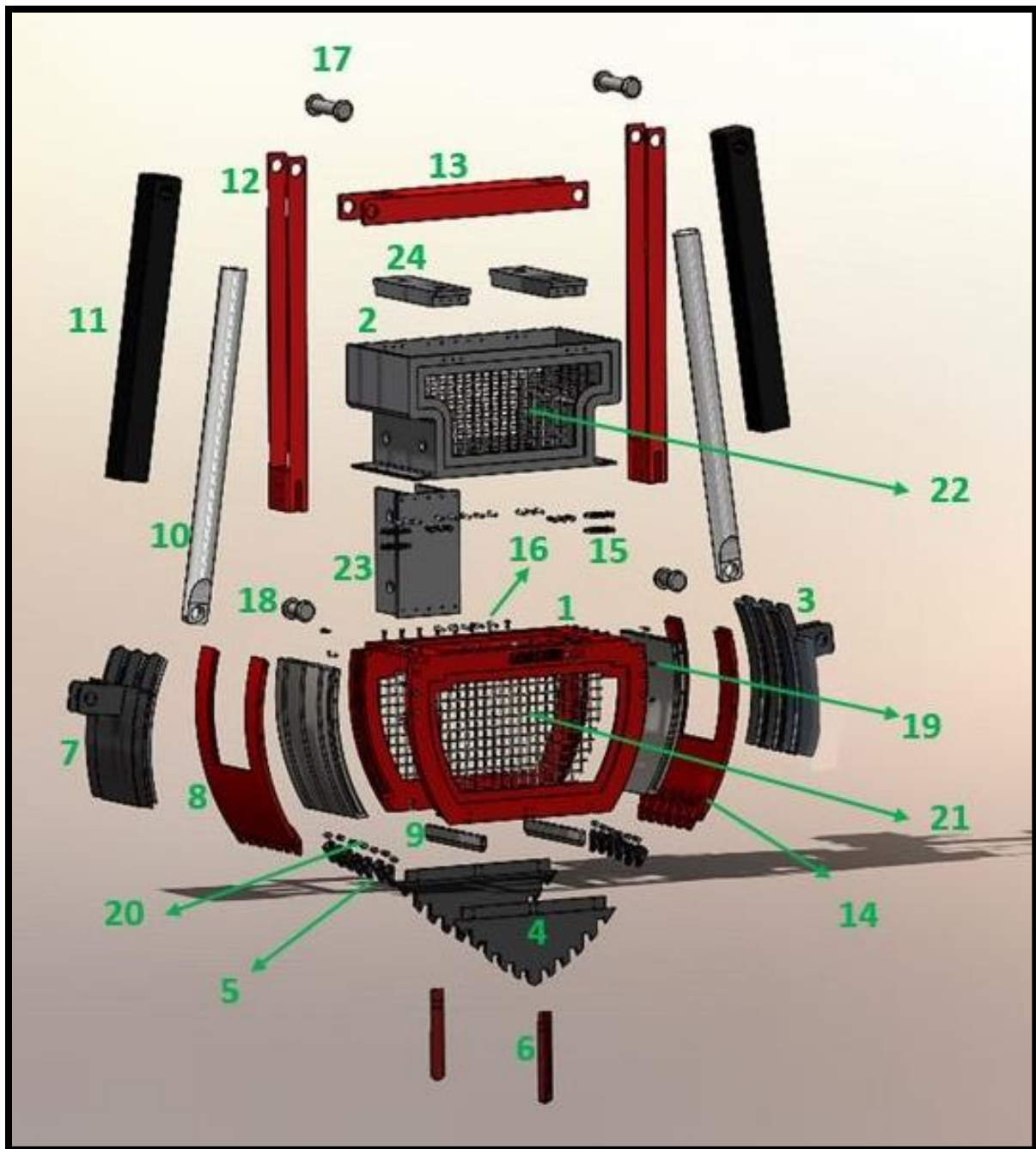


Figure 58: Final design Components

Table 14: List of Components for Final Design

Number	Parts	QTY
1	Main Body Bottom Frame	1
2	Main Body Top Frame	1
3	Rail	2
4	Fix Blade	2
5	Bucket Tooth	13
6	T-Shape Angle Bar	2
7	Slider	2
8	Moving Blade-Left	1
9	Inside Frame Blade	2
10	Hydraulic Actuator Piston Rod	2
11	Hydraulic Actuator Barrel	2
12	Hydraulic Actuator Connector Frame-Side	2
13	Hydraulic Actuator Connector Frame-Top	1
14	Moving Blade-Right	1
15	Hex Cap Screw M6×65mm	8
16	Hex Cap Screw M6×30mm	74
17	Top Hinge	2
18	Bottom Hinge	2
19	Machine Screw M5×30mm	12
20	Bucket Tooth Pin	13
21	Gridwall Panel-Bottom	2
22	Gridwall Panel-Top	2
23	Tractor Hitch Adapter-Back	1
24	Tractor Hitch Adapter-Top	2

These components, in general, can be considered to fall into one of the following five categories:

- 1) **Frame:** This is the main structure of the mechanism which will be used to hold the sick (roots, stems, leaves, etc.). In Table 14, this would include the Main Body Frames (top & bottom), Hydraulic Actuator Connector Frame, and Gridwall Panels. The size of the main body (top & bottom) is 60cm×30cm×90cm and this mechanism can dig up to a maximum depth of 30cm.
- 2) **Movable components:** This includes all components required for actuation and to bring about the desired motion of the blades. For example, the Rail, Slider, Hydraulic Actuator Piston Rod, and Hydraulic Actuator Barrel.
- 3) **Cutting Sections:** This includes all parts performing the actual digging action in the field and facilitates cutting the soil with ease. These include Fixed Blades, Moving Blades, and Bucket Tooth.
- 4) **Mechanism strength:** To improve the overall rigidity of the system we included a T-Shape Angle Bar on the sides of the main body and Inside Frame Blades which connect two sides of the main body (back-front). The connection between components was brought about using off-the-shelf pins and screws to make it easy to replace, clean, and assemble.
- 5) **Attachments:** This mechanism is designed to easily attach to various types of tractors or other farm equipment. Three possible adapters were designed to attach it to tractors: from the back by Tractor Hitch Adapter-Side, from the Top by Tractor Hitch Adapter-Top, and from the sides where they can be screwed to the holes which are placed on the sides of the Main Body Top Frame.

5.3.2 Parts Specification

In this stage of design of plant extraction mechanism, focus of our group was on finding the most appropriate design for this mechanism, having motion study for it, and building a smaller

model of it for some initial tests. The mechanical design, material selection for various parts and material properties, required power for digging, specification of hydraulic system, and some other details, in future research will be studied and analyzed for the final design.

5.3.3 Motion Study

This roguing machine complete assembly is presented in Fig. 61. Fig. 61-a shows the mechanism when the moving blades are open, yellow arrows show the direction of movement of hydraulic actuators that are connected to the arms. These hydraulic arms will actuate the opening and closing of the jaws while also providing sufficient force to pierce the soil. For closing the blades, the hydraulic system moves down and pushes the blades along the curved rails. Fig. 61-b shows the machine with the blades in the closed position.



Figure 59: Actuation of blades by a hydraulic system in the final design

5.3.4 Designed Attachment for Tractor

One of the advantages of this roguing mechanism, in addition to use as an attachment for this project, is the ability to attach and use on various vehicles in the farms (tractors, excavators, etc.). Because three-point hitches are a very popular way for attaching various attachments to tractors, we decided to design a connection part for the roguing mechanism for attaching it to the three-point hitch in this stage although based on customer needs, other connectors for tractors can be designed later. Fig. 62 & Fig. 63 are shown different views of this connector and after connecting to roguing mechanism respectively. The three-point hitches in tractors usually just have an active hydraulic system for lifting the attachments and a passive one for going down (by the own weight of the attachment). The three-point hitches maximum can lift a 615 kg load.

In most tractors, we can control how fast the mechanism going down. So, in this case, we can set it up to mechanism fall very fast, and because of the weight of it, the soil will be cut by the fixed cutting blades, and then moving blades will cut the rest of the soil.

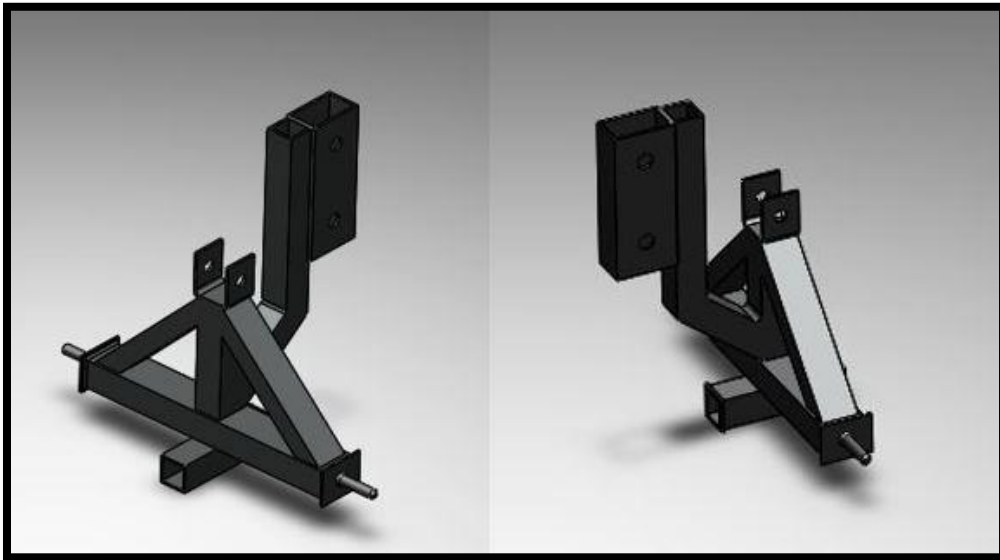


Figure 60: Different views of the designed connection part between roguing mechanism and tractors three-point hitch

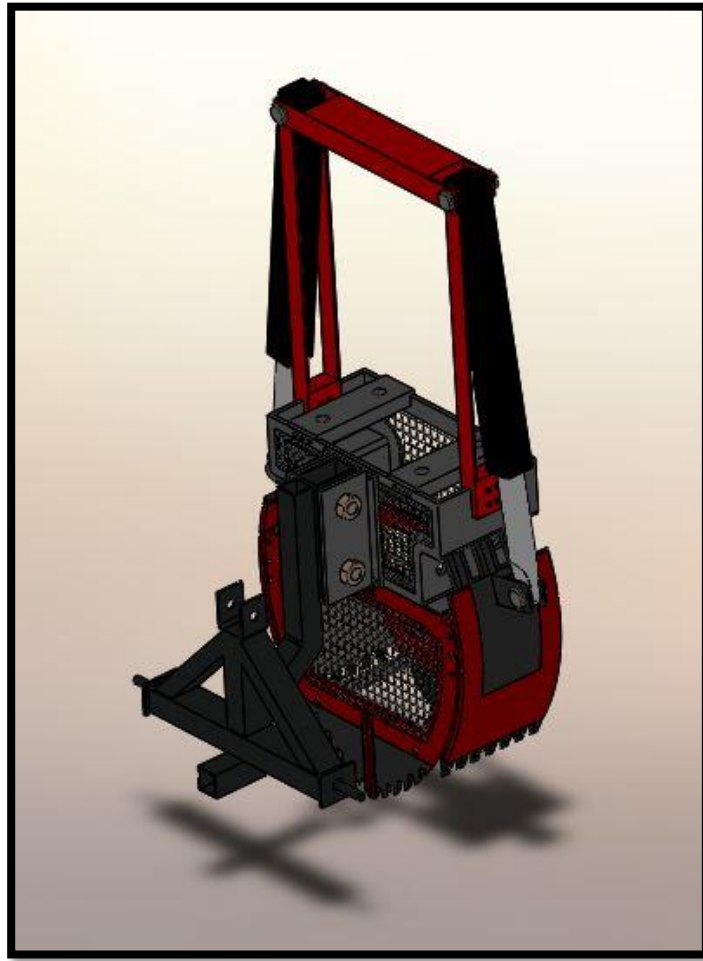


Figure 61: Roguing mechanism with connection part for tractors three-point hitch

5.3.5 Some of the Mechanism Specifications and Information about Extracted Soil

As it was discussed before, the size of the main body (top & bottom) is 60cm×30cm×90cm while this size can be changed on different scales based on customer desires. This size roguing mechanism with all attachments (including a three-point hitch connection) has a weight of around 227 kg and able to dig up to a maximum depth of 30cm. Fig. 64 shows the amount of soil that can be extracted from the field. Based on the range of density for soil from [94] which is between $1.2 \text{ gr/cm}^3 - 1.5 \text{ gr/cm}^3$ the maximum weight of extracted soil would be 12.5 kg. Therefore, the summation of the weight of the extracted soil and the weight of the mechanism together will be less than the maximum allowable load that can be lifted by the three-point hitches.

$$m_{soil_max} = \rho \times V = 1.5 \frac{gr}{cm^3} \times 18845 cm^3 \cong 12500 gr = 12.5kg$$

$$m_{total} = m_{roguing_mechanism} + m_{soil_max} = 227kg + 12.5kg \cong 240kg \ll 615kg$$

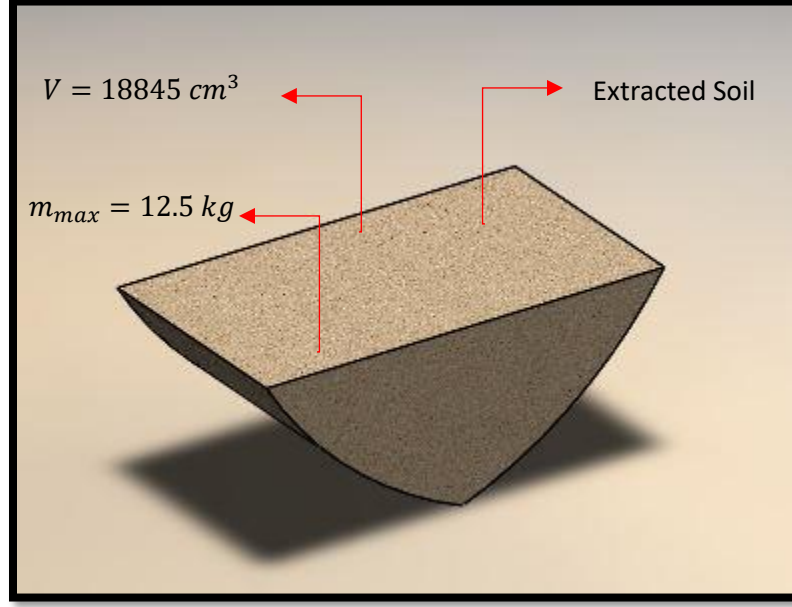


Figure 62: Amount soil can be extracted from the field

5.4 Prototype Model and Actual Test

Fig. 65 shows a prototype of the final design of the roguing machine which was built to 1/3 scale of the actual model. The prototype was used for testing the motion and functionality of the system.

There will be some differences between the final design and this prototype to accommodate in filed operation. First, the final design will be about three times larger than this prototype. In the final design, all major components are divided into sub-systems for ease of replacement and cleaning. Other small changes are related to improving the functionality of system and attachments needed to integrate the prototype to commonly used farm equipment.

Fig. 65-a shows the prototype connected to an ABB robotic platform, Fig. 65-b shows the tracks along which the jaws will move, Fig. 65-c shows the jaws in a completely closed position,

Fig. 65-d shows the teeth at the end of the jaws to help pierce the soil, Fig. 65-e shows a bottom views of the rouging mechanism with the jaws in a completely closed position with the teeth interlocking, Fig. 65-f shows the bucket in which the sample to be removed will be collected and disposed off the field. The catch bucket grills can be modified based on the type of sample being collected.

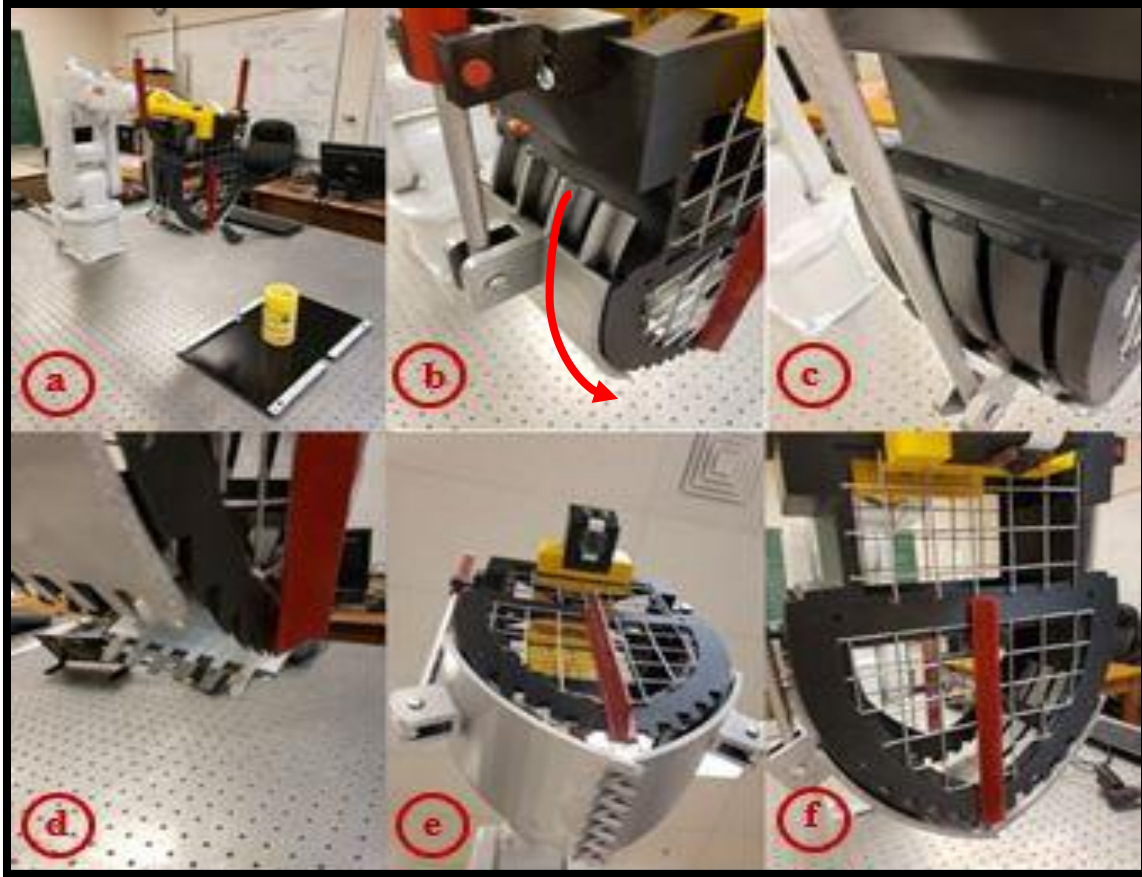


Figure 63: Prototype of the mechanism (1/3 of the real size)

Fig. 66 shows the rouging process of a sample plant by the prototype mechanism. In Fig. 66-a, the robotic arm pushes the mechanism down and the soil is cut by the fixed blades. In Fig. 66-b & Fig. 66-c, the moving blades will be closed and collecting the soil from the sides and keeping the plant inside of the cage. In Fig. 66-d, the robotic arm moves the mechanism up with the plant and soil inside.



Figure 64: Process of roguing the sample plant by prototype mechanism

*** This roguing mechanism filed as a provisional patent (Application Serial No.: 63/104,937 Filing date: 10/23/2020) and results of this design has been submitted to “5th IFToMM Symposium on Mechanism Design for Robotics – MEDER, 2021” (In press).**

CHAPTER 6. SINGULARITY ANALYSIS

6.1 Kinematic Synthesis of the Five-Fingered Multi-fingered Hand

The singularity of robotic mechanisms and manipulators is one of the important factors in designing a robotic system. Most of the works found focus on avoiding singularities or creating singularity-free trajectories with an algorithm based on a Probabilistic Road Map. In robotic hands, for applications such as agriculture, we want complex motion of the fingers, but we don't want to have many actuators in the hand, because that makes it more expensive, more fragile and harder to control. So, we want to use some kind of coupling mechanism for the dofs. One possibility which gives a robust mechanism is to use other linkages for coupling, such as the SS chain. But the problem is that, in doing so, you introduce non-obvious singularities, unless you design it with care. However, in this section, we want to use SS chains to couple RR fingers for the design of wristed, multi-fingered robotic hands. Unlike previous approaches, in this work, the focus is on designing the mechanism for specific singular configurations at desired positions. This approach can be useful to make sure the designed mechanism will stop at specific locations, or have motion between two specific points, corresponding to the two singular points. In the following sections, the derived equations are explained, and examples are included to test the method.

The object of this work is to study the singularity for a wristed, five-fingered hand which is a member of the single-jointed tree topology family studied in [86]. It has a single joint at the wrist and a single joint for each of the five fingers attached to the wrist with a single palm, see Fig. 67. It is solvable for $m_p = 2$ positions, and that means if all the dofs are actuated simultaneously for a given set of angles, the mechanism can be designed for a pick-and-release, or a single action task, when in general, and considering each finger acting separately, we can target more tasks. Each

finger has the same connectivity, and single mobility, plus the common mobility at the wrist. Definition for all concepts that are mentioned here (wrist, mobility, task, etc.) can be found in [17].

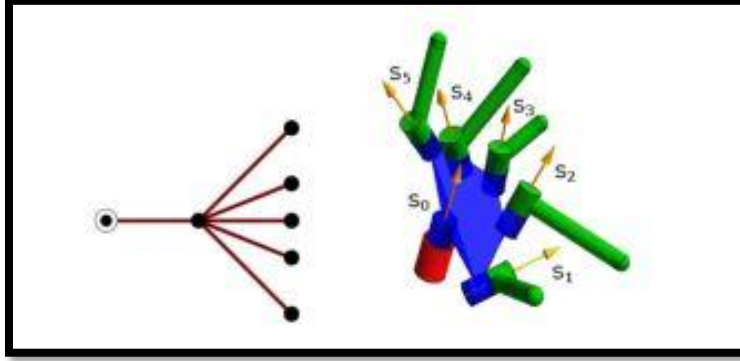


Figure 65: The tree graph of the 1-(1, 1, 1, 1, 1) hand, left; the kinematic sketch, right

The dimensional synthesis of this hand was studied in [87]. The complete description of the methodology for the synthesis can be found in [88], and it consists of solving the system of equations $F(S, \Delta\theta)$, composed of the forward kinematics equations of each branch, equated to the relative displacement of the corresponding fingertip. For $b = 5$ branches and a simultaneous task of $m_p = 2$ finite positions per finger, we have the set of equations:

$$F(S, \Delta\theta) = \hat{P}_{12}^c - e^{\frac{\Delta\theta_0}{2} S_0} e^{\frac{\Delta\theta_c}{2} S_c}, \quad c = 1, \dots, 5 \quad (8)$$

Where \hat{P}_{12}^c is the relative displacement from position 1 to position 2 for each finger “c”. The six joints have Plucker coordinates $S_i = s_i + \varepsilon s_{i0}$ for $i = 0, \dots, 5$, and the rotation angle about each joint is θ_i . The relative forward kinematics is computed as the product of exponentials for each branch. An algebraic derivation for this problem can be found in [87] and it yields two solutions.

The two positions shown in Table 15 for the first finger and in Fig. 68 are selected. The solution from the synthesis problem yields the hand shown in Fig. 68. In this sketch, the wrist is connected to the fingers through several rigid links forming the palm. The connection between the

joints is drawn at the common perpendicular line between axes. The twist angles between the wrist joint and each finger joint are shown in Table 16.

Table 15: The two positions used for the synthesis of finger 1, expressed as dual quaternions

Finger	Position 1	Position 2
Finger 1	$0.18 - 0.25i - 0.11j + 0.94k$ $+\varepsilon(2.46 - 3.3i - 1.4j - 1.5k)$	$0.0 - 0.10i - 0.01j + 0.99k$ $+\varepsilon(0.0 - 1.86i + 0.20j - 0.20k)$

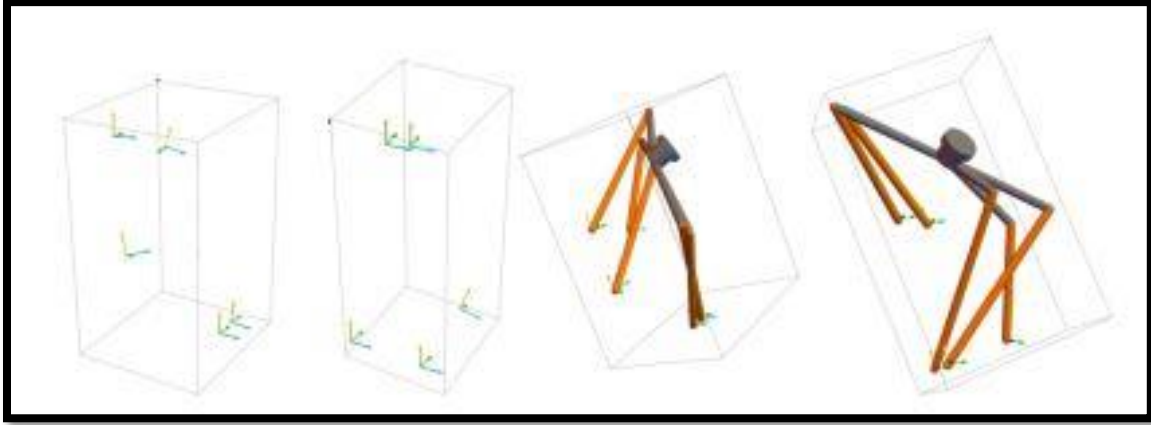


Figure 66: First and second positions for each fingertip, left and a schematic sketch of hand in both

Table 16: Twist angles α_{ij} between axis S_i and axis S_j

Twist Angle	α_{01}	α_{02}	α_{03}	α_{04}	α_{05}
Value (degrees)	60.7	11.8	6.0	7.4	-57.1

It is clear from the example that, even though the hand is theoretically capable of performing the task, its implementation is not straightforward.

6.2 Hand Optimization

The link-based optimization developed in [89] is used to select the best placement for the joints, that is, the dimensions and angles of the links. The method is based on optimizing the links' locations along each axis to satisfy a set of performance requirements.

Here, the objective function is formulated to minimize the overall length of the hand by considering the lengths between the wrist joint and each of the five finger joints, as well as the length to the five end-effectors. The sliding scalar values along each of the six axes to define the anchoring points are the parameters. Minimum and maximum link sizes were considered and formulated as non-linear constraints. Another important criterion is avoiding the self-intersection of hand parts. For this, links and end-effectors are considered cylinders that must maintain a user-defined distance with respect to each other. These conditions create another set of nonlinear constraints. The formulation was made in Mathematica and run in MATLAB using ga and fmincon. The optimization took an average of 15 generations and less than a minute. The resulting sliding parameters for each joint are shown in Table 17. These sliding values are measured from the intersection points at the common normal so that their initial value is zero. Fig. 69, shows the sketch of the hand before and after optimization at position 1. It can be seen how all the link and finger lengths are more balanced after the optimization.

Table 17: Resulting values for the sliding parameters of the joints

t_s	t_0	t_1	t_2	t_3	t_4	t_5
values	-0.656	1.843	-0.242	1.549	0.300	-10.468

An automatic modeling method developed in [90] was used on the optimization results to generate an initial model of the hand.

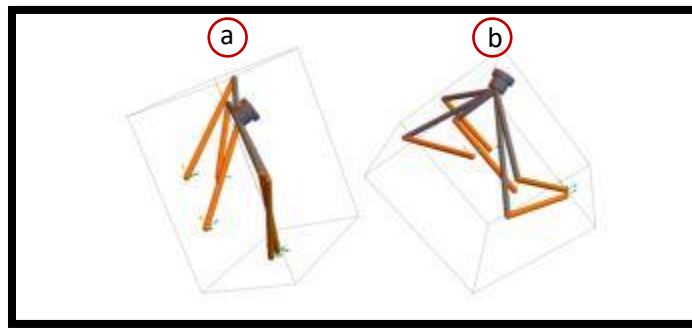


Figure 67: a) Schematic sketches of the hand in position 1 before optimization b) after optimization

6.3 Underactuated Coupling Mechanisms

To reduce the complexity in the control and to allow for adaptive motion, different types of coupling mechanisms are used so that the hand can perform the desired motion with a smaller number of actuators. For this design, a single actuator should perform the desired motion for all five fingers. Most of the mechanisms currently used are restricted to particular arrangements of the joint axes that are being coupled. The most common situation is that of joints with parallel axes. The table below intends to be a non-exhaustive enumeration of the most popular coupling mechanisms and their applicability to different arrangements of the joint axes.

Table 18: Mechanisms to implement coupling between joint axes

Mechanism	Applicability
Spur Gears	Parallel joint axes
Helical Gears	Generally-oriented joint axes
Bevel Gears	Intersecting axes
Belts and Cables	Mostly parallel axes
Closed-loop linkages	Generally-oriented axes

The use of some types of gears could be a good solution but must be complemented with another transmission such as a cable because the distance between the axes is limited by the gear ratio and the size of the elements. This can be solved by using a combined gear + cable system.

Belts and cables present a similar problem; the force at the belt is perpendicular to the rotation axis for parallel axes, and those mainly tangential forces are optimal to create the desired torque and angular velocity. When the axes are skew, axial force components appear. The problem increases when the anchor points are not located at the common perpendicular line between axes. Those axial components increase the friction and require specific solutions to avoid the cable to slip from the pulley.

The use of additional links to create closed-loop linkages is a very common solution for parallel axes because it yields a low-friction, low-maintenance and high rigidity (if desired)

coupling mechanism. The simplest way to connect two revolute joints with a linkage to yield a 1-dof system is the use of two more joints, to create a spatial four-bar linkage [91].

The simplest of the four-bar linkages consists of four revolute joints, and for skew joints, the only movable four-bar linkage is the Bennett linkage. However, its use as a coupling mechanism for an existing R-R chain is limited.

The synthesis of the five-fingered hand yields two solutions. Connecting both solutions yields a Bennett linkage for each finger. Fig. 70 shows the Bennett linkages for this example, and it illustrates the limitations in the use of this method. Because there is only one option for coupling the hand, the designer has no control over the placement and dimensions of the coupling mechanism, which is not an acceptable solution in general.

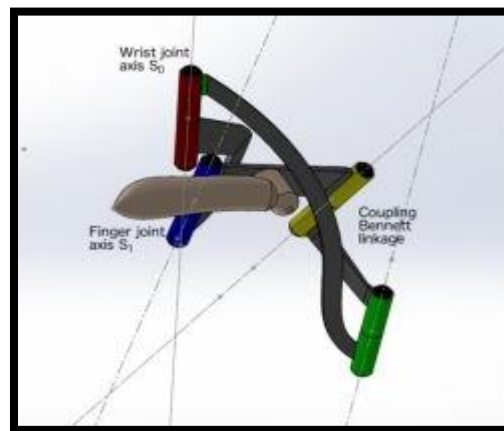


Figure 68: The R-R chain for wrist joint and first finger, coupled using the complementary R-R chain

Other spatial-four-bar linkages contain cylindric joints. Cylindric joints in general present problems of friction and linear motion range, yielding them also impractical as a coupling mechanism. Finally, the use of spherical joints in the design has several advantages. They are small and compact, and they yield non-overconstrained mechanisms, which increase the search space to optimize their placement and dimensions. One of the few drawbacks of this linkage is that the range of the spherical joints is limited.

6.4 The RRSS Mechanism

In designs for which the robot size is important and the mechanism has to work in a small space, the required number of actuators plays an important role in minimizing the final size of the robot. Therefore, the smaller the number of actuators, the more control the designer has over the size of the robot to target smaller dimensions. The R-R-S-S mechanism is a non-overconstrained spatial four-bar linkage with mobility equal to one. This mechanism is regularly used for instance for function generation.

In the present work, for designing an RRSS mechanism, the first step is to synthesize an RR chain based on the design objective, mainly the positions that the system must reach which was explained before.

A spherical joint S can be expressed using dual quaternions as:

$$\hat{S}(\alpha) = \alpha_0 + \begin{Bmatrix} \alpha_1 \\ \alpha_2 \\ \alpha_3 \end{Bmatrix} + \epsilon \begin{Bmatrix} c_x \\ c_y \\ c_z \end{Bmatrix} \times \begin{Bmatrix} \alpha_1 \\ \alpha_2 \\ \alpha_3 \end{Bmatrix} \quad (9)$$

Where the position of the center point of the joint is $C = [C_x, C_y, C_z]$ and α contains the rotation components. When the SS chain is attached to the RR chain to form the RRSS linkage, the SS will have the same relative displacement as the RR chain. Consider the relative motion in dual quaternion form $\hat{P}_{12} = P_0 + P_1i + P_2j + P_3k + \epsilon (P_4i + P_5j + P_6k + P_7)$. The relation between S joints and relative motion shows in Equation 10. In this equation (α) and (β) are rotation components that belong to first and second S joint respectively.

$$\hat{S}_2(\beta) = \hat{S}_1^*(\alpha) \hat{P}_{12} \quad (10)$$

Finally, we impose that the SS chain goes to the desired positions in Equation 11. In this equation, the determinant of the 8×8 matrix M has to be zero (not a full rank). Thus, Equation 12

would be a condition for the S joints in the RRSS mechanism to reach the same relative position as the RR chain.

$$\begin{bmatrix} p_0 & p_3 & -p_2 & -p_1 & 1 & 0 & 0 & 0 \\ -p_3 & p_0 & p_1 & -p_2 & 0 & 1 & 0 & 0 \\ p_2 & -p_1 & p_0 & -p_3 & 0 & 0 & 1 & 0 \\ -p_1 & -p_2 & -p_3 & -p_0 & 0 & 0 & 0 & 1 \\ c_{1y}p_2 + c_{1z}p_3 + p_7 & -c_{1z}p_0 - c_{1x}p_2 + p_6 & c_{1y}p_0 - c_{1x}p_3 - p_5 & -p_4 & 0 & -c_{2z} & c_{2y} & 0 \\ c_{1z}p_0 - c_{1y}p_1 - p_6 & c_{1x}p_1 + c_{1z}p_3 + p_7 & -c_{1x}p_0 - c_{1y}p_3 + p_4 & -p_5 & c_{2z} & 0 & -c_{2x} & 0 \\ -c_{1y}p_0 - c_{1z}p_1 + p_5 & c_{1x}p_0 - c_{1z}p_2 - p_4 & c_{1x}p_1 + c_{1y}p_2 + p_7 & -p_6 & -c_{2y} & c_{2x} & 0 & 0 \\ -c_{1z}p_2 + c_{1y}p_3 - p_4 & c_{1z}p_1 - c_{1x}p_3 - p_5 & -c_{1y}p_1 + c_{1x}p_2 - p_6 & -p_7 & 0 & 0 & 0 & 0 \end{bmatrix} \begin{Bmatrix} \alpha_1 \\ \alpha_2 \\ \alpha_3 \\ \alpha_4 \\ \beta_1 \\ \beta_2 \\ \beta_3 \\ \beta_4 \end{Bmatrix} = \mathbf{0} \quad (11)$$

$$\det[M] = 0 \quad (12)$$

In the RRSS mechanism, by coupling the RR chain with two S joints, the degree of freedom of the system would be equal two which one of them being the idle rotation about the link connecting the two spherical joints. So, the RRSS mechanism will have just one degree of freedom. This helps to minimize the number of required actuators for the mechanism. Fig. 71 shows the final design for this mechanism with 5 RRSS closed linkages, which is designed for grasping a mobile phone.

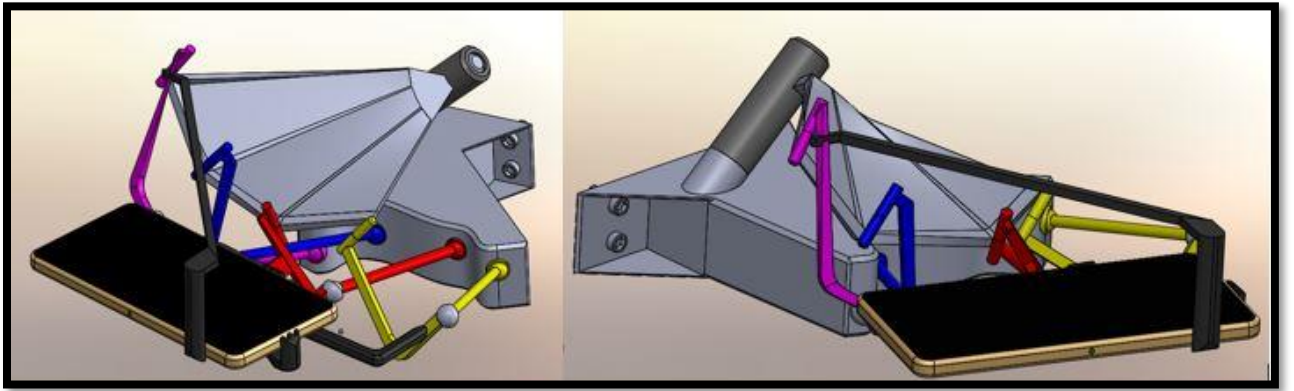


Figure 69: Mechanism with 5 RRSS chains designed for grasping a mobile phone

6.5 Singularity Design for RRSS Mechanism

Any closed-loop chain can be characterized as having input and output joint angles, which are represented with n-dimensional vectors θ_{in} and i-dimensional vectors θ_{out} respectively. These input and output vectors are related to each other according to the overall number of degrees of freedom of the system.

One of the methods to characterize singularities [92] is using loop closure equations. This is shown in Equation 13.

$$[J][\dot{\theta}_{in}] = [J^*][\dot{\theta}_{out}] \quad (13)$$

In general, there are three types of singularities, which can occur separately or simultaneously [1].

For the first type of singularity,

$$[\dot{\theta}_{in}] = 0 \quad \& \quad [\dot{\theta}_{out}] \neq 0 \quad (14)$$

Therefore:

$$\det[J^*] = 0 \quad (15)$$

The second type of singularity happens when,

$$[\dot{\theta}_{out}] = 0 \quad \& \quad [\dot{\theta}_{in}] \neq 0 \quad (16)$$

Therefore:

$$\det[J] = 0 \quad (17)$$

Finally, the third type of singularity is a combination of first and second types of singularity.

In other words, $\det[J] = \det[J^*] = 0$ or both matrices J and J^* become singular at the same time

[92]. The present work focuses on an RRSS linkage, a single-loop mechanism. Fig. 72, shows a single RRSS closed chain.

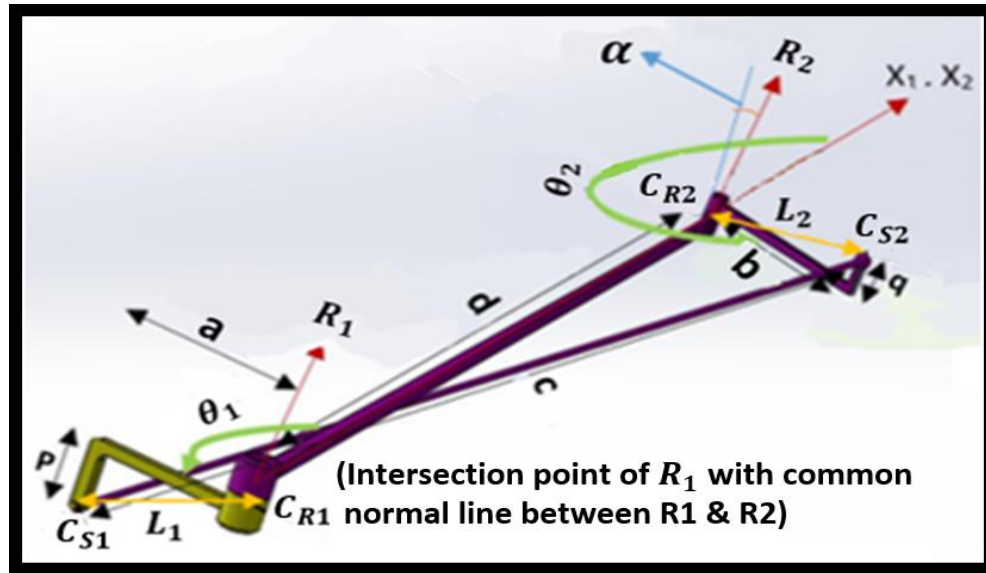


Figure 70: Single RRSS chain

As it was stated before, the RR chain is designed for a given task and later will be coupled by the SS. That means that RR parameters (Plucker coordinates (R_1, R_2) , twist angle α , the distance between R joints d) are known. However, locations of S joints and input/output angles (θ_1, θ_2) are unknown. To calculate the closure equation for this mechanism, we create a distance constraint by taking the two paths originating from joint R_1 . Equation 18 shows the transformation needed to reach C_{S1} (the center point of first S joint) from R_1 in the global coordinate. In the following equation, R and T represent rotation and translation along common normal lines in a homogeneous format respectively.

$$C_{S1} = [G][R_{\theta_1}][T_{\alpha}][T_p] \begin{Bmatrix} 0 \\ 0 \\ 0 \\ 1 \end{Bmatrix} \quad (18)$$

In which $[G]$ is a transformation from the first revolute joint (R_1) coordinate, where we considered our local frame origin, to the global coordinate. The same procedure applies to the right leg starting from R_1 and leading to the location of the point C_{s2} (the center point of second S joint):

$$C_{s2} = [G][T_d][R_\alpha][R_{\theta_2}][T_b][T_q] \begin{Bmatrix} 0 \\ 0 \\ 0 \\ 1 \end{Bmatrix} \quad (19)$$

Having the coordinates of the two spherical joints in terms of the structural parameters and joint variables of the mechanism, the final loop closure can be formulated as Equation 20, where c^2 is the square of the length of the link between the two spherical joints, which can be computed by the difference between the location of the center point of S joints from the left and right legs, Equations 18 and 19.

$$F = (C_{s1} - C_{s2}) \cdot (C_{s1} - C_{s2}) - c^2 = 0 \quad (20)$$

Therefore, loop closure in Equation 21 is computed as a function of (a, b, c, p, q) which are link lengths and the input and output angles (θ_1 and θ_2). Singularity equations for type 1 and type 2 can be found from Equations 22 and 23 where the output and input velocity is not zero respectively. Any solution to (Equation 21) and one of Equations 22 or 23 forces the mechanism to be singular at a particular point.

$$F(\theta_1, \theta_2, a, b, p, q, c) = 0 \quad (21)$$

$$\frac{\partial F}{\partial \theta_2} = 0 \quad (22)$$

$$\frac{\partial F}{\partial \theta_1} = 0 \quad (23)$$

For each particular value for θ_1 , we create a singular pose for which two equations need to be satisfied. We can keep adding these singular points up to the maximum number of singularities

for the linkage. In the present work, the equations are solved for two singular poses for which we can write the following set of equations:

$$\theta_{11} => \begin{cases} F(\theta_{21}, a, b, p, q, c) = 0 \\ \frac{\partial F}{\partial \theta_1}(\theta_{21}, a, b, p, q, c) = 0 \end{cases} \quad (24)$$

$$\theta_{12} => \begin{cases} F(\theta_{22}, a, b, p, q, c) = 0 \\ \frac{\partial F}{\partial \theta_1}(\theta_{22}, a, b, p, q, c) = 0 \end{cases} \quad (25)$$

Adding Equations 12 to 25 provides a system of equations whose solution is an RRSS mechanism with two specified singular poses and a workspace which includes the poses that the RR chain was synthesized for. We transform the design into an optimization problem whose objective function, G , is the sum of the squares of the lengths of all links (except “d” as it was calculated in the RR synthesis step) to have some control over the total size of the mechanism. Equation 26 shows this objective function. This objective function was chosen to design a mechanism with the most appropriate size.

$$G = a^2 + b^2 + p^2 + q^2 + c^2 \quad (26)$$

6.6 Solution Procedure and a Numerical Example

For designing a single RRSS chain and to show that the proposed method can be applied to any arbitrary RRSS, we start with selecting two random task positions and find the appropriate RR chain for these points from synthesis. Two task positions and two points on the axis of R joints are included in Table 19. Also, the Plucker coordinates for each of the R joints are shown in Table 20. Then we can couple this RR chain with an SS linkage under the conditions mentioned in Equation 12 for S joints.

Table 19: Two task positions and two points on each R joint axis

Parameters	X(cm)	Y(cm)	Z(cm)
Task Position	5.2	-7	-3
Task Position	0	-3.75	.4
Axis of R Joint 1- Point 1	-7.02	20.73	-1.63
Axis of R Joint 1- Point 2	-7.65	20.49	-2.24
Axis of R Joint 2- Point 1	-8.07	-0.10	-0.36
Axis of R Joint 2- Point 2	-10.46	4.38	6.85

Table 20: Plucker coordinates for the R joints

Joints	\mathcal{S}	\mathcal{S}^0
1st R Joint	-0.70, -0.26, -0.67	-14.32, -3.57, 16.23
2nd R Joint	-0.27, 0.51, 0.82	0.095, 6.69, -4.13

For this design with two specific singular positions, we have five equations (four of them from Equations 24 & 25 plus one main condition for S joints from Equation 12), and seven unknown design parameters ($a, b, c, p, q, \theta_{21}, \theta_{22}$). All five equations are nonlinear and they will be added as equality constraints to an optimization problem. The two arbitrary input angles (θ_{11}, θ_{12}) where we want the mechanism to be singular, are selected and presented in Table 21. For solving the optimization problem, we use a genetic algorithm (ga) with an upper limit of 400 generations, Constraint Tolerance (TolCon) of $1e-6$. The objective function was defined as minimizing the sum of squares of the length of each link.

Table 21: Information about the relation between R joints and input values for θ_1 to define two singular positions

Parameters	Value (cm) or (rad)
Length of link d	18.71
Angle α	1.06
Angle θ_{11}	0.39
Angle θ_{12}	1.05

The optimization test was run 20 times and the best result based on the minimum objective function, time of the test, and the number of generations was selected. In the best result, the optimization finished after 200 generations and a total time of 170.92 s. The final value for the objective function was 454.208 cm. After finding unknown parameters, the center point for each of S joints can be found. Table 22 expresses the results for all unknown parameters and the center point of S joints.

Table 22: Result for unknown parameters and the center point of S joints for RRSS with two specified singular positions

Parameters	Value (cm) or (rad)
Length of link a	14.92
Length of link b	-7.70
Length of link p	1.81
Length of link q	-10.05
Length of link c	6.06
θ_{21}	5.55
θ_{22}	5.67
1st S Joint	-4.45, 6.58, 2.47
2nd S Joint	-2.01, 4.28, -2.57

The final design of the model is shown in Fig. 73. In this case, the finger (RR chain) is designed to move from point 1 to point 2. These two points are objective design values, which are defined for RR chain synthesis. Also, two selected singularity points for this robot are in $\theta_{11} = \pi/8$ and $\theta_{12} = \pi/3$, which would occur at points 1 and 3. Fig. 74 shows the angles for these two singularity points.

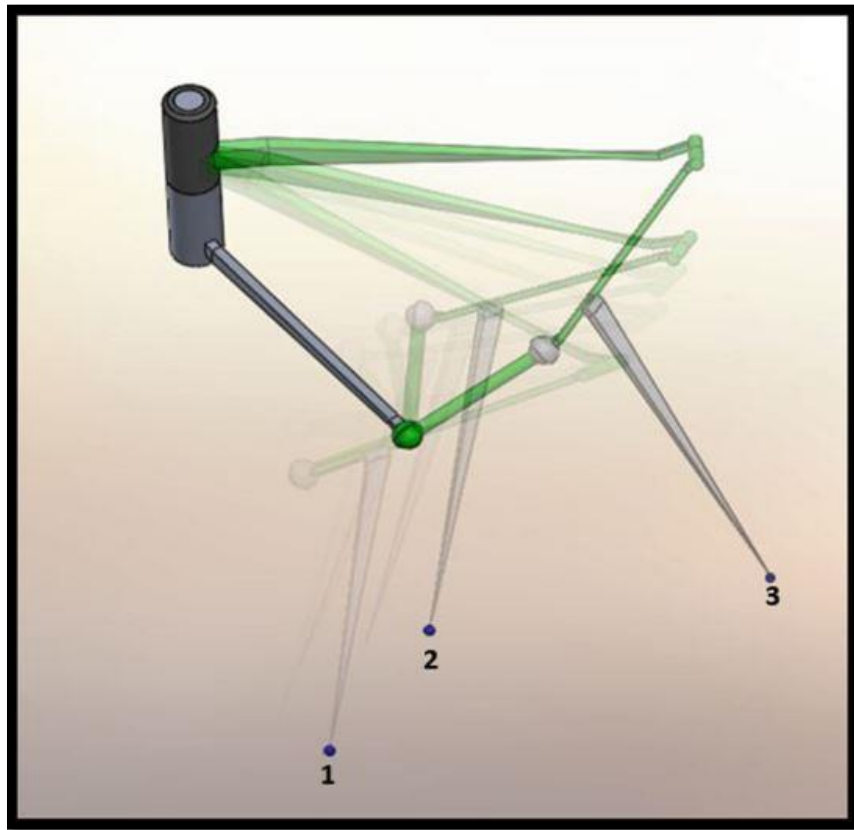


Figure 71: Motion of RRSS chain between points 1 and 2 (the points the RR chain was synthesized for) plus singular positions at point 1 and 3

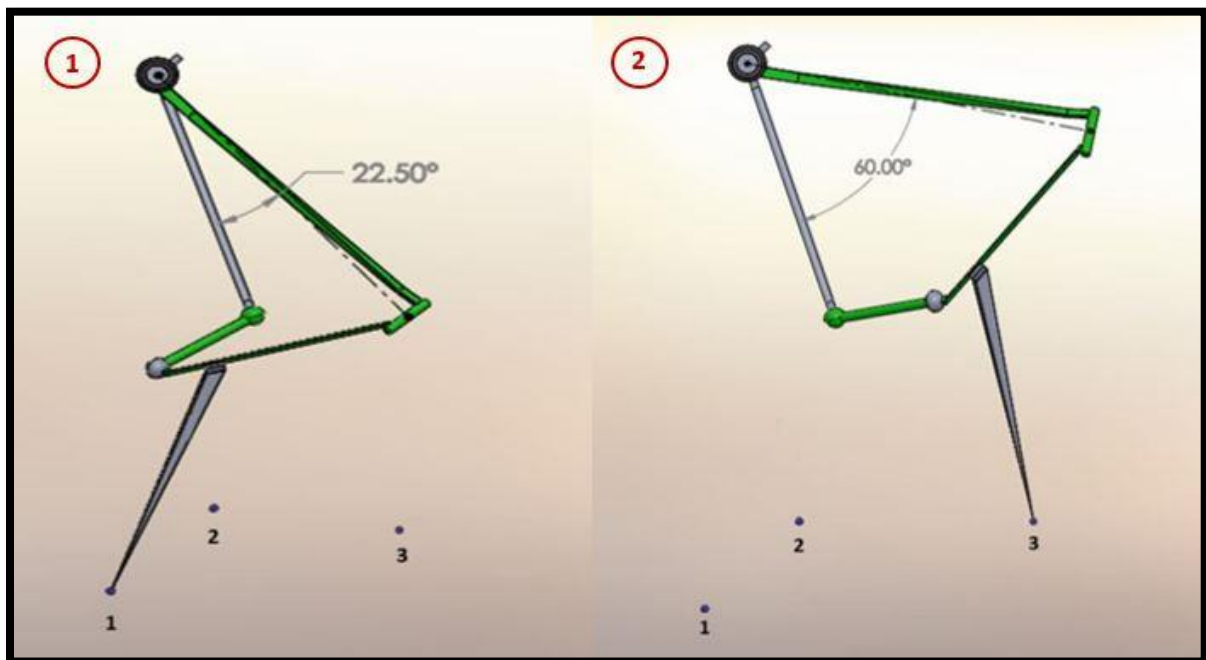


Figure 72: Angle for θ_{11} at the first singularity position (left), Angle for θ_{12} at the second singularity position (right)

The velocity of the output angle can be found from $\frac{\partial F}{\partial \theta_2} \times \frac{\partial \theta_2}{\partial t}$. In the points where the sign of the velocity changes (and velocity becomes zero), the mechanism becomes singular. Therefore, if we sketch the graph for $\frac{\partial F}{\partial \theta_2}$ respect to θ_2 for any specific θ_1 , we can find singular points for this mechanism.

Fig. 75 shows the results for the example above. From this figure, there are two possible singular points for each selected θ_1 . Also, the relation between θ_1 and θ_2 for loop closure is presented in Fig. 76, which shows just one of these singular points from Fig. 75 for each θ_1 belonging to the workspace of the robot. This coincides with the point selected to be singular. These values are mentioned in Table 23.

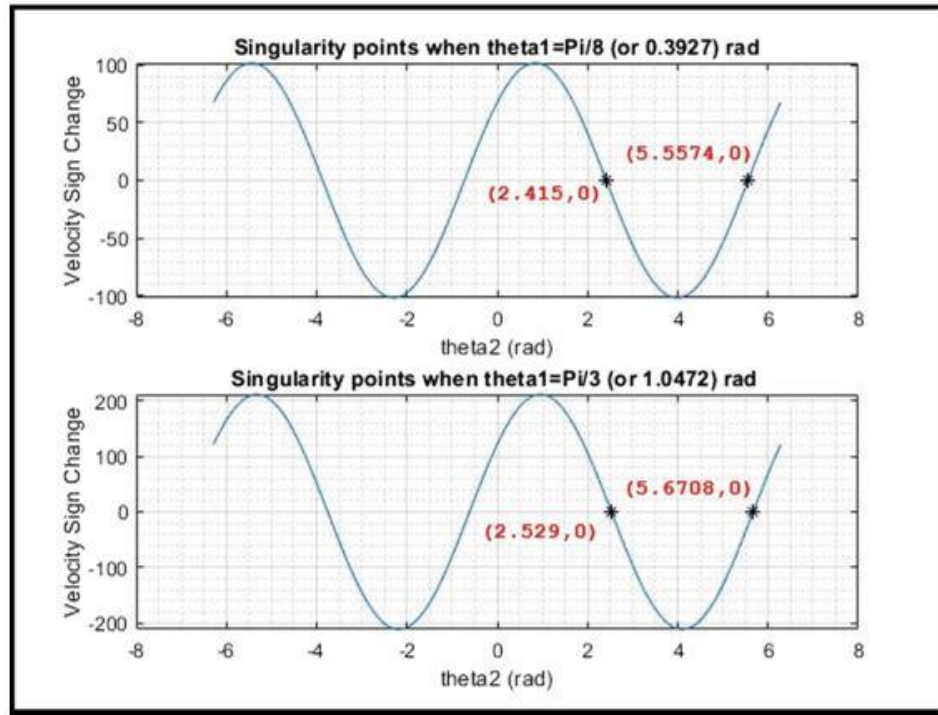


Figure 73: Possible singular points for each selected θ_1

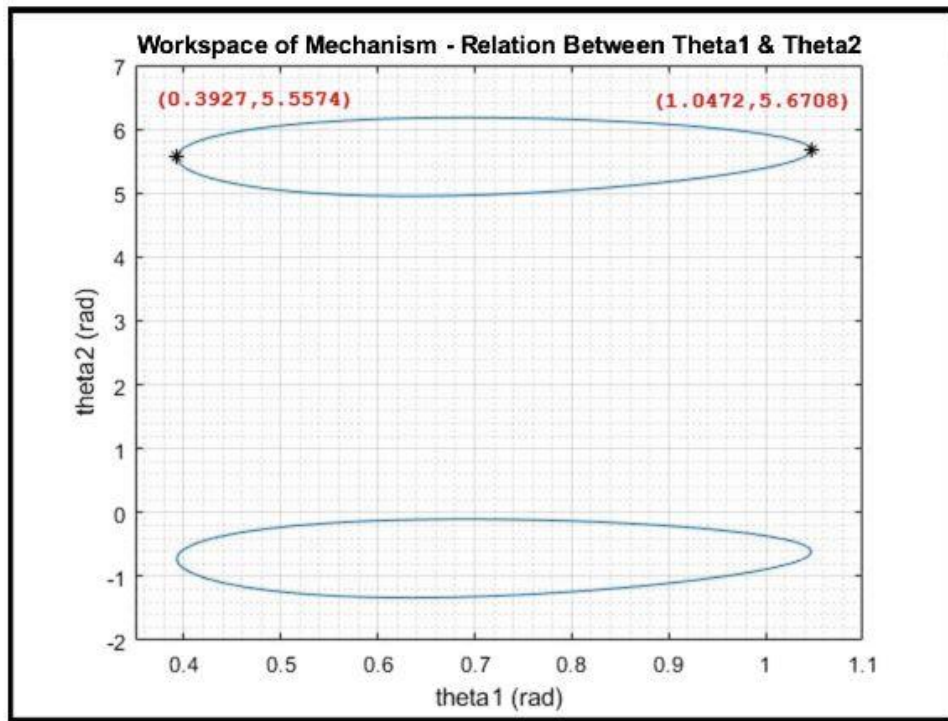


Figure 74: The relation between θ_1 & θ_2 for the loop closure

Table 23: Possible singularity points and valid one respect to work-space of robot

θ_1	θ_2	Description	Validity
0.39	2.41	Extra possible singular point	Out of Robot Workspace
0.39	5.56	Singular point defined by designer	Inside of Robot Workspace
1.05	2.52	Extra possible singular point	Out of Robot Workspace
1.05	5.67	Singular point defined by designer	Inside of Robot Workspace

* The results for designing the optimized multi-finger hand were presented and published in IFToMM Symposium on Mechanism Design for Robotics (MEDER) 2018, pages 344–352. Springer.

* The results for singularity design were presented and published in USCToMM Symposium on Mechanical Systems and Robotics (MSR) 2020, pages 287–297. Springer.

CHAPTER 7. CONCLUSIONS

The population of the world has gone from 3 billion in the 1960s to 7.7 billion in 2019. This dramatic rise in the World population has caused a food shortage around the world and right now, about 9% of the World's population (around 700 million people) are hungry [95]. This has put significant stress on agricultural capabilities. More and more farm equipment and farming methods are turning to automation and smart technologies. PVY as one of the main problems for farmers significantly affects the quantity and quality of their products and each year damage millions of dollars of products.

In this research, various parts of an autonomous system for agricultural purposes were designed and implemented. That included the design of a chassis for a prototype model, navigation system, obstacle avoidance, vision system, and roguing mechanism for this AGV. Except for these parts for designing the autonomous system, in theoretical research, a method for hand design and singularity avoidance was analyzed and formulated. Although finally the theoretical solution for hand design was not used and the roguing mechanism was preferred, to interact with the very complex systems in the agro world is needed.

In the first section, the process of chassis design for an autonomous ground robot for agriculture was discussed. First, using the Genetic Algorithm, we calculated the optimum size of the chassis and selected the best material for the application while minimizing weight. Next, we performed the force analysis of the chassis. Finally, based on possible stress on the chassis, we did seven stress analysis tests in SolidWorks, 4 bending tests, and 3 torsion tests. The maximum stress and displacement occur when two wheels in the left are assumed fixed and force was applied to the two right wheels. However, final results show this chassis is very capable and can withstand

all the possible simulated stresses. The autonomous vehicle with the above-described chassis was fully assembled and successfully was tested in a field.

The AGV designed and built in this project has an extremely accurate RTK GPS and combined with the Pixhawk navigational firmware is a suitable testing platform for an autonomous agricultural robot. The robot and components were relatively inexpensive but robust enough to handle typical terrains the robot will be operational in. Since it uses the Pixhawk it is extremely customizable as well. These features, along with obstacle avoidance in the future, make it extremely useful not just for this project but for many agricultural robot applications.

Because of error in GPS finding the center of a sick plant with just using GPS is impossible. Thus, for finding the exact location of the sick plant, we will combine the results from GPS coordinate with results from an image processing algorithm to find the exact center of the target plant. However, because this image processing algorithm supposed to use in the potato field and for a wide range of green colors, the HSL format was the most proper format for detecting the target object. We found a proper range for H, L, and S for detecting the target object. Also, we defined two different algorithms for finding the center of a sick plant, and the best one was selected.

A novel mechanism for a roguing system was designed. Multiple designs, grasping types were considered, all relevant mechanisms were analyzed, and three mechanisms based on primary analysis were considered for the study. On comparing the advantages and disadvantages of each of these three options, the final mechanism was designed utilizing the best combination of each design's strengths and capabilities. Although this mechanism is designed to work in a potato field due to its versatility and ease of coupling to various tractors or farm equipment, it could potentially be used for roguing other crops and work in different environments.

Next, a prototype was built to 1/3rd scale of the actual model and successfully tested for motion and it performed exceptionally well to achieve the desired results. In the near future, we are going to build a real-sized model to test it in the potato field. Also, a connection part for attaching roguing mechanism to the tractors' three-point hitch was designed.

As a theoretical part of this research, the last section of the present work is an attempt to further investigate the implementation of nonstandard robotic hands designed for specific tasks. In most cases, they present skew axes that increase the complexity when designing detailed parts and transmissions. In particular, a linkage-based transmission for underactuated hands with skew axes is studied. This consists of coupling the R-R joint corresponding to the wrist joint and finger joint with an S-S mechanism, creating a 1-dof system that can be actuated at the joint. The RRSS linkage allows enough flexibility to be able to state the design problem as an optimization problem to obtain optimum values for length, placement, and obstacle avoidance.

Then a general method for defining the singularity points in RRSS closed linkage was found and an RRSS with known singular poses was designed by coupling an SS chain to an already-synthesized RR chain. A constraint equation and the singularity condition of type one have been utilized to specify singular poses. These equations are populated by new values for the input angle to create a system of design equations whose solution is a mechanism with desired singular poses. The method has been validated by a numerical example and simulation. Future work will explore generalizing the concept for other closed linkages.

Most of the parts in this stage are designed in prototype form and smaller scale than the final model. In the next step, they need to be built in the real size, assemble and attach, and test the final complete autonomous system in a potato field.

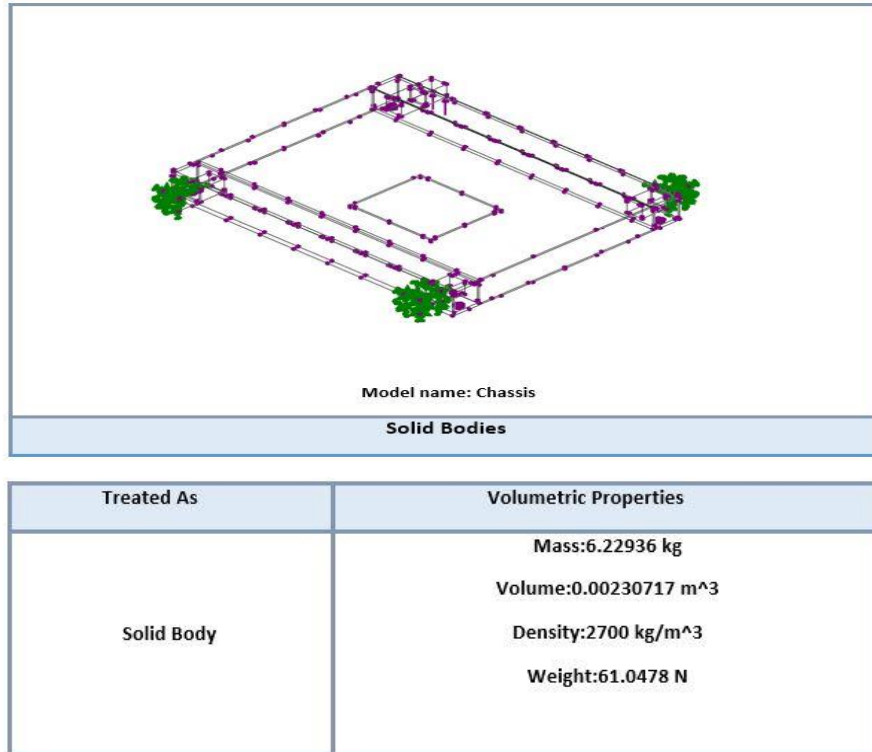
Generally, before this project, farmers used the traditional method of detection and removal PVY by sending specialists to the potato fields which according to the expanse of a potato field, that was not an efficient method. The final goal of this project was to increase the accuracy of detection and speed of removal the sick plants from the field. Based on these requirements and considering the potato field conditions, different parts of a AGV was designed and implemented. That was includes an optimized chassis, a navigation and obstacle avoidance system, an innovative image processing algorithm and robot vision system for sick plant detection and a novel roguing mechanism for sick plant extraction plus finding a new method for singularity design for mechanisms. Outcome of this research had been including one provisional patent and four published conference papers, one conference paper under reviewed, and three journal papers in preparation.

APPENDIX

A. STRESS ANALYSIS FOR CHASSIS

Test 1: One wheel bending analysis

Model Information



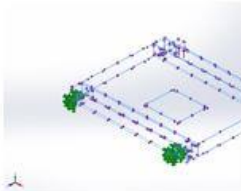
Units

Unit system:	SI (MKS)
Length/Displacement	mm
Temperature	Kelvin
Angular velocity	Rad/sec
Pressure/Stress	N/m ²


Study Properties

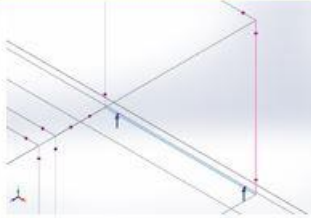
Study name	Test1
Analysis type	Static
Mesh type	Solid Mesh
Thermal Effect:	On
Thermal option	Include temperature loads
Zero strain temperature	298 Kelvin
Include fluid pressure effects from SOLIDWORKS Flow Simulation	Off
Solver type	FFEPlus
Inplane Effect:	Off
Soft Spring:	Off
Inertial Relief:	Off
Incompatible bonding options	Automatic
Large displacement	Off
Compute free body forces	On
Friction	Off
Use Adaptive Method:	Off

Material Properties

Model Reference	Properties	Components
	Name: 6061 Alloy	Chassis
	Model type: Linear Elastic Isotropic	
	Yield strength: 5.51485e+007 N/m ²	
	Tensile strength: 1.24084e+008 N/m ²	
	Elastic modulus: 6.9e+010 N/m ²	
	Poisson's ratio: 0.33	
	Mass density: 2700 kg/m ³	
	Shear modulus: 2.6e+010 N/m ²	
	Thermal coefficient: 2.4e-005 /Kelvin	

Loads and Fixtures

Fixture name	Fixture Image	Fixture Details		
Fixed-1		Entities: 9 face(s)		
		Type: Fixed Geometry		
Resultant Forces				
Components	X	Y	Z	Resultant
Reaction force(N)	-0.00386631	-192.31	0.0102177	192.31
Reaction Moment(N.m)	0	0	0	0

Load name	Load Image	Load Details		
Force-1		Entities: 1 edge(s) Reference: Edge< 1 > Type: Apply force Values: ---, ---, 192.3 N		

Mesh information

Mesh type	Solid Mesh
Mesher Used:	Standard mesh
Automatic Transition:	Off
Include Mesh Auto Loops:	Off
Jacobian points	4 Points
Element Size	0.831685 in
Tolerance	0.0415842 in
Mesh Quality Plot	High

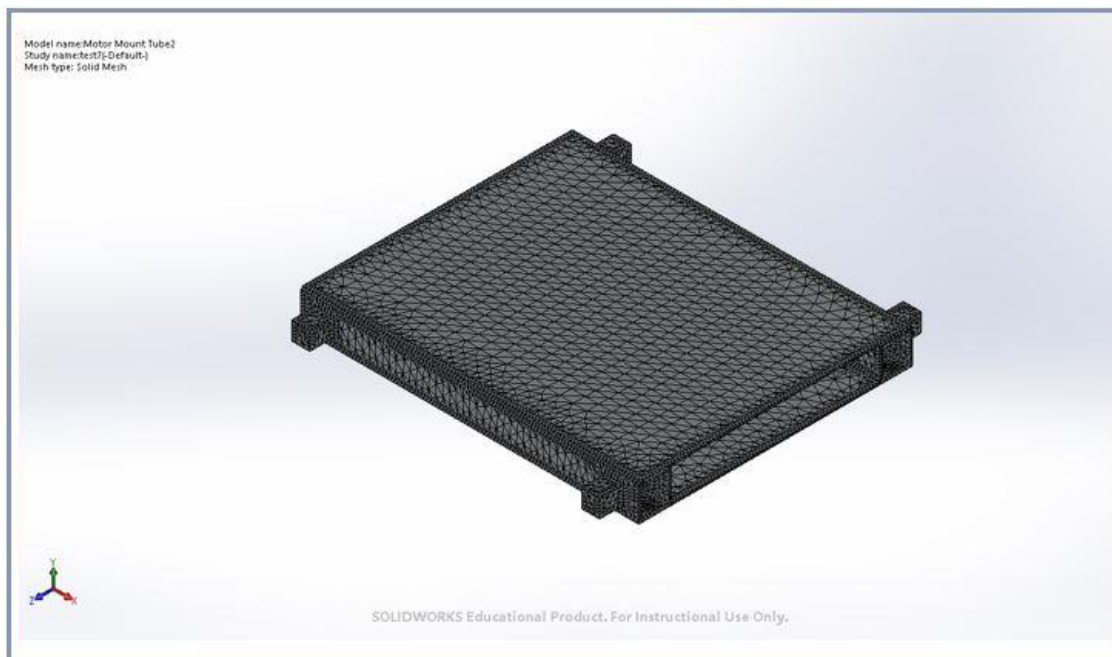
Resultant Forces

Reaction forces

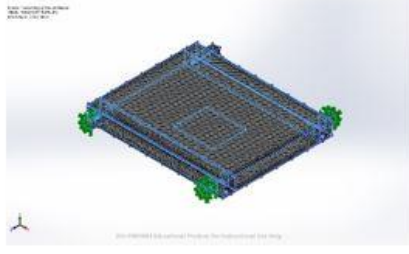
Selection set	Units	Sum X	Sum Y	Sum Z	Resultant
Entire Model	N	-0.00386631	-192.31	0.0102177	192.31

Mesh information – Details

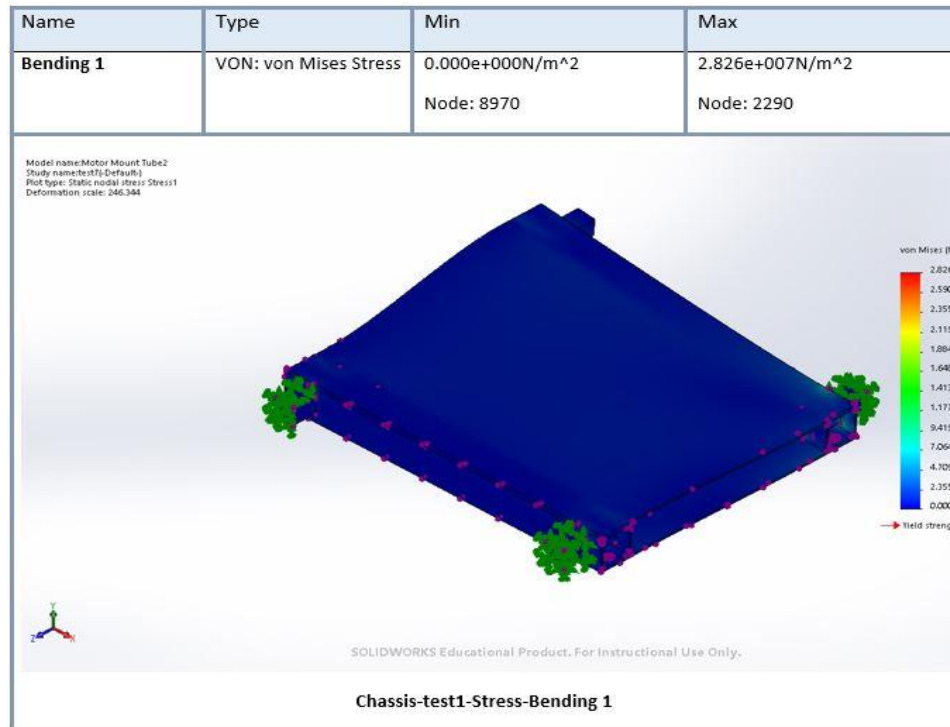
Total Nodes	79959
Total Elements	41264
Maximum Aspect Ratio	13.933
% of elements with Aspect Ratio < 3	66.4
% of elements with Aspect Ratio > 10	0.172
% of distorted elements(Jacobian)	0
Time to complete mesh(hh:mm:ss):	00:00:11

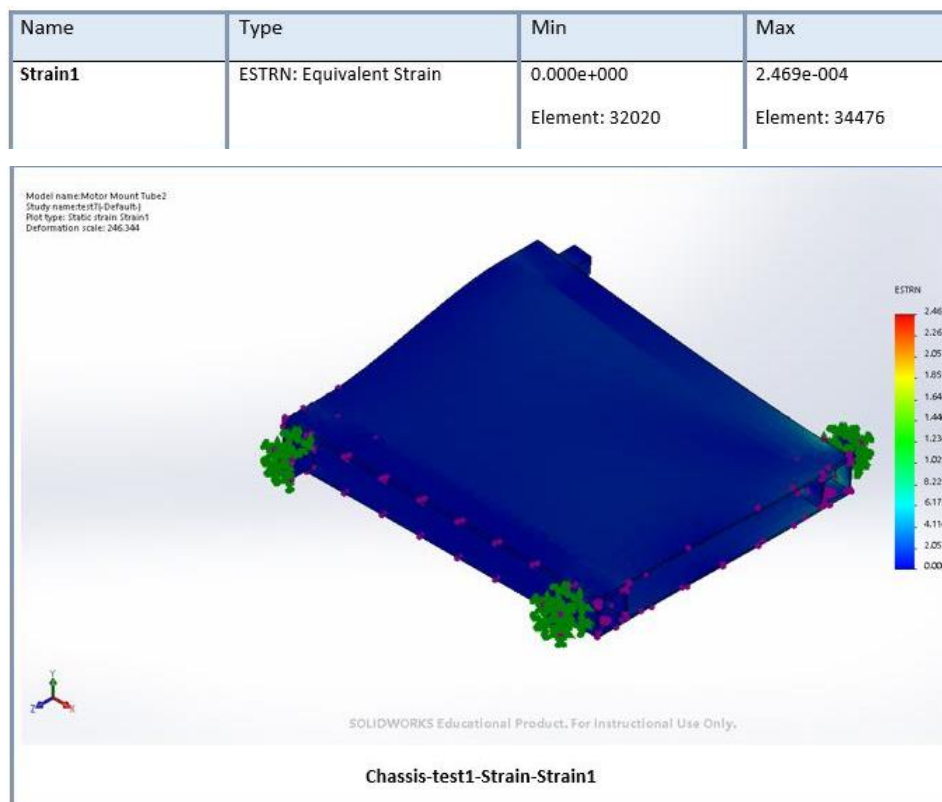
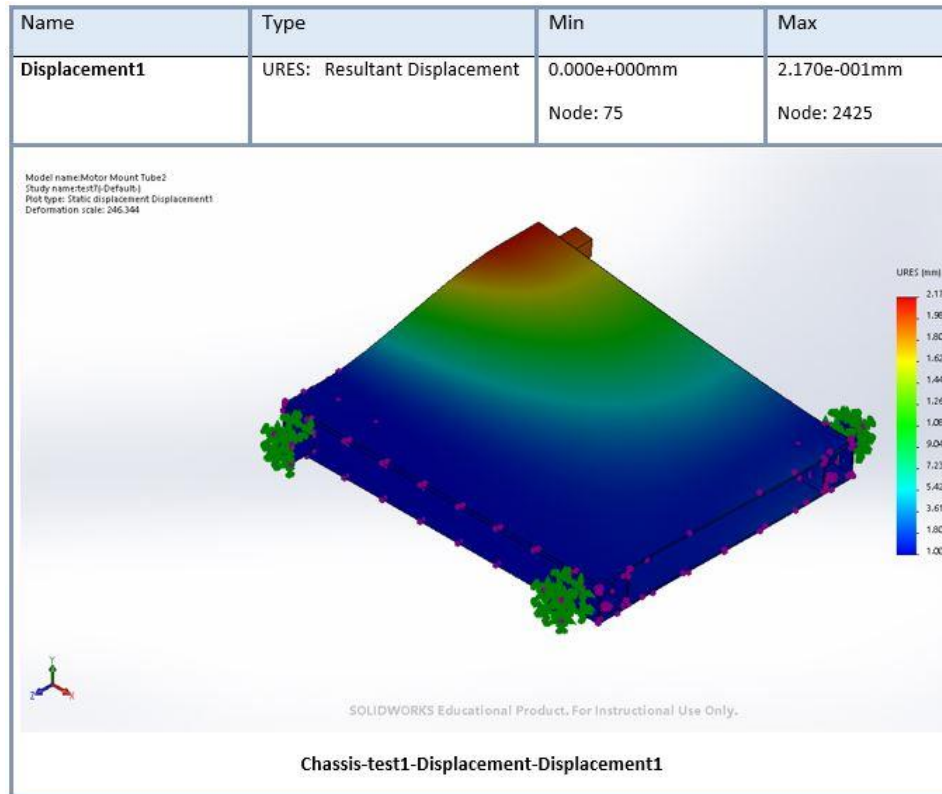


Mesh Control Information

Mesh Control Name	Mesh Control Image	Mesh Control Details
Control-1		<p>Entities: 177 edge(s)</p> <p>Units: in</p> <p>Size: 0.2</p> <p>Ratio: 1.5</p>

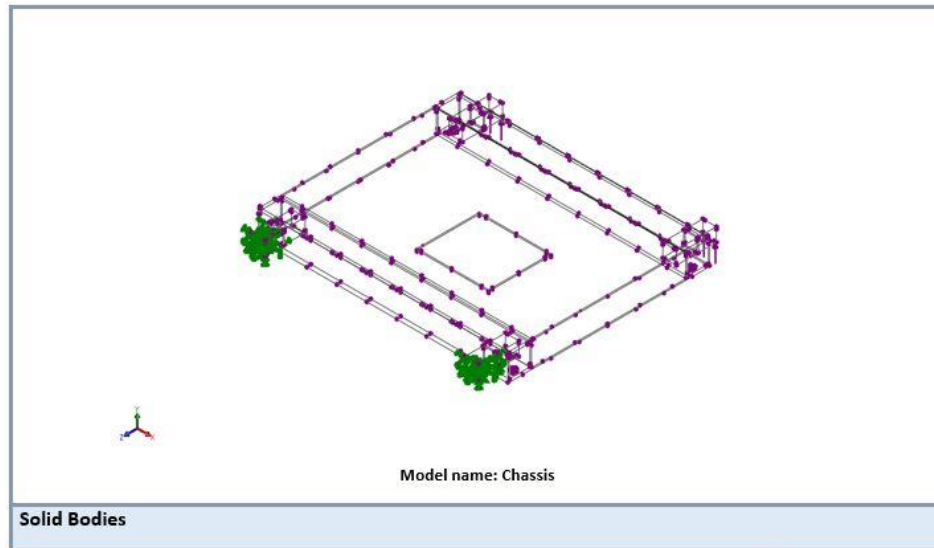
Study Results



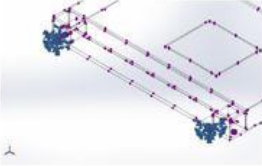


Test 2: Right- left bending analysis

Model Information



Loads and Fixtures

Fixture name	Fixture Image	Fixture Details
Fixed-1		Entities: 6 face(s) Type: Fixed Geometry

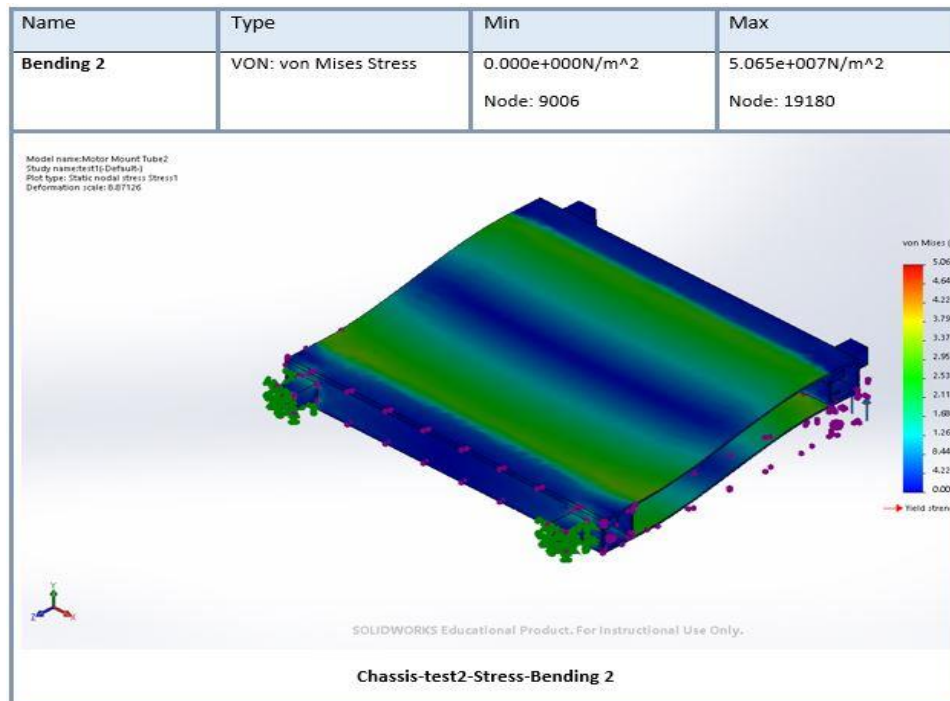
Resultant Forces				
Components	X	Y	Z	Resultant
Reaction force(N)	0.0973787	-384.564	-0.193329	384.564
Reaction Moment(N.m)	0	0	0	0

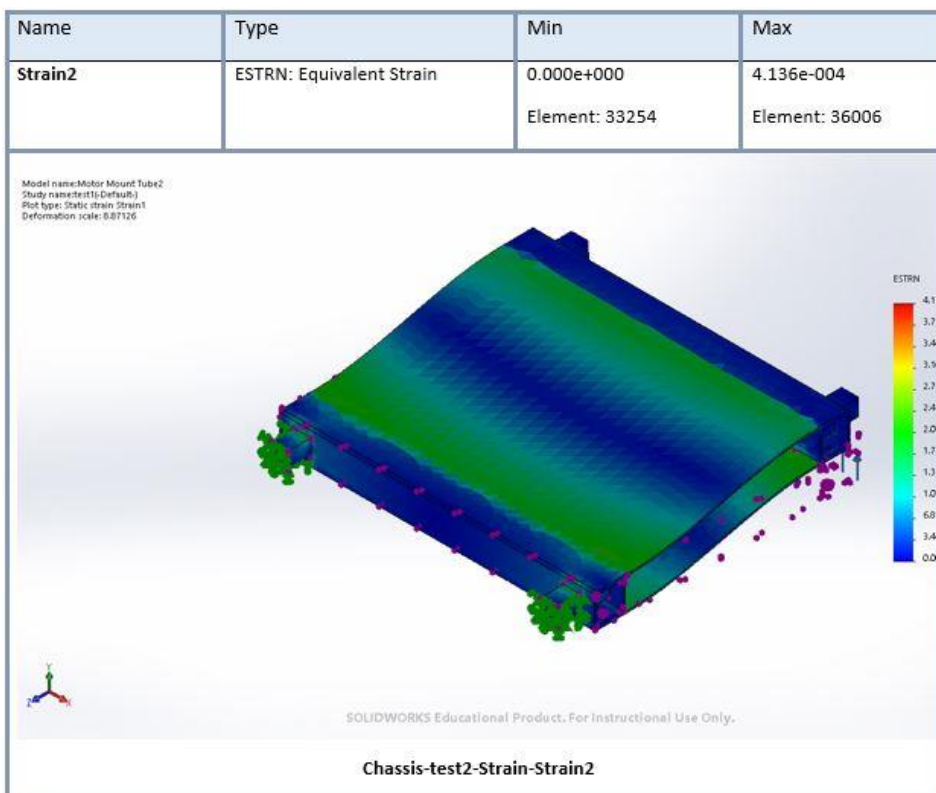
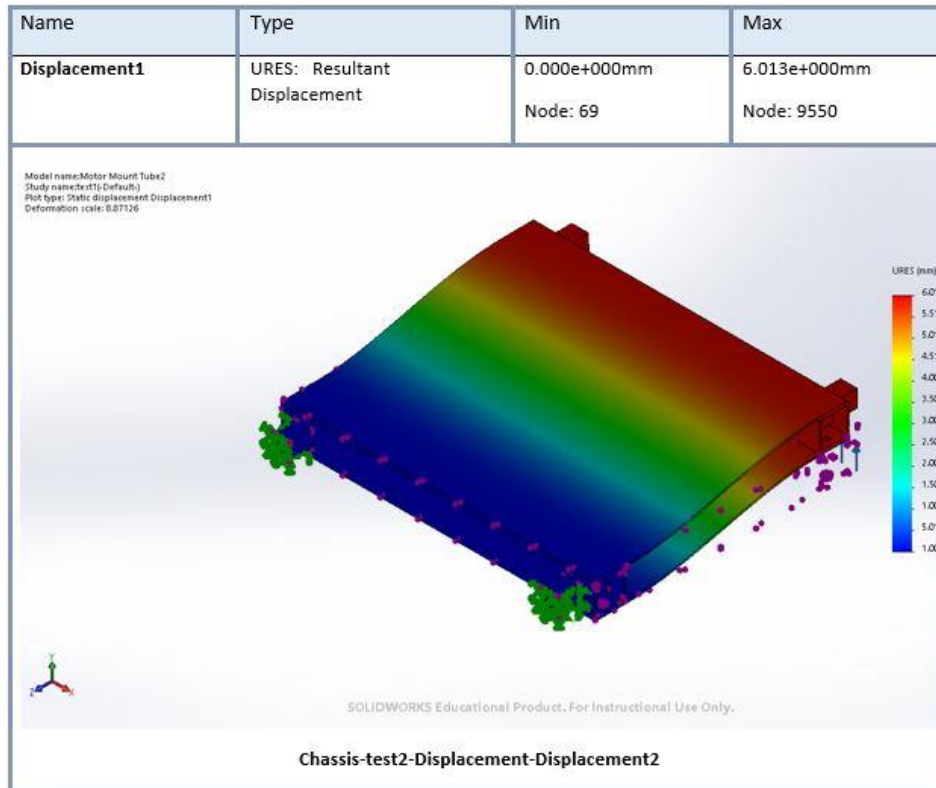
Resultant Forces

Reaction forces

Selection set	Units	Sum X	Sum Y	Sum Z	Resultant
Entire Model	N	0.0973787	-384.564	-0.193329	384.564

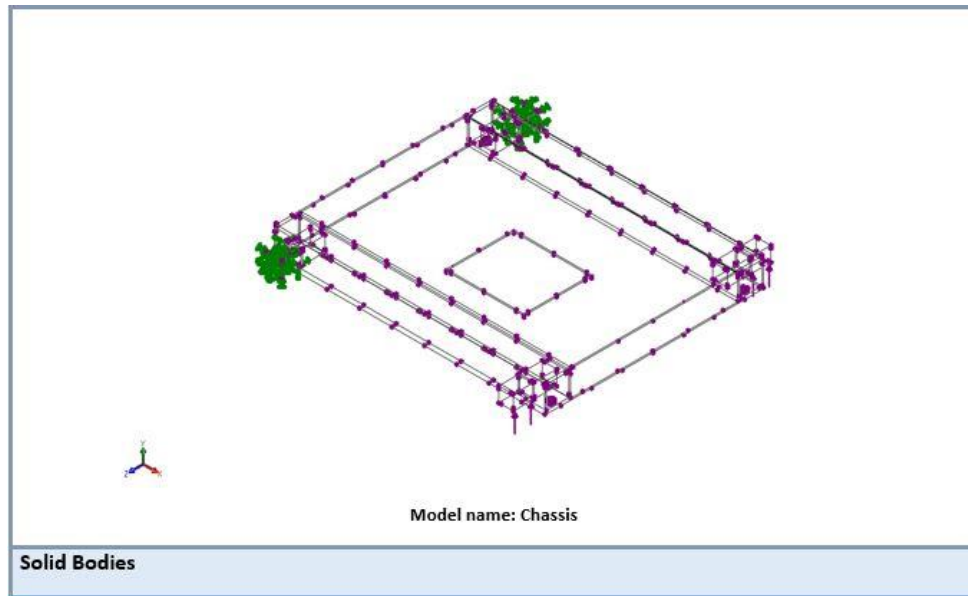
Study Results



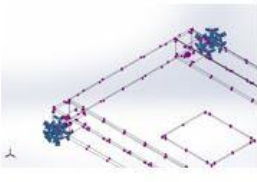


Test 3: Front- back bending analysis

Model Information



Loads and Fixtures

Fixture name	Fixture Image	Fixture Details
Fixed-1		Entities: 6 face(s) Type: Fixed Geometry

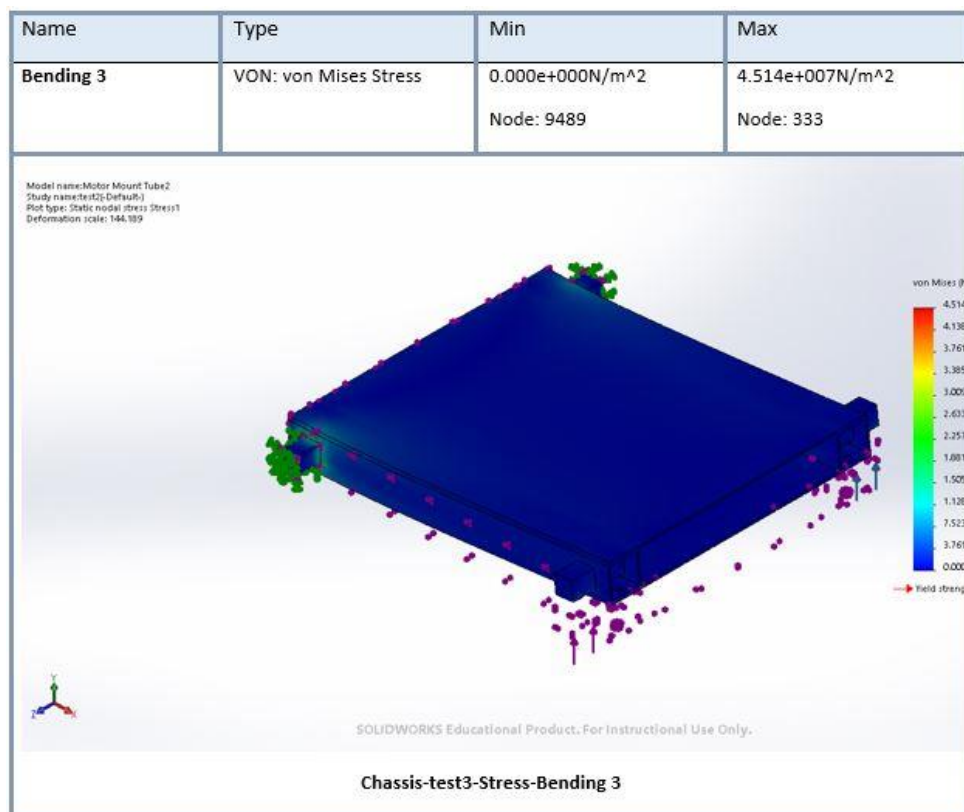
Resultant Forces				
Components	X	Y	Z	Resultant
Reaction force(N)	-0.0243378	-384.679	0.0522804	384.679
Reaction Moment(N.m)	0	0	0	0

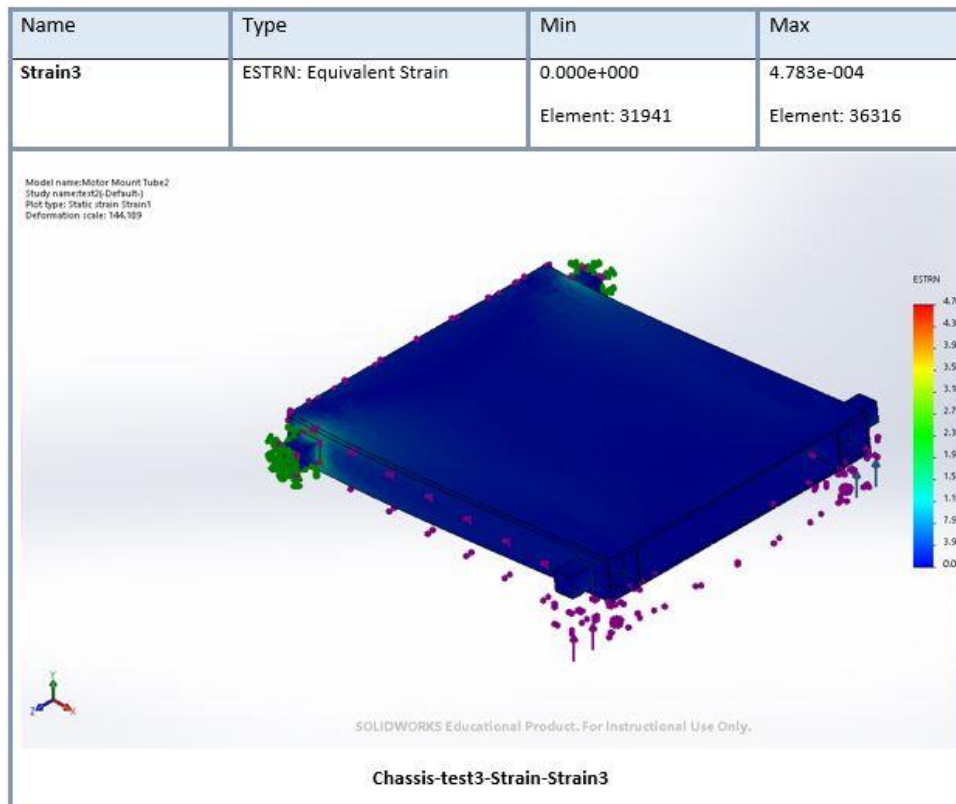
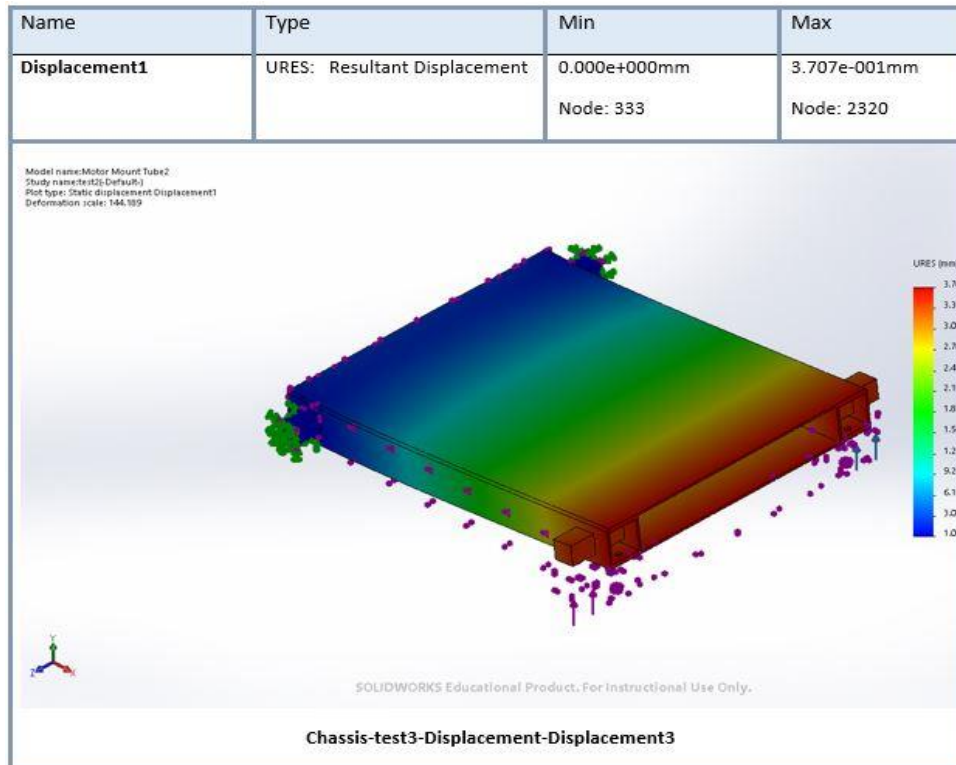
Resultant Forces

Reaction forces

Selection set	Units	Sum X	Sum Y	Sum Z	Resultant
Entire Model	N	-0.0243378	-384.679	0.0522804	384.679

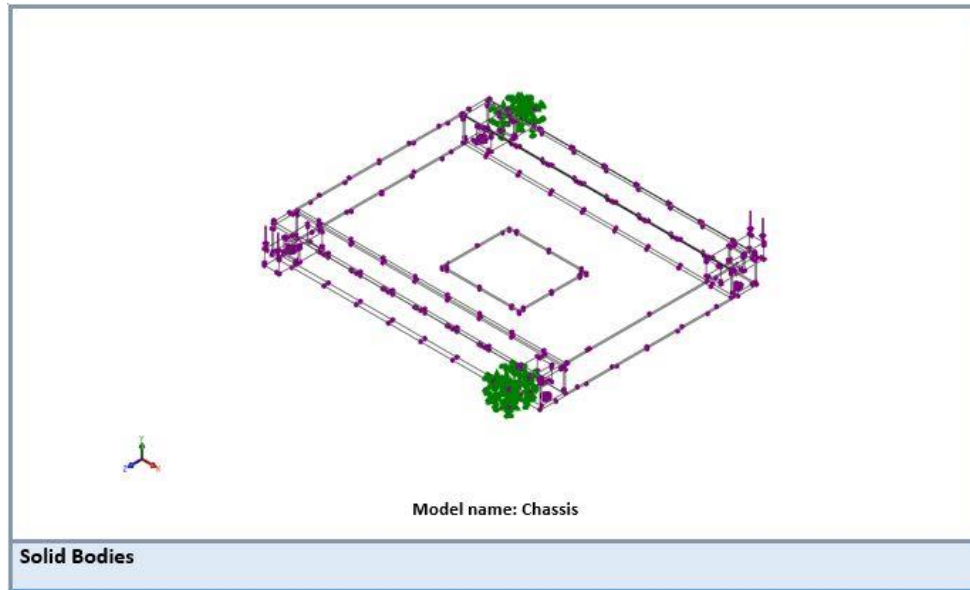
Study Results



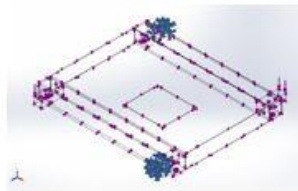


Test 4: Cross wheels bending analysis

Model Information



Loads and Fixtures

Fixture name	Fixture Image	Fixture Details
Fixed-1		Entities: 6 face(s) Type: Fixed Geometry

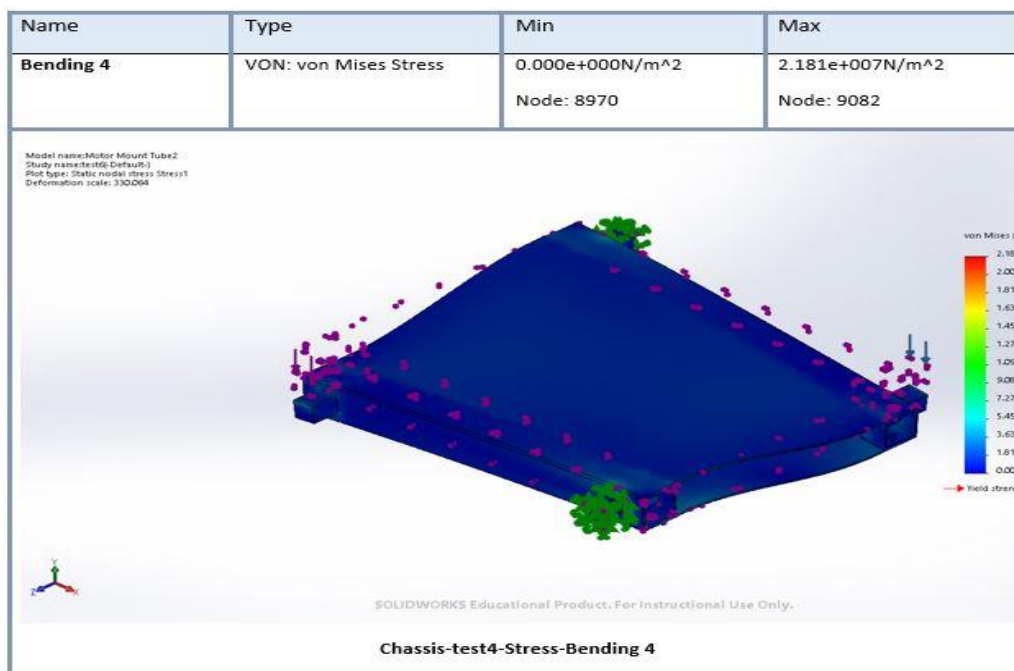
Resultant Forces				
Components	X	Y	Z	Resultant
Reaction force(N)	-0.00495148	384.576	-0.00206041	384.576
Reaction Moment(N.m)	0	0	0	0

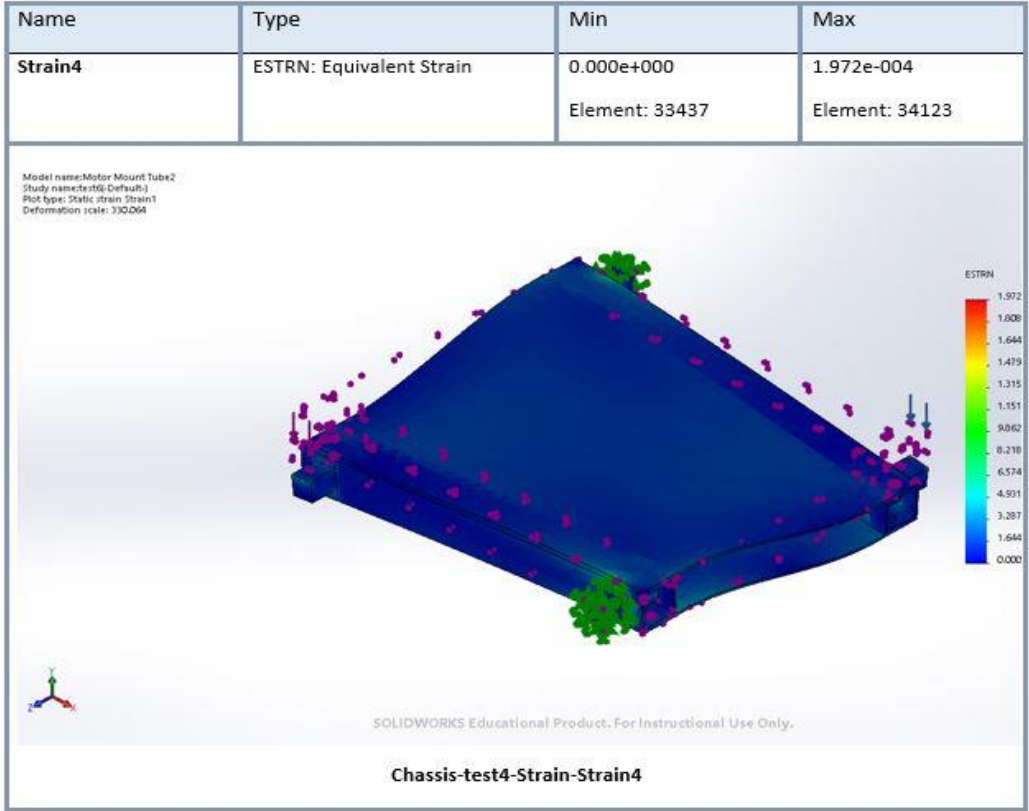
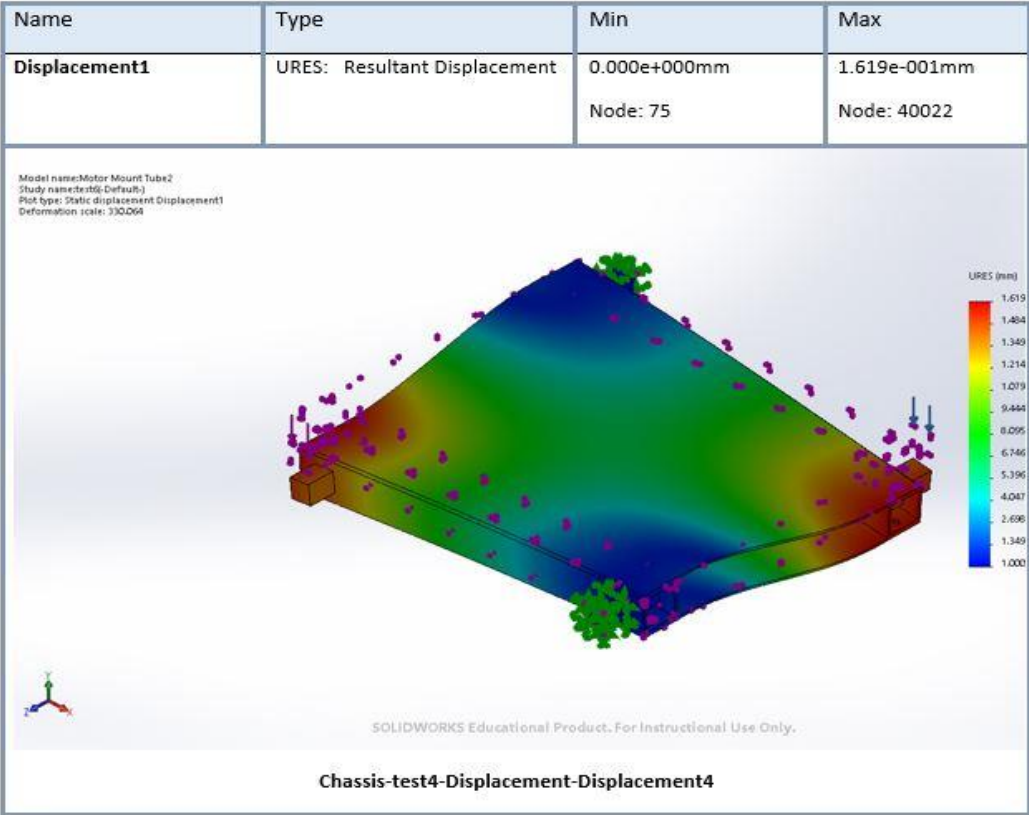
Resultant Forces

Reaction forces

Selection set	Units	Sum X	Sum Y	Sum Z	Resultant
Entire Model	N	-0.00495148	384.576	-0.00206041	384.576

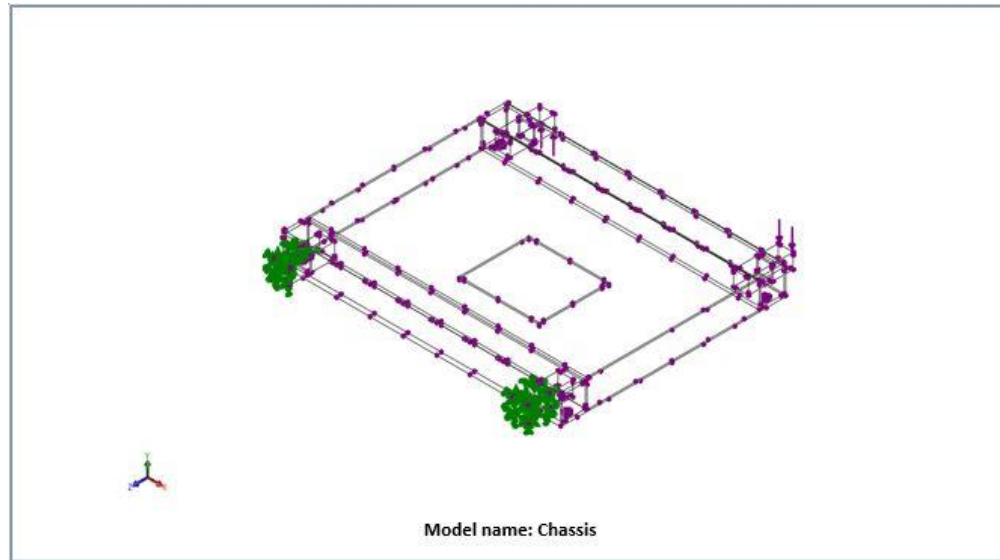
Study Results



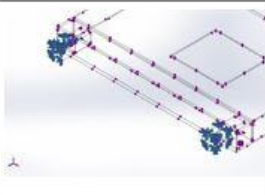


Test 5: Right- left torsion analysis

Model Information



Loads and Fixtures

Fixture name	Fixture Image	Fixture Details
Fixed-1		Entities: 6 face(s) Type: Fixed Geometry

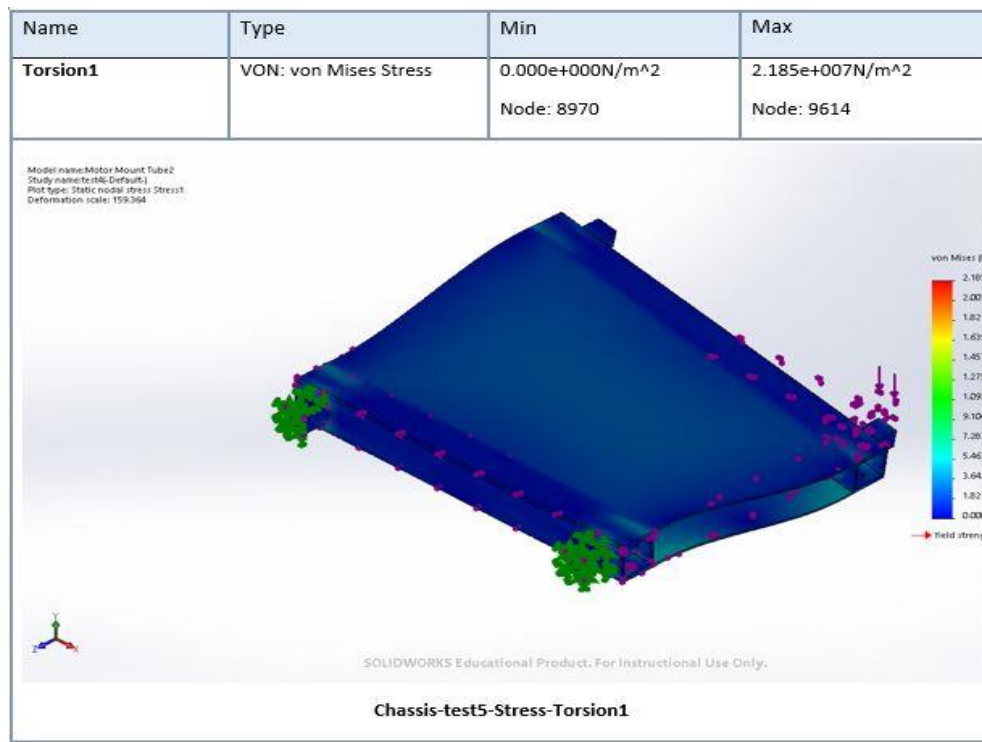
Resultant Forces				
Components	X	Y	Z	Resultant
Reaction force(N)	0.0036397	0.00279236	0.00056076	0.00462159
Reaction Moment(N.m)	0	0	0	0

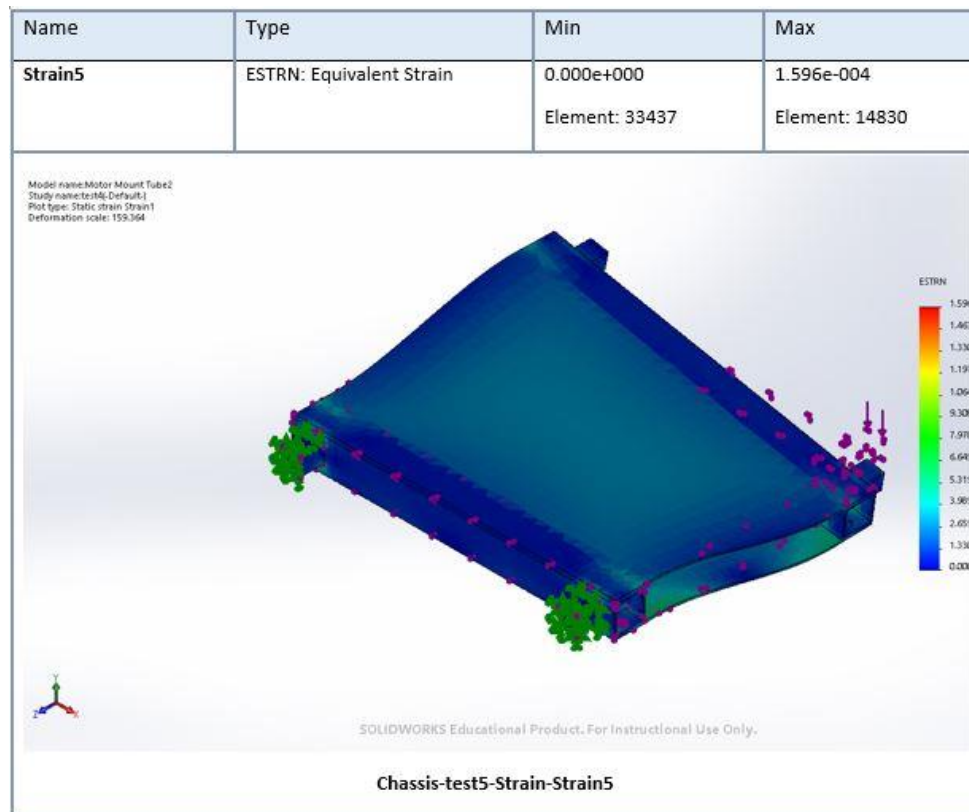
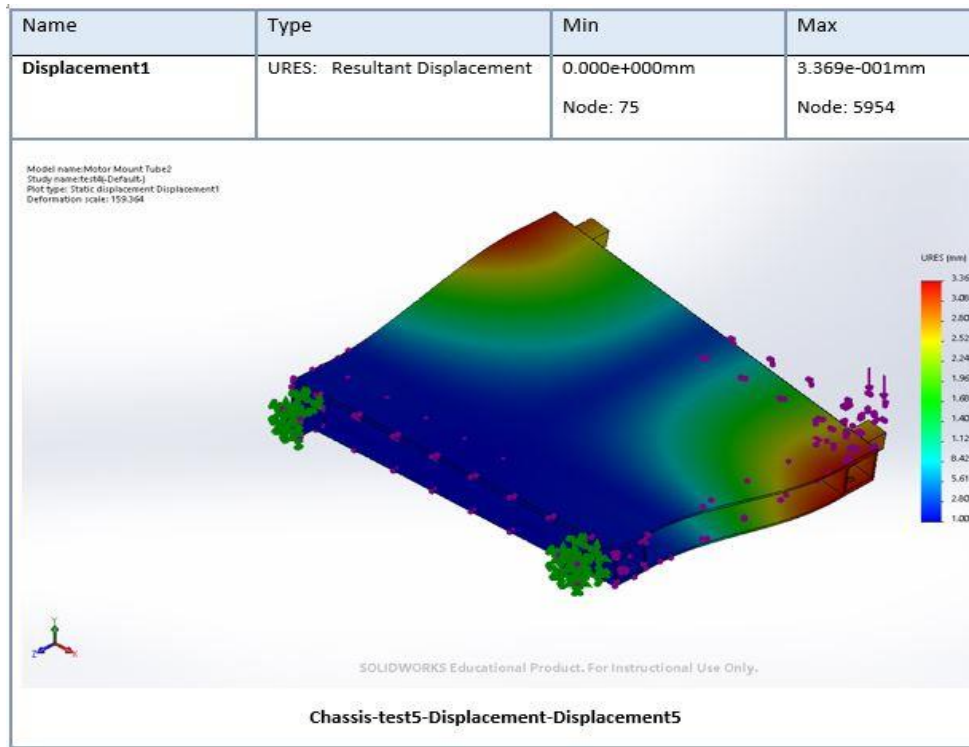
Resultant Forces

Reaction forces

Selection set	Units	Sum X	Sum Y	Sum Z	Resultant
Entire Model	N	0.0036397	0.00279236	0.00056076	0.00462159

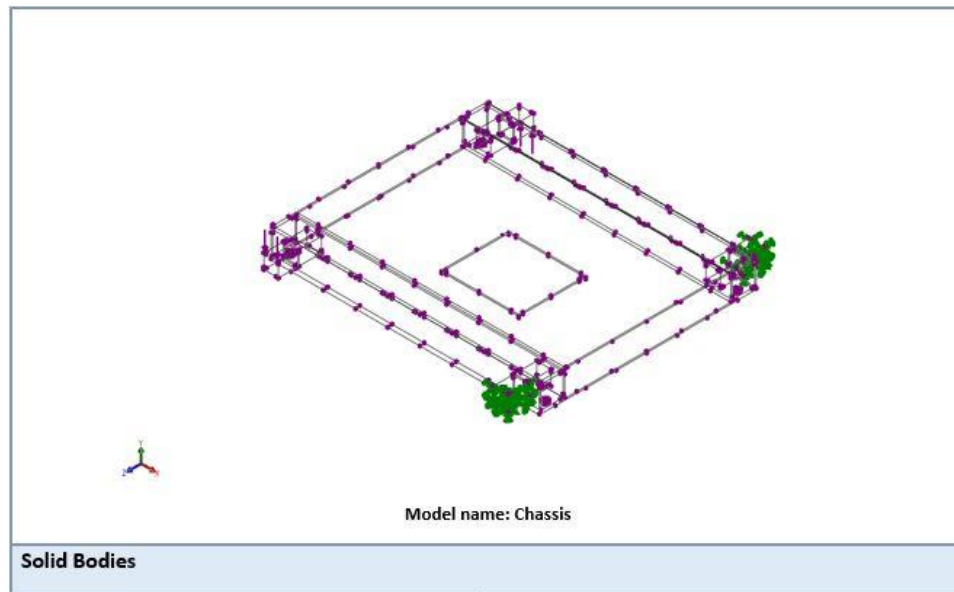
Study Results



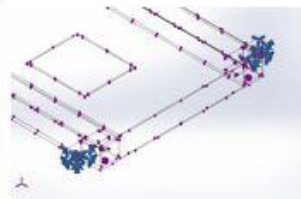


Test 6: Front- back torsion analysis

Model Information



Loads and Fixtures

Fixture name	Fixture Image	Fixture Details
Fixed-1		Entities: 6 face(s) Type: Fixed Geometry

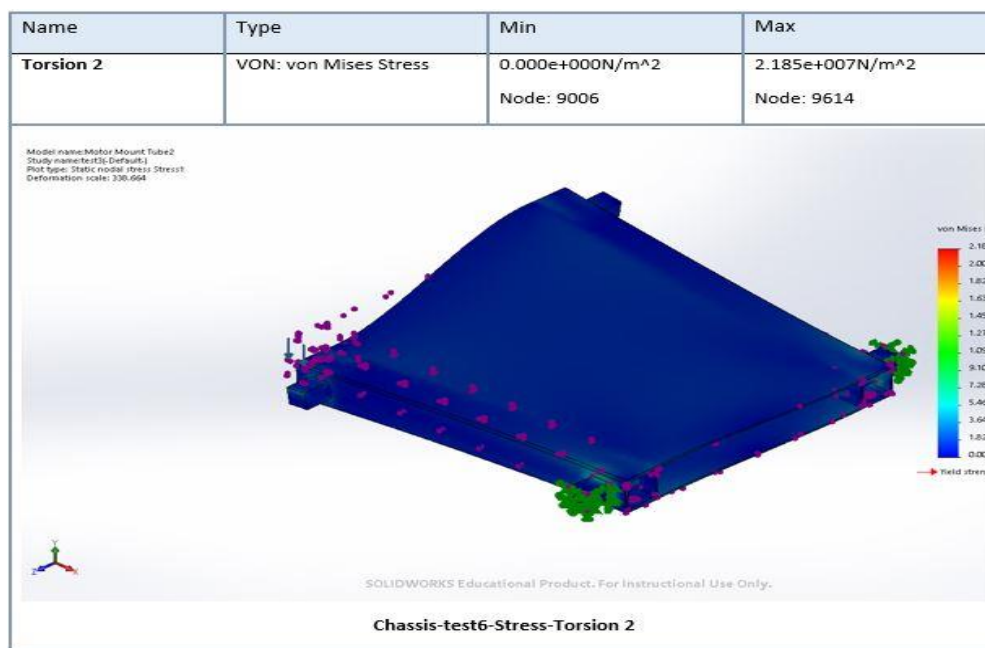
Resultant Forces				
Components	X	Y	Z	Resultant
Reaction force(N)	-0.00527191	0.00790405	-0.00816536	0.0125276
Reaction Moment(N.m)	0	0	0	0

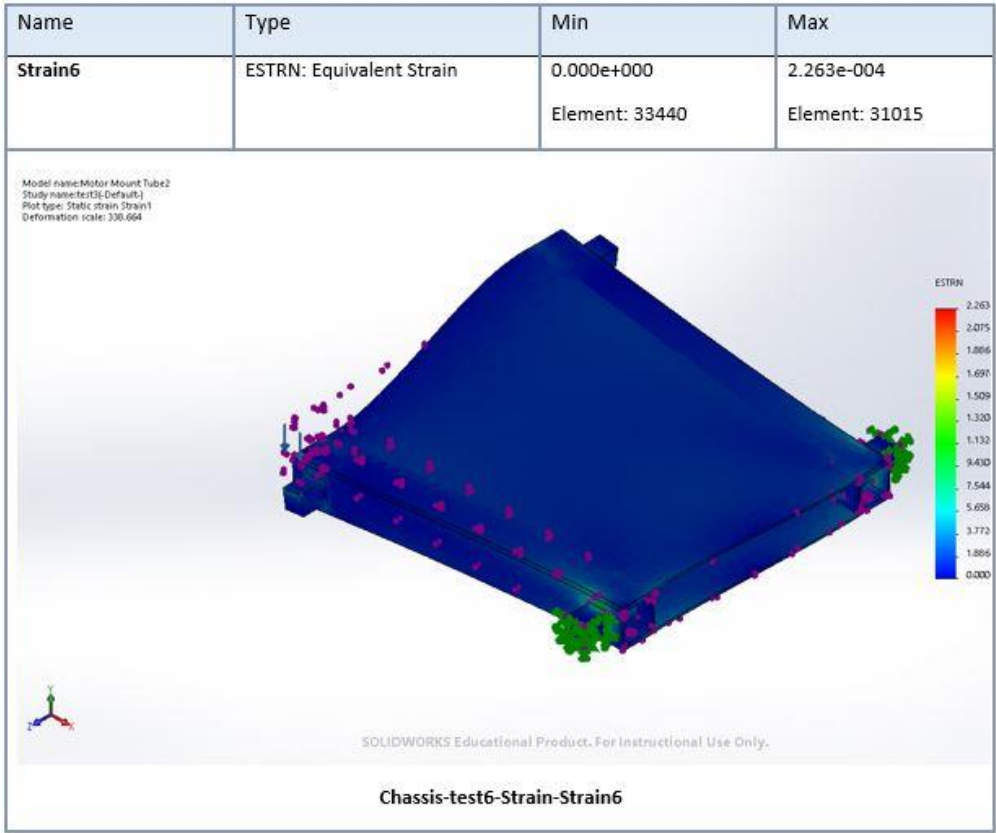
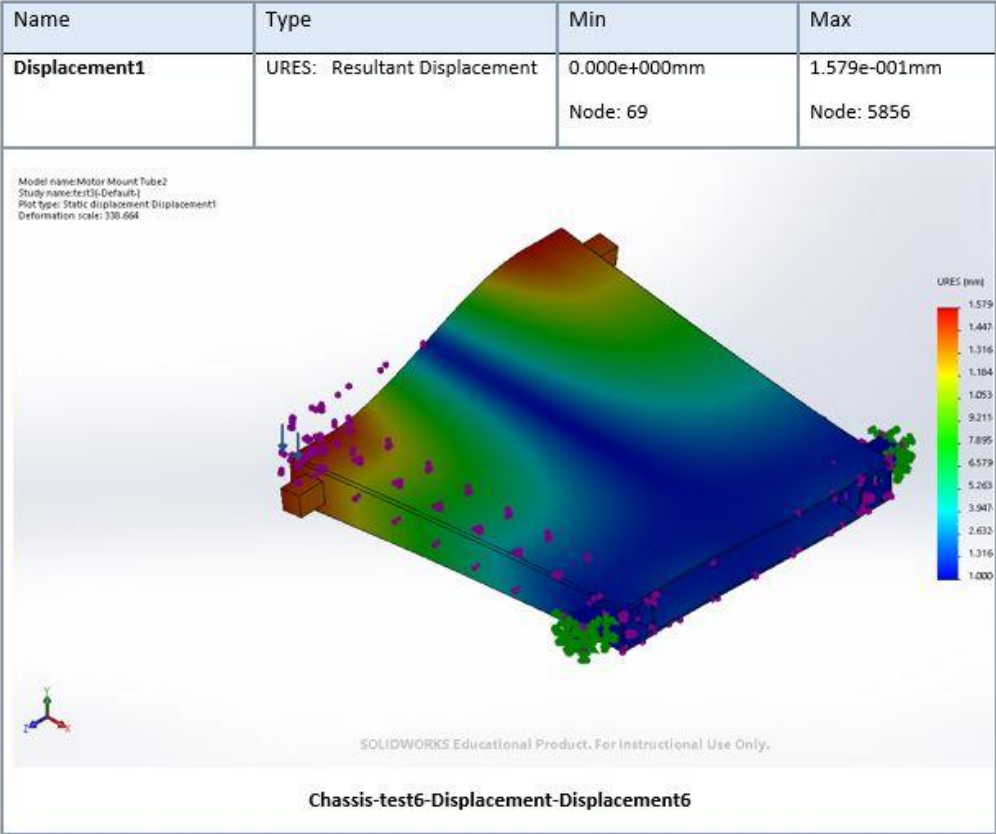
Resultant Forces

Reaction forces

Selection set	Units	Sum X	Sum Y	Sum Z	Resultant
Entire Model	N	-0.00527191	0.00790405	-0.00816536	0.0125276

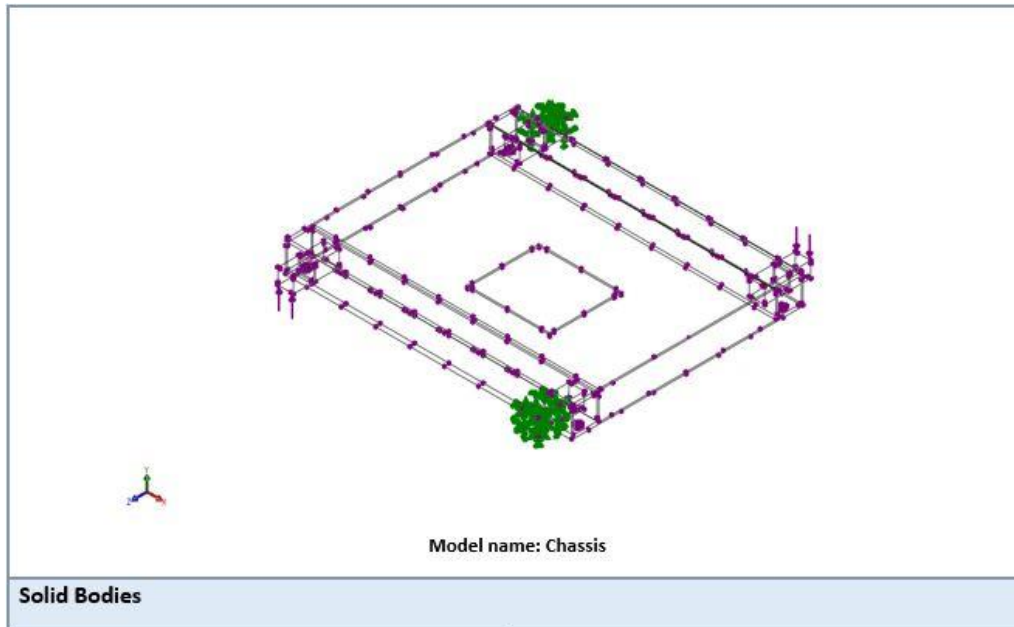
Study Results



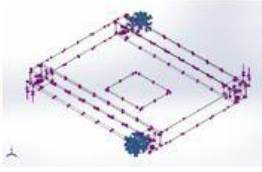


Test 7: Cross wheels bending analysis

Model Information



Loads and Fixtures

Fixture name	Fixture Image	Fixture Details
Fixed-1		Entities: 6 face(s) Type: Fixed Geometry

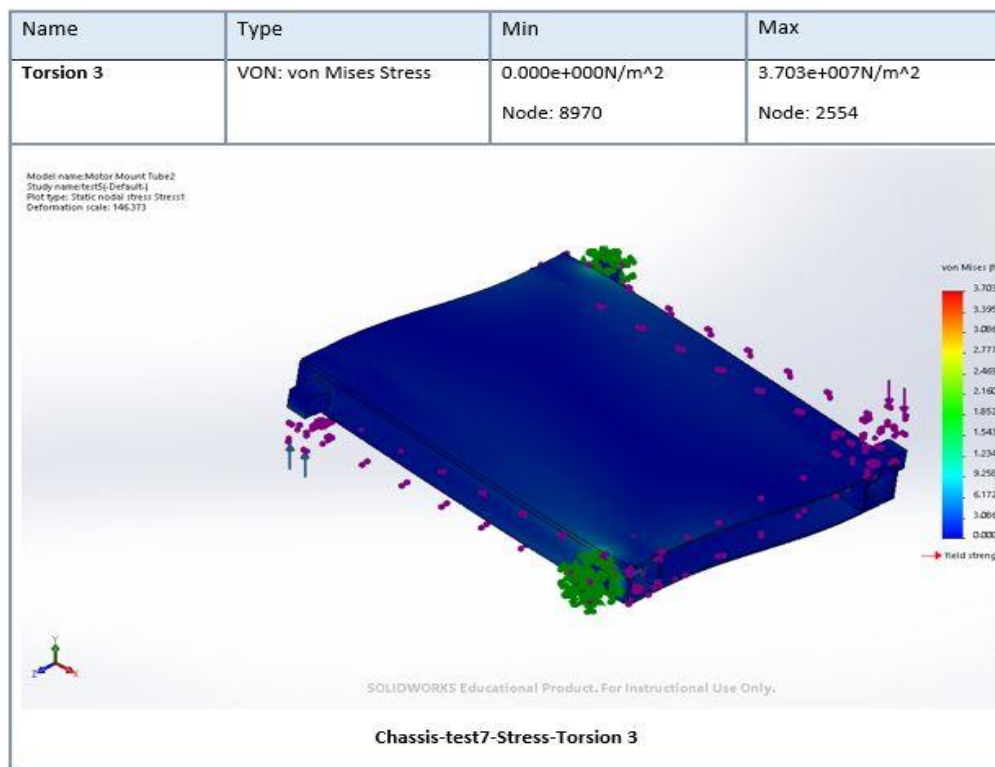
Resultant Forces				
Components	X	Y	Z	Resultant
Reaction force(N)	0.0282288	0.000183105	-0.00393105	0.0285017
Reaction Moment(N.m)	0	0	0	0

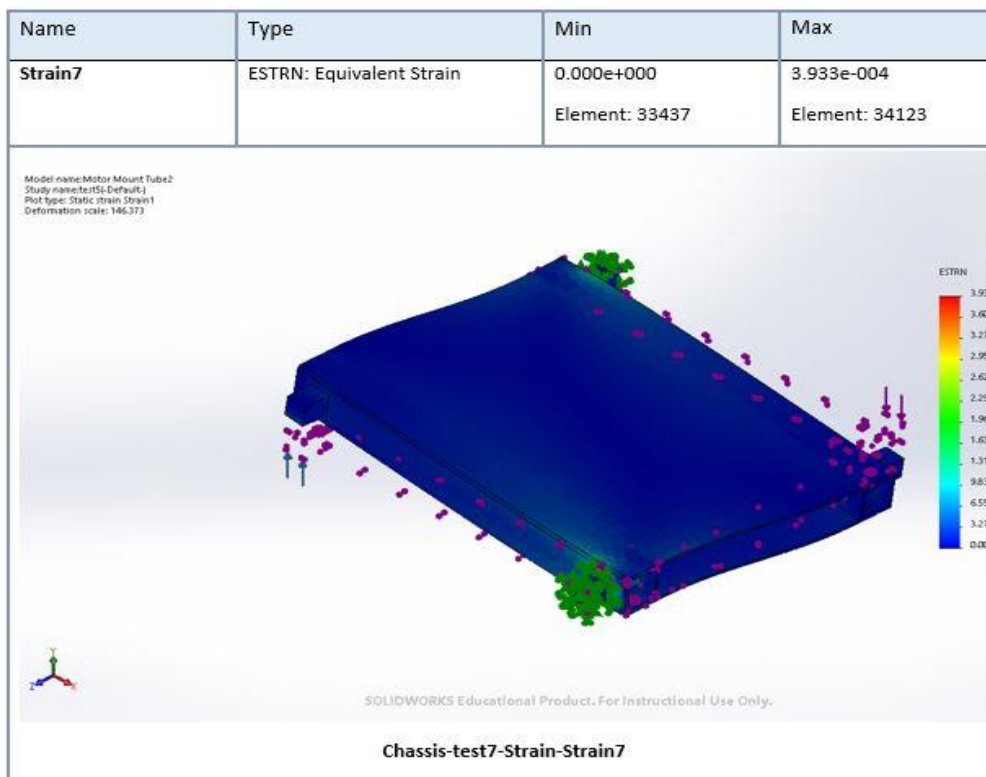
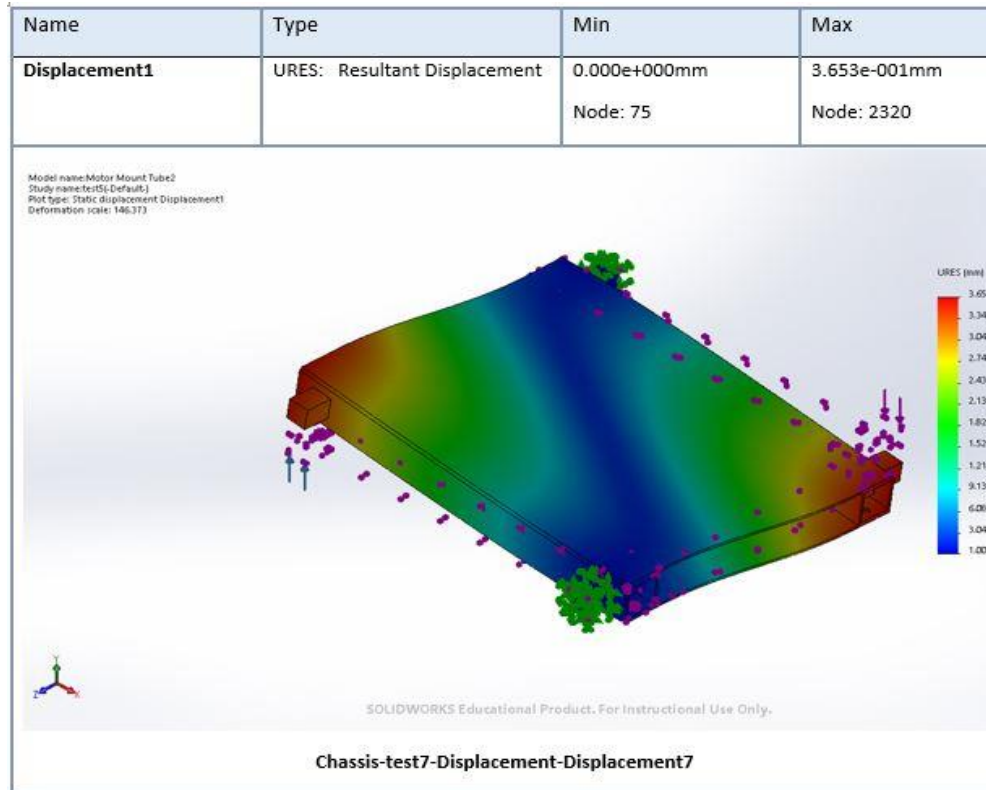
Resultant Forces

Reaction forces

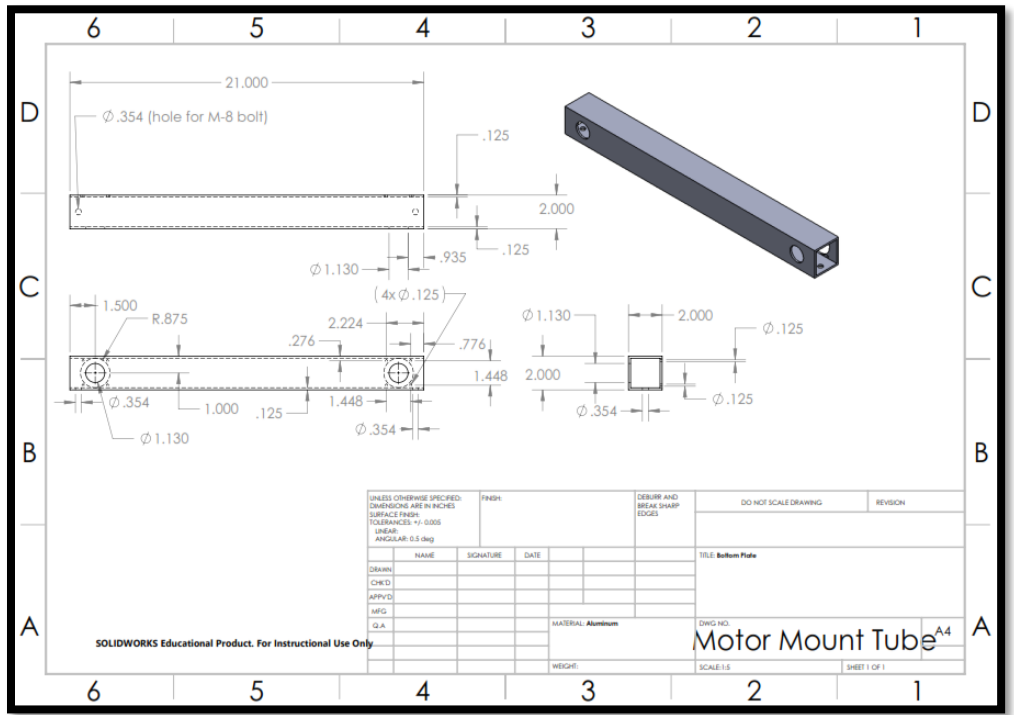
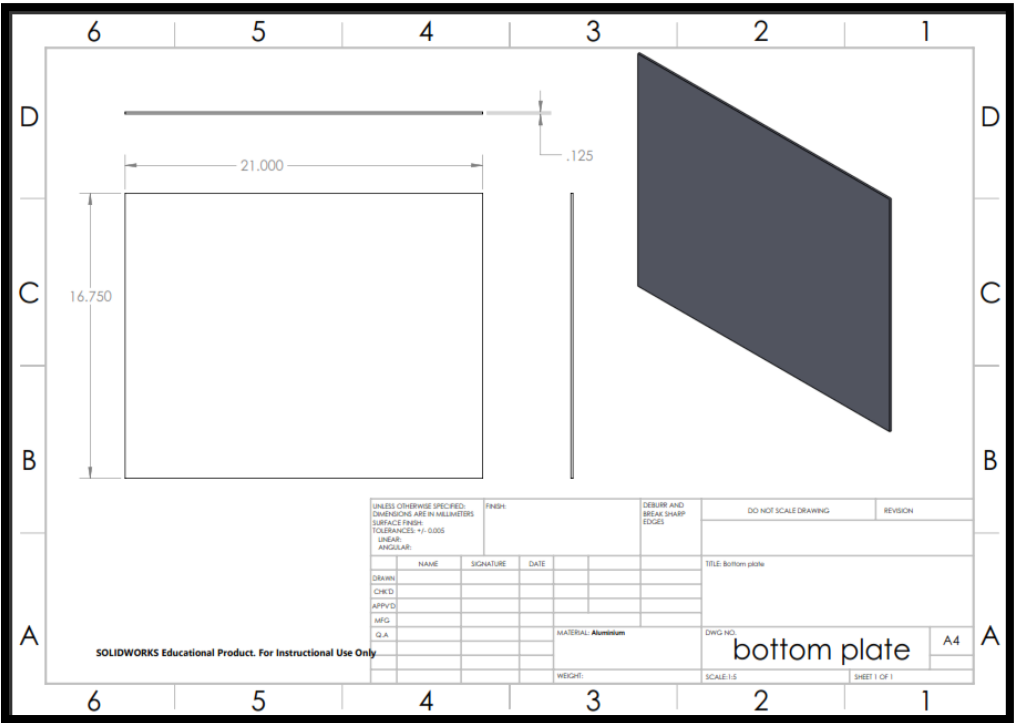
Selection set	Units	Sum X	Sum Y	Sum Z	Resultant
Entire Model	N	0.0282288	0.000183105	-0.00393105	0.0285017

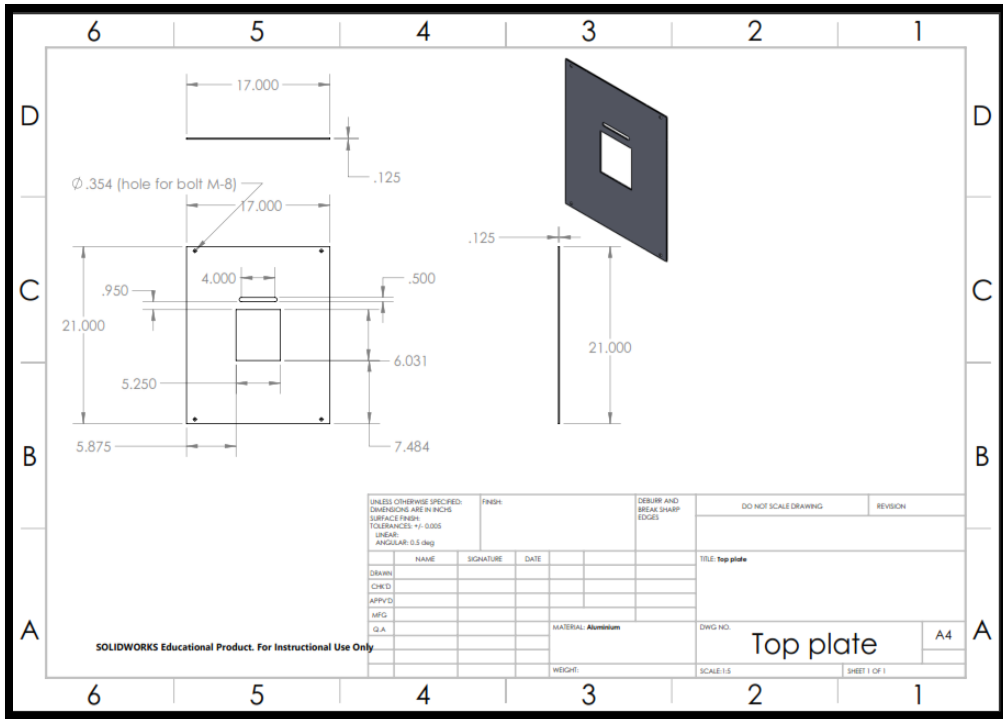
Study Results





Engineering drawing for chassis





B. CHASSIS OPTIMIZATION CODES

Objective Function:

```
% The objective function for the optimization problem. It is formed as a square of
link lengths and offset length of the spatial mechanism

function f = ObjFuncS(x)

t1=x(1);t2=x(2);t3=x(3);b=x(4);h=x(5);q=x(6);r=x(7);

f=(5400*b*h*r - 5400*r*(b - 2*t2)*(h - 2*t2) + 2700*q*r*t1 + 2700*q*r*t3)^2;
```

Constraints Function:

```
function [c,ceq]=Chassisconss(x)

t1=x(1);t2=x(2);t3=x(3);b=x(4);h=x(5);q=x(6);r=x(7);

conx(1)= b - h;

conx(2)= t1 - t2;

conx(3)= t1 - t3;

conx(4)= r/q - 5/4;

nonconx(1)= q - 0.5;

nonconx(2)= 0.4 - q;

nonconx(3)= (12*q*(h/2 + t1/2 + t3/2)*(52974*b*h*r - 52974*r*(b - 2*t2)*(h - 2*t2) + 26487*q*r*t1 + 26487*q*r*t3 + 91/5))/(r*(h + t1 + t3)^3) - 13787125;

nonconx(4)= (r*(h/2 + t1/2 + t3/2)*(52974*b*h*r - 52974*r*(b - 2*t2)*(h - 2*t2) + 26487*q*r*t1 + 26487*q*r*t3 + 91/5))/(2*((b*h^3)/12 + (q*t1^3)/24 + (q*t3^3)/24 - ((b - 2*t2)*(h - 2*t2)^3)/12 + (b*h - (b - 2*t2)*(h - 2*t2))*(abs(h/2 + t3 - ((b*h - (b - 2*t2)*(h - 2*t2))*(h/2 + t3) + (q*t3^2)/4 + (q*t1*(h + t1/2 + t3))/2)/(b*h + (q*t1)/2 + (q*t3)/2 - (b - 2*t2)*(h - 2*t2)))^2)^(1/2) + (q*t1*(abs(h + t1/2 + t3 - ((b*h - (b - 2*t2)*(h - 2*t2))*(h/2 + t3) + (q*t3^2)/4 + (q*t1*(h + t1/2 + t3))/2)/(b*h + (q*t1)/2 + (q*t3)/2 - (b - 2*t2)*(h - 2*t2)))^2)^(1/2))/2 + (q*t3*(abs(t3/2 - ((b*h - (b - 2*t2)*(h - 2*t2))*(h/2 + t3) + (q*t3^2)/4 + (q*t1*(h + t1/2 + t3))/2)/(b*h + (q*t1)/2 + (q*t3)/2 - (b - 2*t2)*(h - 2*t2)))^2)^(1/2))/2)) - 13787125;

nonconx(5)=t1-0.004;

nonconx(6)=-t1+0.003;

nonconx(7)=-b+0.05;

nonconx(8)=b-0.06;

nonconx(9)=-q+0.001;

nonconx(10)=-r+0.001;

c=[nonconx(1),nonconx(2),nonconx(3),nonconx(4),nonconx(5),nonconx(6),nonconx(7),nonconx(8),nonconx(9),nonconx(10)];

ceq=[conx(1),conx(2),conx(3),conx(4)];
```

Main Optimization Script File:

```
close all;
clear;
clc;

x0=rand(1,7);
options = gaoptimset('Generations',200, 'crossoverFcn',@
@crossoverscattered, 'MutationFcn',@mutationadaptfeasible, 'PlotFcns',{@gaplotbestf,
@gaplotstopping}, ...
    'Display','iter','HybridFcn',@fmincon);

[x,fval,exitflag,output,lambda]=ga(@ObjFuncS,7,[],[],[],[],[],[],@Chassisconss,
options);

save('dataxsn','x')
```

C. IMAGE PROCESSING CODES

RGB to HSL Function [115]:

```
function hsl=rgb2hsl(rgb_in)
%Converts Red-Green-Blue Color value to Hue-Saturation-Luminance Color value
%
%Usage
%       HSL = rgb2hsl(RGB)
%
%       converts RGB, a M [x N] x 3 color matrix with values between 0 and 1
%       into HSL, a M [x N] X 3 color matrix with values between 0 and 1
%
%See also hsl2rgb, rgb2hsv, hsv2rgb
% (C) Vladimir Bychkovsky, June 2008
% written using:
% - an implementation by Suresh E Joel, April 26,2003
% - Wikipedia: http://en.wikipedia.org/wiki/HSL\_and\_HSV
rgb=reshape(rgb_in, [], 3);
mx=max(rgb,[],2);%max of the 3 colors
mn=min(rgb,[],2);%min of the 3 colors
L=(mx+mn)/2;%luminance is half of max value + min value
S=zeros(size(L));
% this set of matrix operations can probably be done as an addition...
zeroidx= (mx==mn);
S(zeroidx)=0;
lowlidx=L <= 0.5;
calc=(mx-mn)./(mx+mn);
idx=lowlidx & (~ zeroidx);
S(idx)=calc(idx);
hilidx=L > 0.5;
calc=(mx-mn)./(2-(mx+mn));
idx=hilidx & (~ zeroidx);
S(idx)=calc(idx);
hsv=rgb2hsv(rgb);
H=hsv(:,1);
hsl=[H, S, L];
hsl=round(hsl.*100000)./100000;
hsl=reshape(hsl, size(rgb_in));
```

IMOVERLAY_OLD Function [116]:

```
function out = imoverlay_old(in, mask, color)
%IMOVERLAY_OLD Create a mask-based image overlay.
% This function has been superseded by the Image Processing Toolbox
% function IMOVERLAY, which shipped with R2016a.
%
% OUT = IMOVERLAY_OLD(IN, MASK, COLOR) takes an input image, IN, and a
% binary image, MASK, and produces an output image whose pixels in the
% MASK locations have the specified COLOR.
%
% IN should be a grayscale or an RGB image of class uint8, uint16, int16,
% logical, double, or single. If IN is double or single, it should be in
% the range [0, 1]. If it is not in that range, you might want to use
% mat2gray to scale it into that range.
%
% MASK should be a two-dimensional logical matrix.
%
% COLOR should be a 1-by-3 vector of values in the range [0, 1]. [0 0 0]
% is black, and [1 1 1] is white.
%
% OUT is a uint8 RGB image.
%
% Examples
% -----
% Overlay edge detection result in green over the original image.
%
%     I = imread('cameraman.tif');
%     bw = edge(I, 'canny');
%     rgb = imoverlay_old(I, bw, [0 1 0]);
%     imshow(rgb)
%
% Treating the output of peaks as an image, overlay the values greater than
% 7 in red. The output of peaks is not in the usual grayscale image range
% of [0, 1], so use mat2gray to scale it.
%
%     I = peaks;
%     mask = I > 7;
%     rgb = IMOVERLAY_OLD(mat2gray(I), mask, [1 0 0]);
%     imshow(rgb, 'InitialMagnification', 'fit')
%
% Steven L. Eddins
% Copyright 2006-2012 The MathWorks, Inc.
%
% If the user doesn't specify the color, use white.
DEFAULT_COLOR = [1 1 1];
if nargin < 3
    color = DEFAULT_COLOR;
end
% Force the 2nd input to be logical.
```



```

mask = (mask ~= 0);

% Make the uint8 the working data class. The output is also uint8.
in_uint8 = im2uint8(in);
color_uint8 = im2uint8(color);

% Initialize the red, green, and blue output channels.
if ndims(in_uint8) == 2
    % Input is grayscale. Initialize all output channels the same.
    out_red = in_uint8;
    out_green = in_uint8;
    out_blue = in_uint8;
else
    % Input is RGB truecolor.
    out_red = in_uint8(:, :, 1);
    out_green = in_uint8(:, :, 2);
    out_blue = in_uint8(:, :, 3);
end

% Replace output channel values in the mask locations with the appropriate
% color value.
out_red(mask) = color_uint8(1);
out_green(mask) = color_uint8(2);
out_blue(mask) = color_uint8(3);

% Form an RGB truecolor image by concatenating the channel matrices along
% the third dimension.
out = cat(3, out_red, out_green, out_blue);

```

Main Function:

```
%% Main function for detect the plant in Rea-Time video camera

function Plant_detector()
clear;close all;clc;imaqreset;
%% Setup Image Acquisition

% rpi = raspi('192.168.0.15','pi','raspberry');
% hCamera=cameraboard(rpi,'Resolution','640x480');
hCamera=webcam;
% Create a handle to an imshow figure for faster updating
hShow = imshow(zeros(720,1280,3,'uint8'));title('detector');

%% Quantize images and outputing to the screen

frames=2000;
for i=1:frames
    % Acquire an image from the webcam
    vid_img=snapshot(hCamera);

    % Call the live segmentation function
    Plant_detected=Segmentation_Fn(vid_img);

    % Update the imshow handle with a new image
    set(hShow,'CData',Plant_detected);
    drawnow;

    % Shutdown webcam by deleting handle

end
    stop(hCamera);
    delete(hCamera);

end
```

Segmentation Function for Method A:

```
function [detected_Plant]=Segmentation_Fn(img)
global xt;

%% Thresholding the image on each color plane
Im=im2double(img);
hsl=rgb2hsl(Im);
%% Extract individuals plane from RGB image
imh=squeeze(hsl(:, :, 1));
ims=squeeze(hsl(:, :, 2));
iml=squeeze(hsl(:, :, 3));
%% Threshold Image
imgT1=imh >0.1765 & imh<0.6078;
imgThresh1=imgT1.*imh;

imgT2=ims >0.2353 & ims<1;
imgThresh2=imgT2.*ims;

imgT3=iml >0.0196 & iml<0.89;
imgThresh3=imgT3.*iml;

imgThresh=(imgThresh1&imgThresh2&imgThresh3);

%% Fill in Regions
detectedareal = bwareaopen(imgThresh, 100);

%% Binarize the image
binaryImage = imfill(detectedareal, 'holes');

%% Overlay Onto Original Image
% Utility from File Exchange
% imgboth1=imoverlay_old(imgl,detectedareal,[1 0 0]);
imgboth2=imoverlay_old(img,binaryImage,[1 0 0]);
%figure;
%imml=imshow(imgboth2);
detected_Plant=imgboth2;
%% Label the image.
xt=0;
yt=0;

[labeledImage, numberOfBlobs] = bwlabel(binaryImage);
numberOfBlobs
if numberOfBlobs == 1
    blobMeasurements = regionprops(labeledImage, 'Centroid', 'Area');
    allAreas = [blobMeasurements.Area];
    xCenter = [blobMeasurements(1).Centroid(1)]
    yCenter = [blobMeasurements(1).Centroid(2)]
    hold on;
    plot(xCenter, yCenter, 'g*', 'MarkerSize', 10, 'LineWidth', 2);
    hold off
```

```

elseif numberOfBlobs > 1

for i = 1 : numberOfBlobs
blobMeasurements = regionprops(labeledImage, 'Centroid', 'Area');
allAreas = [blobMeasurements.Area];
x=blobMeasurements(i).Centroid(1);
y=blobMeasurements(i).Centroid(2);
hold on;
plot(x,y, 'b*', 'MarkerSize', 10, 'LineWidth', 2);
xt=x+xt;
yt=y+yt;
end
xCenter = [xt]/numberOfBlobs
yCenter = [yt]/numberOfBlobs
plot(xCenter, yCenter, 'g*', 'MarkerSize', 10, 'LineWidth', 2);
hold off

    %(when X become in the mid get signal and stop moving camera and hand)
end
end

```

Segmentation Function for Method B:

```
function [detected_Plant]=Segmentation_Fn(img)

%% Thresholding the image on each color plane
Im=im2double(img);
hsl=rgb2hsl(Im);
%% Extract individuals plane from RGB image
imh=squeeze(hsl(:,:,1));
ims=squeeze(hsl(:,:,2));
iml=squeeze(hsl(:,:,3));
%% Threshold Image
imgT1=imh >0.1765 & imh<0.6078;
imgThresh1=imgT1.*imh;

imgT2=ims >0.2353 & ims<1;
imgThresh2=imgT2.*ims;

imgT3=iml >0.0196 & iml<0.89;
imgThresh3=imgT3.*iml;

imgThresh=(imgThresh1&imgThresh2&imgThresh3);

%% Fill in Regions
detectedareal = bwareaopen(imgThresh, 100);

%% Binarize the image
binaryImage = imfill(detectedareal, 'holes');

%% Overlay Onto Original Image
% Utility from File Exchange
% imgboth1=imoverlay_old(imgl,detectedareal,[1 0 0]);
imgboth2=imoverlay_old(img,binaryImage,[1 0 0]);
%figure;
%imml=imshow(imgboth2);
detected_Plant=imgboth2;
%% Label the image.
xmax=0;
xmin=1300;
ymax=0;
ymin=1300;
[labeledImage, numberOfBlobs] = bwlabel(binaryImage);
numberOfBlobs
if numberOfBlobs == 1
    blobMeasurements = regionprops(labeledImage, 'Centroid', 'Area','Extrema');
    allAreas = [blobMeasurements.Area];
    extr=blobMeasurements.Extrema;
    xmax=extr(3,1);
    xmin=extr(8,1);
    ymax=extr(6,2);
```

```

        ymin=extr(1,2);

elseif numberOfBlobs > 1

    for i = 1 : numberOfBlobs
        blobMeasurements = regionprops(labeledImage, 'Centroid', 'Area','Extrema');
        allAreas = [blobMeasurements.Area];
        extr=blobMeasurements(i).Extrema;
        xr=extr(3,1);
        xl=extr(8,1);
        yb=extr(6,2);
        yt=extr(1,2);

        if xr>xmax
            xmax=xr;
        end
        if xl<xmin
            xmin=xl;
        end
        if yb>ymax
            ymax=yb;
        end
        if yt<ymin
            ymin=yt;
        end

    end
    xmax;
    xmin;
    ymax;
    ymin;
    hold on
    xCenter=(xmin+xmax)/2
    yCenter=(ymin+ymax)/2
    plot(xCenter, yCenter, 'g*', 'MarkerSize', 10, 'LineWidth', 2);
    hold off

    %(when X become in the mid get signal and stop moving camera and hand)
end
end

```

D. RELATED PUBLICATIONS AND PATENT

Publications:

- **T. Deemyad** and A. Sebastian, “Mobile Manipulator and EOAT for In-Situ Virus Detection and Removal”, In 5th IFToMM Symposium on Mechanism Design for Robotics (MEDER), Springer (In press)
- **T. Deemyad**, R. Moeller, and A. Sebastian, “Chassis design and analysis of an autonomous ground vehicle (AGV) using genetic algorithm”, In Intermountain Engineering, Technology, and Computing Conference (I-ETC, Oct-2020). IEEE
- R. Moeller, **T. Deemyad**, and A. Sebastian, “Autonomous navigation of an agricultural robot using RTK GPS and Pixhawk”, In Intermountain Engineering, Technology, and Computing Conference (I-ETC, Oct-2020). IEEE
- **T. Deemyad**, O. Heidari, and A. Perez-Gracia, 2020, May. Singularity Design for RRSS Mechanisms. In USCToMM Symposium on Mechanical Systems and Robotics (pp. 287-297). Springer, Cham.
- **T. Deemyad**, N. Hassanzadeh, and A. Perez-Gracia, 2018, August. Coupling mechanisms for multi-fingered robotic hands with skew axes. In IFToMM Symposium on Mechanism Design for Robotics (pp. 344-352). Springer, Cham.

Patent:

- **Taher Deemyad**, Anish Sebastian, and Alba Perez-Gracia, the provisional patent application for “**Agricultural Roguing Machine**” **Application Serial No. : 63/104,937, Filing date: 10/23/2020**

E. REFERENCES

- [1] D. Tilman, C. Balzer, J. Hill, and B.L. Befort. “Global Food Demand and the Sustainable Intensification of Agriculture”, *Proc. Natl. Acad. Sci. USA*, 108(50):20260-4, 2011.
- [2] J.L. Araus, J.E. Cairns. “Field high-throughput phenotyping: The new crop breeding frontier”, *Trends Plant Science*, 19: 52–61, 2014.
- [3] J.M. McGuire, L. Wright Morton, J.G. Arbuckle Jr and A.D. Cast. “Farmer identities and responses to the social–biophysical environment”, *Journal of Rural Studies*, 39 (2015): 145-155. 2015.
- [4] L.E. Ehler. “Integrated Pest Management (IPM): Definition, Historical Development and Implementation, and the Other IPM”, *Pest Management Science*, 1526–498X, 2006.
- [5] S. Haneklaus, H. Lilienthal and E. Schnug. “25 Years Precision Agriculture in Germany – A Review”, 13th Int. Conference on Precision Agriculture, St Louis, MI, USA, 2016.
- [6] P. Nolte, J.M. Alvarez and J.L. Whitworth. “Potato Virus Y Management for the Seed Potato Producer”, *CIS 1165*, 2009.
- [7] P. Nolte, J.M. Alvarez and J.L. Whitworth. “Potato Virus Y Management for the Seed Potato Producer”, *CIS 1165*, 2009.
- [8] M. Dadvar, S. Moazami, H. R. Myler, and H. Zargarzadeh. “Multiagent task allocation in complementary teams: a hunter-and-gatherer approach,” *Complexity*, vol. 2020, Article ID 1752571, 15 pages.
- [9] M. Dadvar, S. Moazami, H. R. Myler, and H. Zargarzadeh. “Exploration and coordination of complementary multi-robot teams in a hunter and gatherer scenario,” 2019, {<https://arxiv.org/abs/1912.07521>}.
- [10] M. C. Mayer. “Early detection of virus infections in potato by aphids and infrared remote sensing”, MS Thesis, Department of Crop Production Ecology, Swedish Univ. of Agricultural Sciences, 2016.

- [11] M. C. Mayer. “Early detection of virus infections in potato by aphids and infrared remote sensing”, MS Thesis, Department of Crop Production Ecology, Swedish Univ. of Agricultural Sciences, 2016.
- [12] A.V. Karasev and S.M. Gray, 2013. Continuous and emerging challenges of Potato virus Y in potato. *Annual Review of Phytopathology*, 51, pp.571-586.
- [13] W. Buhrig, M.K. Thornton, N. Olsen, D. Morishita and C. McIntosh, 2015. The influence of ethephon application timing and rate on plant growth, yield, tuber size distribution and skin color of red LaSoda potatoes. *American journal of potato research*, 92(1), pp.100-108.
- [14] L.M. Griffel, D. Delparte, J. Edwards. Using Support Vector Machines classification to differentiate spectral signatures of potato plants infected with Potato Virus Y. *Computers and Electronics in Agriculture*. 2018; 153:318-324. doi:DOI: 10.1016/j.compag.2018.08.027.
- [15] T. Deemyad, N. Hassanzadeh, and A. Perez-Gracia. Coupling mechanisms for multi-fingered robotic hands with skew axes. In *Mechanism Design for Robotics (MEDER)*. Springer, 2018.
- [16] T. Deemyad, O. Heidari, and A. Perez-Gracia. Singularity Design for RRSS Mechanisms. In *USCToMM Symposium on Mechanical Systems and Robotics (MSR) Conferences*. Springer, 2020.
- [17] T. Deemyad. Design of Five-fingered Underactuated Hand for Two-position Tasks (Master’s Thesis, Idaho State University), 2016.
- [18] S. Habibian. "Analysis and Control of Fiber-Reinforced Elastomeric Enclosures (FREEs)." (Master’s Thesis. 229, Bucknell University), 2019.
- [19] J. A. de Bokx, and H. Huttinga, 1981. Potato Virus Y. *Descriptions of Plant Viruses*, No. 242. Commonwealth Mycological Institute and Association of Applied Biologists, Kew, England.
- [20] P. Nolte, J. L. Whitworth, M. K. Thornton and C. S. McIntosh (2004). Effect of Seedborne Potato virus Y on Performance of Russet Burbank, Russet Norkotah, and Shepody Potato. *Plant Disease*, 88(3), 248–252. doi: 10.1094/pdis.2004.88.3.248

[21] G. Polder, P.M. Blok, H.A. de Villiers, J.M. van der Wolf, and J. Kamp, 2019. Potato virus Y detection in seed potatoes using deep learning on hyperspectral images. *Frontiers in plant science*, 10, p.209.

[22] D. Krezhova, K. Velichkova, N. Petrov, and S. Maneva (2017). The Effect Of Plant Diseases On Hyperspectral Leaf Reflectance And Biophysical Parameters. *RAD Conference Proceedings*. doi: 10.21175/radproc.2017.5

[23] D. D. Krezhova, N. M. Petrov, S. N. Maneva, “Hyperspectral remote sensing applications for monitoring and stress detection in cultural plants: viral infections in tobacco plants,” in *Proc. of Remote Sensing for Agriculture, Ecosystems, and Hydrology Conf.*, Edinburgh, UK, 2012, pp. 24-27. DOI: 10.1117/12.974722

[24] Z. Ni, Z. Liu, H. Huo, Z. H. Li, F. Nerry, Q. Wang, X. Li, “early Water Stress Detection Using Leaf-Level Measurements of Chlorophyll Fluorescence and Temperature Data,” *Remote Sens.*, vol. 7, no. 3, pp. 3232-3249, Mar. 2015. DOI 10.3390/rs7030232

[25] R. Moeller, T. Deemyad, and A. Sebastian, 2020, October. Autonomous Navigation of an Agricultural Robot Using RTK GPS and Pixhawk. In *2020 Intermountain Engineering, Technology and Computing (IETC)* (pp. 1-6). IEEE.

[26] T. Deemyad, R. Moeller and A. Sebastian, 2020, October. Chassis Design and Analysis of an Autonomous Ground Vehicle (AGV) using Genetic Algorithm. In *2020 Intermountain Engineering, Technology and Computing (IETC)* (pp. 1-6). IEEE.

[27] <https://www.flickr.com/photos/johnbeales/1270734523>

[28] J. Bengochea-Guevara, J. Conesa-Muñoz, D. Andújar, and A. Ribeiro (2016). Merge Fuzzy Visual Servoing and GPS-Based Planning to Obtain a Proper Navigation Behavior for a Small Crop-Inspection Robot. *Sensors*, 16(3), 276. doi: 10.3390/s16030276

[29] S.M. Pedersen, S. Fountas, H. Have, and B.S. Blackmore, 2006. Agricultural robots—system analysis and economic feasibility. *Precision agriculture*, 7(4), pp.295-308.

- [30] X. Gao, J. Li, L. Fan, Q. Zhou, K. Yin, J. Wang, C. Song, L. Huang, and Z. Wang, 2018. Review of wheeled mobile robots' navigation problems and application prospects in agriculture. *IEEE Access*, 6, pp.49248-49268.
- [31] J. Ma, X. Li, H. Wen, Y.Y. Chen, Z.T. Fu, and L. Zhang, 2015. Monitoring video capture system for identification of greenhouse vegetable diseases. *Transactions of the Chinese of the Society for Agricultural Machinery*, 46(3), pp.282-287.
- [32] J. Ma, X. Li, H. Wen, Z. Fu, and L. Zhang, 2015. A key frame extraction method for processing greenhouse vegetables production monitoring video. *Computers and electronics in agriculture*, 111, pp.92-102.
- [33] J. Ma, H. Wen, and X. Li, 2017. Downy mildew diagnosis system for greenhouse cucumbers based on image processing. *Nongye Jixie Xuebao/transactions of the Chinese Society of Agricultural Machinery*, 48(2), pp.195-202.
- [34] S. Zhang, X. Wu, Z. You, and L. Zhang, 2017. Leaf image based cucumber disease recognition using sparse representation classification. *Computers and electronics in agriculture*, 134, pp.135-141.
- [35] J.G.A. Barbedo, 2016. A review on the main challenges in automatic plant disease identification based on visible range images. *Biosyst. Eng.* 144, 52–60.
- [36] M. Rooker, P. Horstrand, A.S. Rodriguez, S. Lopez, R. Sarmiento, J. Lopez, R.A. Lattarulo, J.M.P. Rastelli, Z. Slavik, D. Pereira and M. Pusenius, 2018, April. Towards improved validation of autonomous systems for smart farming. In *Smart Farming Workshop*.
- [37] C. Saravanan, 2010, March. Color image to grayscale image conversion. In *2010 Second International Conference on Computer Engineering and Applications (Vol. 2, pp. 196-199)*. IEEE.
- [38] G. Saravanan, G. Yamuna and S. Nandhini, 2016, April. Real time implementation of RGB to HSV/HSI/HSL and its reverse color space models. In *2016 International Conference on Communication and Signal Processing (ICCSP)* (pp. 0462-0466). IEEE.

- [39] L. J. Kutz, G. E. Miles, P. A. Hammer, G. W. Krutz (1987). Robotic Transplanting of Bedding Plants. 1987 American Society of Agricultural Engineers 0001-2351/87/3003-0586.
- [40] K. C. Ting, G. A. Giacomelli, S. J. Shen, W. P. Kabala (1990). ROBOT WORKCELL FOR TRANSPLANTING OF SEEDLINGS, PART II - END-EFFECTOR DEVELOPMENT. American Society of Agricultural Engineers 0001-2351 / 90 / 3303-1013.
- [41] B. Allotta, G. Buttazzo, P. Dario, F. Quaglia, and P. Levi (1990). A FORCE/TORQUE SENSOR-BASED TECHNIQUE FOR ROBOT HARVESTING OF FRUITS AND VEGETABLES. IEEE International Workshop on Intelligent Robots and Systems IROS '90.
- [42] W. Simonton, 1990. Automatic geranium stock processing in a robotic work cell. Transactions of the ASAE, 33(6), pp.1274-1280.
- [43] Y. Edan, 1995. Design of an autonomous agricultural robot. Applied Intelligence, 5(1), pp.41-50.
- [44] M. Monta, N. Kondo, Y. Shibano (1995). Agricultural Robot in Grape Production System. IEEE International Conference.
- [45] R. Ceres, J.L. Pons, A.R. Jiménez, J.M. Martín and L. Calderón (1998). Design and implementation of an aided fruit-harvesting robot (Agribot). Industrial Robot Volume 25 · Number 5 · 1998 · pp. 337–346 © MCB University Press · ISSN 0143-991X.
- [46] M. Ceccarelli, G. Figliolini, E. Ottaviano, A.S. Mata, and E.J. Criado, 2000. Designing a robotic gripper for harvesting horticulture products. Robotica, 18(1), pp.105-111.
- [47] N. Kondo, K. Yamamoto, K. Yata and M. Kurita, 2008. A machine vision for tomato cluster harvesting robot. In 2008 Providence, Rhode Island, June 29–July 2, 2008 (p. 1). American Society of Agricultural and Biological Engineers.
- [48] N. Kondo, K. Yata, M. Iida, T. Shiigi, M. Monta, M. Kurita and H. Omori, 2010. Development of an end-effector for a tomato cluster harvesting robot. Engineering in Agriculture, Environment and Food, 3(1), pp.20-24.

- [49] Z. Li, P. Li, H. Yang and Y. Wang, 2013. Stability tests of two-finger tomato grasping for harvesting robots. *Biosystems engineering*, 116(2), pp.163-170.
- [50] S. Hayashi, K. Ganno, Y. Ishii and I. Tanaka, 2002. Robotic harvesting system for eggplants. *Japan Agricultural Research Quarterly: JARQ*, 36(3), pp.163-168.
- [51] S. Sakai, K. Osuka, H. Fukushima and M. Iida 2002. Watermelon harvesting experiment of a heavy material handling agricultural robot with LQ control. In *IEEE/RSJ International Conference on Intelligent Robots and Systems* (Vol. 1, pp. 769-774). IEEE.
- [52] S. Sakai, M. Iida, K. Osuka and Umeda, M., 2008. Design and control of a heavy material handling manipulator for agricultural robots. *Autonomous Robots*, 25(3), pp.189-204.
- [53] S.M. Mizanoor Rahman, Ryojun Ikeura, Soichiro Hayakawa & Hideki Sawai (2011). Design guidelines for power assist robots for lifting heavy objects considering weight perception, grasp differences and worst-cases. *Int. J. Mechatronics and Automation*, Vol. 1, No. 1, 2011.
- [54] G. Muscato and M. Prestifilippo, Nunzio Abbate, Ivan Rizzuto (2005). A prototype of an orange picking robot: past history, the new robot and experimental results. *Industrial Robot: An International Journal* 32/2 (2005) 128–138.
- [55] M. M. Foglia and G. Reina (2006), *Agricultural Robot for Radicchio Harvesting*. *Journal of Field Robotics*, Wiley Periodicals, Inc. Published online in Wiley InterScience.
- [56] N. Irie, N. Taguchi, T. Horie, and T. Ishimatsu (2009). Asparagus harvesting robot coordinated with 3-D vision sensor.
- [57] N. Correll, N. Arechiga, A. Bolger, M. Bollini, B. Charrow, A. Clayton, F. Dominguez, K. Donahue, S. Dyar, L. Johnson, and H. Liu, 2009, October. Building a distributed robot garden. In *2009 IEEE/RSJ International Conference on Intelligent Robots and Systems* (pp. 1509-1516). IEEE.
- [58] Y.J. Huang and F.F. Lee, 2010. An automatic machine vision-guided grasping system for *Phalaenopsis* tissue culture plantlets. *Computers and Electronics in Agriculture*, 70(1), pp.42-51.
- [59] R.M. Holladay and S.S. Srinivasa, 2016, March. RoGuE: Robot Gesture Engine. In *AAAI Spring Symposia*.

- [60] A. Silwal, J. R. Davidson, M. Karkee, C. Mo, Q. Zhang and K. Lewis (2017). Design, integration, and field evaluation of a robotic apple harvester. *Journal of Field Robotics*, Wiley Periodicals.
- [61] T. Duckett, S. Pearson, S. Blackmore and B. Grieve (2018). *Agricultural Robotics, The Future of Robotic Agriculture*. UK-RAS White papers.
- [62] S. Stramigioli: *Modeling and IPC Control of Interactive Mechanical Systems – A Coordinate-Free Approach*. LNCIS, vol. 266. Springer, London (2001)
- [63] C. Tischler, A. Samuel, and K. Hunt: Kinematic chains for robot hands - I. Orderly number-synthesis. *Mech. Mach. Theory* 30(8), 1193–1215 (1995)
- [64] I. Chen, G. Yang, and I. Kang: Numerical inverse kinematics for modular reconfigurable robots. *J. Robot. Syst.* 16(4), 213–225 (1999)
- [65] J. Salisbury, and B. Roth: Kinematic and force analysis of articulated mechanical hands. *J. Mech. Transm. Autom. Des.* 105(1), 35–41 (1983)
- [66] C. Tischler, A. Samuel, and K. Hunt: Kinematic chains for robot hands - II. Kinematic constraints, classification, connectivity and actuation. *Mech. Mach. Theory* 30(8), 1217–1239 (1995)
- [67] J.J. Lee, and L. Tsai: Structural synthesis of multi-fingered hands. *ASME J. Mech. Des.* 124, 272–276 (2002)
- [68] E. Ozgur, G. Gogu, Y. Mezouar: Structural synthesis of dexterous hands. In: *Intelligent Robots and Systems (IROS) Conference* (2014)
- [69] A. Tamimi, A. Perez Gracia, M. Pucheta: Structural synthesis of hands for grasping and manipulation tasks. In: *Recent Advances in Robot Kinematics*. Springer (2016)
- [70] E. Simo-Serra, A. Perez-Gracia, H. Moon, and N. Robson: Design of multi fingered robotic hands for finite and infinitesimal tasks using kinematic synthesis. In: *Advances in Robot Kinematics*, Innsbruck, Austria, June 2012
- [71] E. Simo-Serra, and A. Perez-Gracia: Kinematic synthesis using tree topologies. *Mech. Mach. Theory* 72C, 94–113 (2014)

- [72] A. Makhal, and A. Perez-Gracia: Solvable multi-fingered hands for exact kinematic synthesis. In: Advances in Robot Kinematics, Ljubljana, Slovenia, June 2014
- [73] Y. Yihun, K. Bosworth, and A. Perez-Gracia: Link-based performance optimization of spatial mechanisms. *J. Mech. Des.* 136(12) (2014)
- [74] N. Hasanzadeh, X. He, and A. Perez-Gracia: A design implementation process for robotic hand synthesis. In: ASME International Design Engineering Technical Conferences (2015)
- [75] N. Robson, J. Allington, and G. Soh: Development of underactuated mechanical fingers based on anthropometric data and anthropomorphic tasks. In: ASME, Buffalo, USA (2014)
- [76] M. Ceccarelli, and M. Zottola: Design and simulation of an underactuated finger mechanism for LARM hand. *Robotica* (2015)
- [77] H. Wang, S. Fan and H. Liu: Thumb configuration and performance evaluation for dexterous robotic hand design. *J. Mech. Des.* 139, 301–311 (2017)
- [78] J. Angeles and A. Bernier: A general method of four-bar linkage mobility analysis. In: *Journal of Mechanisms, Transmissions, and Automation in Design*, Volume 109, Issue 2, (7 pages), 1987.
- [79] C. Gosselin and J. Angeles: Singularity Analysis of Closed-Loop Kinematic Chains. In: *IEEE Transactions on Robotics and Automation*, Volume: 6, Issue: 3, Page(s): 281 - 290, Jun 1990.
- [80] A. Muller and D. Zlatanov: Kinematic Singularities of Mechanisms Revisited. In: IMA Conference on Mathematics of Robotics, St Anne's College, University of Oxford, September 2015.
- [81] D. Basu and A. Ghosal: Singularity Analysis Of Platform-Type Multi-Loop Spatial Mechanisms. In: *Mechanism and Machine Theory*, 32 (3), (15 pages), April 1997.
- [82] Z. Liu and J. Angeles: Data-Conditioning In The Optimization Of Function-Generating Linkages. In: *Advances in Design Automation*, Volume 65-1, (8 pages) 1993.
- [83] J. Rastegar: Approximated Grashof-Type Movability Conditions for RSSR Mechanisms With Force Transmission Limitations. In: *ASME*, Volume 114, Issue 1, (8 pages), 1992

- [84] P. Grosch, R. Di Gregorio, J. Lopez, and F. Thomas: Motion Planning for a Novel Reconfigurable Parallel Manipulator with Lockable Revolute Joints. In: 2010 IEEE
- [85] W.B. Riley and A.R. George “Design, Analysis and Testing of a Formula SAE Car Chassis” SAE Motorsports Engineering Conference, 2002
- [86] A. Makhal, and A. Perez-Gracia: Solvable multi-fingered hands for exact kinematic synthesis. In: Advances in Robot Kinematics. Ljubljana, Slovenia (June 2014)
- [87] A. Perez-Gracia: Dimensional synthesis of one-jointed multi-fingered hands. In: Recent Advances in Mechanism Design for Robotics, Mechanisms and Machine Science, vol. 33. Springer (2015)
- [88] E. Simo-Serra, A. Perez-Gracia: Kinematic synthesis using tree topologies. Mechanism and Machine Theory 72 C, 94–113 (2014)
- [89] Y. Yihun, K. Bosworth, and A. Perez-Gracia: Link-based performance optimization of spatial mechanisms. Journal of Mechanical Design 136(12) (2014)
- [90] N. Hasanzadeh, X. He, and A. Perez-Gracia: A design implementation process for robotic hand synthesis. In: ASME Int. Design Engineering Technical Conferences (2015)
- [91] K.J. Waldron: A study of overconstrained linkage geometry by solution of closure equations- part ii- four-bar linkages with lower pair joints other than screw joints. Mechanism and Machine Theory 8, 233–247 (1972)
- [92] C. Gosselin and J. Angeles (1990) Singularity analysis of closed-loop kinematic chains. IEEE Trans Robot Autom 6(3):281–290
- [93] G. Saravanan, G. Yamuna, and S. Nandhini, 2016, April. Real time implementation of RGB to HSV/HSI/HSL and its reverse color space models. In 2016 International Conference on Communication and Signal Processing (ICCSP) (pp. 0462-0466). IEEE
- [94] C. Yu, J.J. Cheng, L.G. Jones, Y.Y. Wang, E. Faillace, C. Loureiro, and Y.P. Chia, 1993. Data collection handbook to support modeling the impacts of radioactive material in soil (No. ANL/EAIS--8). Argonne National Lab.

- [95] T.A. Wise, 2019. World hunger is on the rise. Chain Reaction, (136), pp.42-43.
- [96] M. Ryu, J. Yun, T. Miao, I. Ahn, S. Choi and J. Kim, "Design and implementation of a connected farm for smart farming system," 2015 IEEE SENSORS, Busan, Korea (South), 2015, pp. 1-4, doi: 10.1109/ICSENS.2015.7370624.
- [97] F. Sistler, "Robotics and intelligent machines in agriculture," in IEEE Journal on Robotics and Automation, vol. 3, no. 1, pp. 3-6, February 1987, doi: 10.1109/JRA.1987.1087074.
- [98] L. García-Pérez, M.C. García-Alegre, A. Ribeiro, and D. Guinea. An agent of behavior architecture for unmanned control of a farming vehicle. 2008, computers and electronics in agriculture, 60(1), pp.39-48.
- [99] G. Ren, T. Lin, Y. Ying, G. Chowdhary, and K.C. Ting. Agricultural robotics research applicable to poultry production: A review. 2020, Computers and Electronics in Agriculture, 169, p.105216.
- [100] <https://robohub.org/3-types-of-robot-singularities-and-how-to-avoid-them/>
- [101] G. Quaglia, C. Visconte, L.S. Scimmi, M. Melchiorre, P. Cavallone, and S. Pastorelli. Design of the positioning mechanism of an unmanned ground vehicle for precision agriculture. 2019, In IFToMM World Congress on Mechanism and Machine Science (pp. 3531-3540). Springer, Cham.
- [102] J. Underwood, A. Wendel, B. Schofield, L. McMurray, and R. Kimber. Efficient in-field plant phenomics for row-crops with an autonomous ground vehicle. 2017, Journal of Field Robotics, 34(6), pp.1061-1083.
- [103] Z. Wang, J. Yang, P. Liu, X. Long, H. Li, and W., Wei. Development of an agricultural vehicle levelling system based on rapid active levelling. 2019, Biosystems Engineering, 186, pp.337-348.
- [104] H.B. Patil, S.D. Kachave, and E.R. Deore. Stress analysis of automotive chassis with various thicknesses. 2013, IOSR Journal of Mechanical and Civil Engineering, 6(1), pp.44-49.
- [105] H.K. Asker, T.S. Dawood, and A.F. Said. Stress Analysis of standard Truck Chassis during ramping on Block using Finite Element Method". 2012, ARPN Journal of Engineering and Applied Sciences, 7(6), pp.641-648.

- [106] M. Perez-Ruiz, D.C. Slaughter, C. Gliever, and S.K. Upadhyaya. Tractor-based Real-time Kinematic-Global Positioning System (RTK-GPS) guidance system for geospatial mapping of row crop transplant. 2012, *Biosystems engineering*, 111(1), pp.64-71.
- [107] M. Pini, G. Marucco, G. Falco, M. Nicola, and W. De Wilde. Experimental testbed and methodology for the assessment of RTK GNSS receivers used in precision agriculture. 2020, *IEEE Access*, 8, pp.14690-14703.
- [108] S. Gan-Mor, R.L. Clark, and B.L. Upchurch. Implement lateral position accuracy under RTK-GPS tractor guidance. 2007, *Computers and Electronics in Agriculture*, 59(1-2), pp.31-38.
- [109] H. Sun, D.C. Slaughter, M.P. Ruiz, C. Gliever, S.K. Upadhyaya, and R.F. Smith. RTK GPS mapping of transplanted row crops. 2010, *Computers and Electronics in Agriculture*, 71(1), pp.32-37.
- [110] U. Weiss, and P. Biber. Plant detection and mapping for agricultural robots using a 3D LIDAR sensor. 2011, *Robotics and autonomous systems*, 59(5), pp.265-273.
- [111] M. Kragh, R.N. Jørgensen, and H. Pedersen. Object detection and terrain classification in agricultural fields using 3D lidar data. 2015, In *International conference on computer vision systems* (pp. 188-197). Springer, Cham.
- [112] Global Navigation Satellite System: <https://talks.navixy.com/trends/in-depth/how-many-gnss-satellites-work-on-the-earths-orbit/>
- [113] RTK GPS, <https://www.youtube.com/watch?v=pOuYdxBWVyU>
- [114] R. Moeller, 2020. GPS-Guided Autonomous Robot with Obstacle Avoidance and Path Optimization (Master's Thesis, Idaho State University).
- [115] Converting RGB color to HSL format: <https://github.com/Sable/mcbench-benchmarks/blob/master/20292-hsl2rgb-and-rgb2hsl-conversion/rgb2hsl.m>
- [116] <https://www.mathworks.com/matlabcentral/fileexchange/10502-image-overlay>